

UCSF

UC San Francisco Electronic Theses and Dissertations

Title

Modeling Cartilage Extracellular Matrix Stiffness: A Potent Regulator of TGF β -inducible Chondrocyte Differentiation

Permalink

<https://escholarship.org/uc/item/70v5t2c4>

Author

Allen, Jessica Lynn

Publication Date

2012

Peer reviewed|Thesis/dissertation

Modeling Cartilage Extracellular Matrix Stiffness: A Potent Regulator of TGFbeta-inducible
Chondrocyte Differentiation

by

Jessica Allen

DISSERTATION

Submitted in partial satisfaction of the requirements for the degree of

DOCTOR OF PHILOSOPHY

in

Bioengineering

in the

GRADUATE DIVISION

of the

UNIVERSITY OF CALIFORNIA, SAN FRANCISCO

ACKNOWLEDGEMENTS

This dissertation and the completion of my graduate degree would not have been possible without the support and dedication of my family, friends, coworkers, classmates, and mentors.

First to all my mentors, thank you so much for all you've taught me as I've worked to obtain my degree. I'd like to thank my dissertation committee members – Dr. Valerie Weaver, Dr. Ralph Marcucio, and Dr. Lisa Pruitt – for all their support, helpful comments and suggestions. It was through your encouragement that I was able to develop a research project that I am truly proud of. I'd also like to thank Dr. Alfred Kuo, Dr. Tejal Desai, Dr. Omar Akil, and Dr. Xiaojuan Li for their collaboration and guidance. Also, thank you Dr. Paul Hansma for teaching me that being inquisitive and creative with our questions and solutions is what science is all about.

Thank you to all the members of the Alliston Lab: Dr. Carol Chen, Dan Nguyen, Emily Chin, Dr. Simon Tang, Dr. Margaret Cooke, Ellora Berthet, Dr. Dan Thuillier, Jackie Nguyen, Joanna Rys, Dr. Faith Hall-Glenn, Dr. Amanda Whitaker, and Rebecca Usoff. It was wonderful to work every day with such friendly, driven, and ambitious scientists. I think I chose the best possible lab for my graduate degree and I'm only sorry I have to leave so soon. I'd like to thank the other members of the Orthopedic Surgery Department as well. Working alongside the Schneider and Lotz labs added diversity and a spirit of collaboration that was truly inspiring. Thanks especially to Kristin Butcher for sharing her wealth of knowledge. I'd also like to thank the members of the Weaver Lab, particularly Dr. Jon Lakins, Dr. Janna Mouw, and Dr. Inkyung Kang, for help developing

the polyacrylamide gel substrates used extensively in this dissertation. Without your help, I would have given up long ago.

I realize now that the support of my family and friends made grad school so much easier. To my family – Mom, Dad, Jennifer, and Mark – thanks for being there for me. You were always enthusiastic about what I do and that made it easier to keep going when times were tough. Thank you for teaching me to pursue my passion. To my friends – thank you for being there as a much-needed outlet for all of the stresses of grad school. Thanks especially to Emma Essock-Burns for commiserating with me as we both worked to finish writing our dissertations. And to my husband – Dean Allen – thank you for believing in me and for being there for me through good days and bad. And thank you for joining me on this great adventure in California. It is so much easier to work hard when you know there is someone special at home waiting to make you smile.

Finally I would like to thank my advisor and mentor, Dr. Tamara Alliston. I knew from our first meeting that I chose the right mentor. Never lose your spirit and enthusiasm for science. Working that extra hour for that last bit of data is easier when I know you will be just as excited (if not more so) by the results. I am so proud of what we've achieved in the short time we've worked together. Thank you for being such an inspiring mentor and a great friend.

ABSTRACT

The extracellular matrix (ECM) functions hierarchically: macroscopically, it supports the tissue under physiologic loading and microscopically, it acts as a physical cue for the native cell population. Combining these perspectives of an orthopedic tissue, like cartilage, provides comprehensive knowledge of the tissue as a whole. In this dissertation, PA gels were adapted to study cartilage ECM to understand its function at the tissue level and as a physical cue in the cellular microenvironment. Layered PA gels were used to emulate the stratified material properties of articular cartilage and develop a mathematical model of the loading behavior of intact stratified materials. This model, when applied to articular cartilage, led to the finding that osteoarthritis results in a loss of stratified architecture and an increase in the homogeneity of cartilage ECM. Homogeneous PA gels were used in cellular mechanosensing studies as a physical cue to determine the effect of ECM stiffness on chondrocyte differentiation. Chondrocyte gene expression in ATDC5 cells, murine chondrocytes, and mesenchymal stem cells were specifically induced on substrates that mimicked the stiffness of articular cartilage ECM. Addition of exogenous TGF β to cartilage-like substrates induced a synergistic induction in chondrocyte specific gene expression. Chondroinduction on cartilage-like substrates requires autocrine TGF β 1 expression. Smad3 phosphorylation, nuclear localization, and transcriptional activity are also induced on cartilage-like substrates. When TGF β is added exogenously, synergistic induction of chondrocyte gene expression becomes Smad3 independent, acting instead through the p38 MAPK pathway. Combining macroscopic and microscopic perspectives of cartilage ECM from this dissertation may be parlayed into novel therapies and tissue engineering strategies.

TABLE OF CONTENTS

Chapter 1. Introduction	1
Chapter 2. Materials and Methods	8
Chapter 3. Development of Cell Culture Substrates that Mimic the Stiffness of Articular Cartilage	20
Chapter 4. Depth-Dependent Modulus of Articular Cartilage Approaches Homogeneity with Osteoarthritis	31
Chapter 5. ECM Stiffness Primes the TGF β Pathway to Promote Chondrocyte Differentiation	47
Chapter 6. ECM Stiffness Regulates Chondrogenesis in Mesenchymal Stem Cells	72
Chapter 7. Summary and Future Directions	85
References	91
Appendix A. The Use of Polyacrylamide Gels for Mechanical Calibration of Cartilage – A Combined Nanoindentation and Unconfined Compression Study	102
Appendix B. The Tissue Diagnostic Instrument	110

LIST OF TABLES

Table 2.1: Primers for SYBR-green detection of mouse sequences by quantitative RT-PCR analysis.	15
Table 4.1: Elastic moduli of homogeneous polyacrylamide gels.	34
Table 4.2: Composition of stratified polyacrylamide gels.	34
Table 5.1: Physical characteristics of experimental substrates.	52

LIST OF FIGURES

Figure 3.1: PA gel stiffness determined by several mechanical testing methods.	23
Figure 3.2: PA gel protein conjugation method comparison.	25
Figure 3.3: Passive protein coating allows weak and transient cell attachment to PA gels.	27
Figure 4.1: Superficial and underlying moduli of stratified gels	35
Figure 4.2: Model describes loading curves of experimental gel data.	39
Figure 4.3: The stratified moduli of articular cartilage approach homogeneity with OA.	40
Figure 4.4: Applying the stratified gel model to articular cartilage.	42
Supplemental Figure 4.1: Type V Probe Assembly.	46
Figure 5.1: Chondrocyte differentiation is stiffness-sensitive.	53
Figure 5.2: Substrate stiffness and TGF β synergize to induce chondrogenic differentiation.	54
Figure 5.3: Mechanosensitive chondroinduction is mediated by ROCK signaling.	56
Figure 5.4: Mechanosensitive, ROCK-dependent induction of TGF β 1 is required for chondroinduction.	58
Figure 5.5: Smad3 phosphorylation, localization and transcriptional activity are sensitive to ECM stiffness.	60
Figure 5.6: Synergy between TGF β and ECM stiffness requires p38 MAPK, but not Smad3.	62
Figure 5.7: Schematic of the mechanism of chondrocyte integration of cues provided by ECM stiffness and TGF β .	66
Supplemental Figure 5.1: Smad3 mRNA expression is relatively unaffected by substrate.	71
Figure 6.1: Chondrogenic gene expression in murine MSCs is stiffness-sensitive.	74

Figure 6.2: hMSC gene expression is stiffness-sensitive.	75
Figure 6.3: Aggrecan gene expression is repressed in hMSCs by cartilage-like substrates and TGF β .	76
Figure 6.4: hMSCs fail to produce Col2 α 1 PCR product.	77
Figure 6.5: Substrate stiffness and TGF β synergize to induce Sox9 expression	78
Figure 6.6: hMSCs adopt a rounded morphology on 0.5 MPa substrates.	79
Figure 6.7: Stiffness-sensitive Sox9 expression may require ROCK-regulated activation of the TGF β pathway.	80

CHAPTER 1

Introduction

Osteoarthritis (OA) is a detrimental disease currently affects over 27 million Americans (Lawrence *et al.*, 2008). The disease is marked by cartilage degradation, synovial fibrosis, and osteophyte formation in the subchondral bone (Goldring and Goldring, 2007). As cartilage degrades, the material properties of cartilage are diminished, including the stiffness, viscoelastic properties, and overall thickness (Knecht *et al.*, 2006). While the true cause of the disease is unknown, OA has both physical and genetic risk factors. Conditions that generate unnatural loading, including obesity, joint injury, muscle weakness, and joint malalignment, have been identified as risk factors for OA (Aigner and Dudhia, 2003; Goldring and Goldring, 2007; Li *et al.*, 2007a). Genome studies and animal models have also identified specific polymorphisms and mutations that increase susceptibility to OA. Regardless of the impetus, the disease progresses similarly, suggesting a common mechanism underlying the development of OA from physical or biochemical cues.

The difficulty in identifying the mechanism of OA is further compounded by the strong relationship between the physical and biochemical components of this tissue. Cartilage mechanical function correlates strongly with the biochemical structure of the extracellular matrix (ECM), composed of a dense mesh of collagen II enclosing large proteoglycans, like aggrecan (Knecht *et al.*, 2006). Negatively charged groups on the proteoglycans attract cations, creating a positive osmotic pressure which causes the tissue

to swell (Hu and Athanasiou, 2003). In selective degradation experiments, the two main components of cartilage ECM, collagen II and proteoglycans, were found directly responsible for the tissue's dynamic instantaneous and static equilibrium properties, respectively (Knecht *et al.*, 2006). Therefore, the biochemical structure of cartilage matrix is tied directly to the mechanical function of the tissue.

Chondrocytes themselves are also tightly controlled by physical and biochemical cues. Numerous studies have shown that externally applied physical cues, like cyclic loading, intermittent hydrostatic pressure, shear and low intensity ultrasound, increase chondrocyte proteoglycan production in vitro (Grad *et al.*, 2011; McCormack and Mansour, 1998; Nishikori *et al.*, 2002; Parkkinen *et al.*, 1992; Parvizi *et al.*, 1999). These physical cues mimic the external forces found in joints under physiological loading. However, even though the mechanical properties of cartilage ECM are known to be so important to the tissue's function under applied load, little is known about how these intrinsic physical cues affect chondrocyte behavior.

In comparison to intrinsic physical cues, far more is understood about biochemical regulation of chondrocyte phenotype within the microenvironment. Among the biochemical factors important in cartilage maintenance, TGF β plays an important role in all stages of articular cartilage development (van der Kraan *et al.*, 2009). TGF β is the earliest signal in chondrogenesis, inducing recruitment, proliferation and condensation of chondroprogenitor MSCs (Goldring *et al.*, 2006). Upon initiation of chondrogenesis, TGF β stimulates anabolic production of cartilage ECM components, like collagen II and aggrecan in combination with Sox9, the key transcription factor in chondrogenesis. TGF β induces Col2a1 mRNA by activating Sox9 through CBP/p300 recruitment in a

Smad3 dependent manner (Furumatsu *et al.*, 2005). Aggrecan mRNA expression requires Smad2 activation at earlier time points and ERK1/2 and p38 MAPK activation at late timepoints, both regulated by TGF β (Watanabe *et al.*, 2001).

In late stages of chondrocyte differentiation, TGF β inhibits progression of hypertrophy. In the growth plate progression of hypertrophy is controlled indirectly by TGF β produced by perichondrium in response to Ihh and Shh, which slows the progression of hypertrophy by stimulating production of PTHrP (Alvarez *et al.*, 2002; Serra *et al.*, 1999). Hypertrophy is also directly inhibited by TGF β directly, through Smad2/3 and HDAC4 repression of the Runx2 promoter (Ferguson *et al.*, 2000). TGF β also negatively regulates hypertrophic genes induced by Runx2, including Collagen X and MMP13 (Chen *et al.*, 2012; Zhang *et al.*, 2004).

The role of TGF β in OA is complex. Injection of TGF β into the knee space results in an increase in proteoglycan production and cartilage repair, but also an increase in osteophyte formation and synovial thickening. Studies of osteoarthritic cartilage suggest a dramatic reduction in expression of the TGF β ligand and TGF β type II receptor with disease (Blaney Davidson *et al.*, 2007; Pujol *et al.*, 2008). Mice lacking Smad3 or expressing a dominant negative TGF β type II receptor develop OA-like symptoms. (Serra *et al.*, 1997; Yang *et al.*, 2001). Moreover, a newly identified syndrome in humans caused by mutations in Smad3 leads to early-onset OA, underlining this signaling pathway's importance in healthy cartilage maintenance (van de Laar *et al.*, 2011). While the importance of biochemical cues like TGF β in chondrocyte differentiation and disease has been extensively studied, the role of intrinsic physical cues presented by the cartilage ECM in maintenance of healthy cartilage remains elusive.

Recently, intrinsic physical cues from the microenvironment, like ECM stiffness, have been identified as powerful drivers of cell behavior. The cellular mechanotransduction pathway hinges on a balance of forces between the external stimuli in the microenvironment and internal cytoskeletal tension. Cellular connection to the physical microenvironment is mediated through integrin attachment to the ECM. Upon the application of force, integrins cluster to form focal adhesions, which activate actin stress fiber formation and other downstream signaling molecules, like FAK, Rho GTPases and MAPKs (Geiger *et al.*, 2009; Kanchanawong *et al.*, 2010; Miranti and Brugge, 2002). These signaling molecules convert the physical signal into a biochemical response, altering cellular behavior as a result of the external environment. Cell motility is directed toward stiffer substrates in a phenomenon called durotaxis (Lo *et al.*, 2000). Cell cycle, proliferation and apoptosis were found to be directed not only by the compliance of the extracellular matrix, but also size of attachment area (Assoian and Klein, 2008; Chen *et al.*, 1997; Huang and Ingber, 2005; Wang *et al.*, 2000). Interestingly, many studies have found that the stiffness of the physical microenvironment can direct mesenchymal stem cell differentiation in to several lineages (Engler *et al.*, 2006; Leipzig and Shoichet, 2009; Park *et al.*, 2011). Differentiation can be driven toward a particular lineage by presenting a substrate that matches the stiffness of physiological microenvironment for that lineage. For example, neurogenesis is promoted on extremely compliant substrates that mimic the stiffness of brain tissue (Engler *et al.*, 2006). This phenomenon is also present in several diseases, including cancer and liver fibrosis, in which the disease state is perpetuated by a physical cue in the microenvironment (Butcher *et al.*, 2009; Li *et al.*, 2007b; Paszek *et al.*, 2005).

Given these observations, it seems likely that the physical microenvironment of chondrocytes acts as a signal to maintain the chondrocyte phenotype, and aberrant physical cues could result in a development of OA. Remarkably, chondrocyte differentiation in vitro seems to be activated by specific physical conditions. Chondrogenesis in MSCs requires 3D culture and a rounded morphology (Guilak *et al.*, 2009). Chondrocyte differentiation is activated by culture in agarose, alginate, pellet culture, and collagen gels, which induce a rounded morphology and present a stiffness that is far more compliant than tissue culture plastic (Benya and Shaffer, 1982; Hauselmann *et al.*, 1994; Schulze-Tanzil *et al.*, 2002; Takahashi *et al.*, 2007). It seems likely that a component of the success of these culture methods lies in presenting a better representation of the microenvironment, and possibly the physiological stiffness, normally found in cartilage ECM.

Polyacrylamide (PA) gels represent a classical method for simple mechanosensing assays across an easily tunable range of stiffnesses (Wang and Pelham, 1998). Compared to the culture methods described above, PA gels would easily allow application of molecular assays to determining the mechanisms through which stiffness might regulate chondrocyte behavior. However, currently the range of stiffnesses afforded by PA gels is overly compliant to properly model the stiffness of cartilage. Chapter 3 will delve into the development of novel PA substrates that appropriately model the stiffness of articular cartilage ECM.

Previous research has given hints as to how chondrocyte differentiation may be regulated by ECM stiffness. Many of the same pathways involved in mechanosensing have been identified as regulators of chondrocyte differentiation. ERK1/2 and p38

MAPK signaling plays a central role in the induction of chondrogenesis and the regulation of aggrecan expression in chondrocyte differentiation (Stanton *et al.*, 2003). Inhibition of integrin, actin, FAK, and Rho colocalization with nitric oxide inhibits proteoglycan synthesis in bovine chondrocytes (Clancy *et al.*, 1997). Moreover, ROCK, the downstream mediator of Rho GTPase, directly phosphorylates Sox9 in chondrocytes (Haudenschild *et al.*, 2010). On overly stiff tissue culture plastic, inhibition of the actin cytoskeleton in vitro rescues dedifferentiating chondrocytes, indicated by an increase in collagen II and proteoglycan expression (Woods *et al.*, 2007). However, in alginate bead or explant culture, disruption of the actin cytoskeleton reduced pericellular matrix production and proteoglycan expression, suggesting that the role of actin changes with culture conditions (Nofal and Knudson, 2002). Woods, et al demonstrated that Rho/ROCK signaling, which directly mediates actin stress fiber formation, regulates chondrogenesis. However, the effect of Rho inhibition is again dependent on the culture condition, increasing chondrocyte-specific gene expression when Rho is inhibited in monolayer culture on plastic, but decreasing with Rho inhibition in micromass culture (Woods and Beier, 2006). The array of responses to the loss of these mediators of focal adhesions suggests that the chondrocyte phenotype may be tightly regulated by the mechanosensing pathway.

Interestingly, these mechanosensing pathways also intersect with TGF β , an important biochemical cue in articular cartilage. Integrins and internal cellular tension can regulate TGF β ligand activation (Munger *et al.*, 1999; Wipff *et al.*, 2007). Once activated, the ligand signals through a heterotetrameric complex consisting of two type I and two type II serine/threonine kinase receptors, that relay the signal through several

pathways. ‘Canonical’ TGF β signaling is mediated by R-Smads 2 and 3 and the common mediator Smad4 (Wrana, 2000), but TGF β can also act through many non-Smad pathways, including Rho/ROCK and the MAPK pathway, (Derynck and Zhang, 2003). The overlapping pathways for TGF β and mechanosensing mirror the complex interplay between physical and biochemical cues in both healthy and osteoarthritic cartilage. A further investigation into the integration of TGF β with intrinsic physical cues can be found in chapters 5 and 6.

Therefore, in order to understand the integration between ECM stiffness and biochemical cues, like TGF β , in the regulations of chondrocyte differentiation, we sought to (1) determine the mechanisms involved in ECM stiffness regulation of chondrocyte differentiation, (2) determine the mechanisms through which ECM stiffness interacts with the TGF β pathway to regulate chondrocyte differentiation, (3) Determine the extent to which these interactions differ through development and disease.

CHAPTER 2

Materials and Methods

Gel Substrate Preparation: The elastic modulus of polyacrylamide gel substrates was controlled by varying the concentration of the crosslinker, piperazine diacrylamide (PDA) (Bio-Rad, 161-0202), from 1% to 3% (w/v), while maintaining a constant 30% (w/v) concentration of the monomer, acrylamide (Bio-Rad, 161, 0140), in a solution of 0.01M Hepes buffer. Polymerization was initiated by 10% (w/v) ammonium persulfate (APS) added at a 1:200 dilution and enhanced by TEMED (Bio-Rad, 161-0801), added at a 1:2000 dilution. Before adding APS, the acrylamide mixture was vortexed and degassed for one hour. Gels were polymerized in a 1 mm thick vertical glass mold and then stored in phosphate buffered saline at 4°C. The gels prepared in the studies described in this dissertation spanned the stiffness range reported for articular cartilage (Table 4.1 and 5.1).

Stratified gel preparation: To construct a stratified elastic modulus gel, a pre-polymerized “underlying” PA gel was placed in a mold that allowed for the polymerization of a thin “superficial” layer of PA. Compositions of the stratified gels can be found in Table 4.2.

Measuring stratified material properties by reference point microindentation:

Reference point microindentation was performed using the Tissue Diagnostic Instrument (TDI), an indenter previously validated against established mechanical testing methods (Hansma *et al.*, 2009). The TDI concurrently measures force and displacement of a magnetically attached probe. The force generator oscillates at a set frequency of 2 Hz, with maximum displacement of 600 μm . In this study, a type V probe assembly was used, which consisted of a flat reference probe and a flat 1 mm diameter cylindrical indenter (Supplemental Figure 4.1) (Hansma *et al.*, 2009; Tang *et al.*, 2010). The mechanical tests were performed with the PA gels fully immersed in 0.01M HEPES at room temperature. At least 5 cyclic loading curves were sampled at 3 different sites on each composite gel. Proprietary software, included with the indenter, was used to determine the elastic modulus using a formula previously derived for indentation with a flat-ended cylindrical punch (Hansma *et al.*, 2009; Sneddon, 1965; Tang *et al.*, 2010). Measurements at each site were averaged and are represented graphically by a single point. Stratified elastic moduli were compared to moduli of homogeneous gel standards using a 95% confidence interval. Spearman rank correlation test was performed to identify a correlation between crosslinker concentration and elastic modulus. Regression analysis and model-fit was performed using Table Curve (Jandal Scientific Software, San Rafael, CA).

Specimen Preparation: Human articular cartilage samples were obtained from patients in accordance with protocols approved by the Committee on Human Research at the University of California, San Francisco. Tibial plateaus and femoral condyles with the

subchondral bone intact were harvested and fresh frozen from a human cadaver (19yo) and from human total knee arthroplasty with severe clinically confirmed osteoarthritis (> 60yo). Using the type V probe assembly, non-destructive indentation loads were applied to cartilage *in situ* at 2 Hz within a PBS bath. Three sites each were tested on the cadaveric sample and across two osteoarthritic samples. At least five measurements were taken at each site. Loading curves were obtained from these measurements, and analyzed with the software included with the indenter. For statistical analysis of the cadaveric and osteoarthritic tissue, the average moduli and standard error of the mean were calculated from measurements at multiple sites, each of which is an average of five measurements. Student t-tests were used to identify statistical significance between cadaveric and osteoarthritic cartilage samples.

Preparing PA Gels for Cell Culture Studies: Cell attachment was facilitated by covalently attaching collagen II (Sigma, C9301) to the polyacrylamide gel as described previously (Reinhart-King *et al.*, 2005), modified to use acrylic acid n-hydroxysuccinimide ester (N2, Sigma, A8060). A 1.8% (w/v) solution of N2 in 50% ethanol was diluted 1:6 into a solution containing 0.01% (w/v) bisacrylamide (Bio-Rad, 161-0142), 0.17% (w/v) Irgacure 2959 (BASF, 55047962), and 0.05 M Hepes NaOH (pH 6). Polyacrylamide gel slabs were cut into 3 cm diameter disks with a stainless steel biscuit cutter. The gel disks were covered with 200 μ l of N2 solution and sandwiched horizontally between two large glass slides prior to exposure to UV light (306 nm) for 10 mins, followed by rinsing with PBS. Collagen II was dissolved in 0.1 M acetic acid at a concentration of 1 mg/ml and then diluted 1:100 in 1 M HEPES (pH 8). Each gel was

incubated with 1 ml of the collagen II solution at 4°C overnight in ultra-low attachment 6 well plates (Costar, 3471) with constant agitation. Gel substrates were washed once more with PBS and allowed to equilibrate for at least 3 hours in media (50/50 DMEM/F12) at 4°C before seeding cells. Plastic controls were coated with 1 mg/ml collagen II in acetic acid, diluted 1:100 in sterile water for a minimum of 4 hours at room temperature. The remaining solution was then removed and the plates were left to dry overnight at 4°C followed by a rinse with PBS before seeding cells.

The composition of PA gels polymerized with 3% (w/v) 2-acrylamido-2-methylpropane sulfonic acid (AMPSA) (Sigma, 282731) was adjusted to 29.3% acrylamide and 2% PDA. AMPSA is negatively charged and therefore should electrostatically attract proteins to the gel surface to facilitate cell attachment. 300 µl of collagen II (0.5 mg/ml) dissolved in water was pooled on the top of the AMPSA gel for 1 hour before cell seeding.

To prepare PA gels for protein conjugation with hydrazine hydrate (Sigma, 225819), gels were cut into 6.5 x 9 cm slabs and placed in a glass container. PA gels were fully immersed in hydrazine hydrate for 4 hours on an orbital shaker and then washed with 5% glacial acetic acid. To remove any trace of hydrazine hydrate, gels were washed in sterile water 4 times for 15 mins each on an orbital shaker. Hydrazine-treated gels were stored for up to two months in sterile PBS at 4°C. Prior to the addition of collagen II, hydrazine-treated gel slabs were cut with a 3 cm diameter biscuit cutter. Collagen II was dissolved in 0.1 M acetic acid at a concentration of 1mg/ml and then diluted 1:10 in 50 mM sodium acetate buffer (pH 4.5). To oxidize the collagen, Sodium periodate was added at a concentration of 3.6 mg/ml. The oxidized collagen solution was

diluted 1:5 0.1 M sodium acetate. 305 μ l of the oxidized collagen solution was pooled on the surface of each gel and incubated at room temperature for 1 hour. Gels were then rinsed with PBS 3 times for 10 mins each, and stored in DMEM/F12 without FBS at 4°C overnight before cell seeding. Poly-l-lysine (Sigma, P4707) was added to hydrazine-treated gels at a concentration that matched that normally used for collagen II protein conjugation.

To determine the collagen II ligand density for each substrate, an indirect ELISA assay was performed on collagen II coated gels and plastic using an primary mouse antibody raised against collagen II (C11C1, Development Studies Hybridoma Bank, Iowa) and an Alexa Fluor 488 goat-anti-mouse secondary (Invitrogen, A11029). A dilution series of collagen II coated on plastic, prepared as for the experimental conditions, served as a standard curve. Fluorescence was measured in a SpectraMax M5 plate reader (Molecular Devices) and normalized to the standard curve. The given values are averages of four replicates. Collagen densities between substrates were found to be statistically indistinguishable through ANOVA analysis (Table 5.1).

Cell Culture: A majority of the studies used ATDC5 cells, a murine chondroprogenitor cell line (RIKEN, RCB0565). Growth media for ATDC5 cells consisted of 50/50 DMEM/F12 with 5% FBS and was also used for experiments lasting less than 48 hours. Experiments lasting 7 days were performed in differentiation media consisting of growth media supplemented with 10 μ g/ml insulin (Sigma, I9278), 10 μ g/ml transferrin (Gibco, 02-0124SA), 3×10^{-8} M sodium selenite (Sigma, S5261), and 1% penicillin/streptomycin.

For Alcian blue staining, differentiation media was supplemented with 25 µg/ml of ascorbic acid (Sigma, A8960).

Primary chondrocytes were isolated from 5 day old mice, as described previously (Thirion and Berenbaum, 2004). Briefly, cartilage from the femoral heads, tibial plateaus, and femoral condyles were removed, cleaned of all extraneous tissue through a serial digestion in cell culture medium, consisting of DMEM supplemented with 2 mM L-glutamine, and 0.5% penicillin/streptomycin, with 3 mg/mL collagenase D (Roche, 11 088 858 001) twice for 45 mins, and finally overnight in cell culture medium with 0.5 mg/ml collagenase D. The remaining cell suspension was passed through a sterile 48-µm mesh and then plated directly on to experimental substrates at a density similar to that of ATDC5 cells (6000 cells/cm²). Differentiation experiments were performed in media consisting of 50/50 DMEM/F12 supplemented with 10% FBS, 0.5% penicillin/streptomycin, 10 µg/ml insulin, 10 µg/ml transferrin, 3 x 10⁻⁸ M sodium selenite.

Mouse mesenchymal stem cells (mMSCs) were isolated from the bone marrow of two month old mice. Differentiation experiments were conducted in chondrogenic media consisting of high glucose DMEM supplemented with 1% penicillin/streptomycin, 10 µg/ml insulin, 10 µg/ml transferrin, 3 x 10⁻⁸ M sodium selenite, 50 µg/ml ascorbic acid, 40 µg/ml L-proline, 0.1 µM dexamethasone, and 110 µg/ml pyruvate.

Growth media for human mesenchymal stem cells (hMSCs) (Lonza, PT-2501) consisted of low glucose DMEM supplemented with 10% FBS, and 1% penicillin/streptomycin. Experiments lasting less than 48 hours were conducted in this media formulation. For chondrogenesis experiments hMSCs were cultured in

chondrogenic media consisting of high glucose DMEM supplemented with 10% FBS, 1% non-essential amino acids, 1% penicillin/streptomycin, 0.01 M HEPES, 10 µg/ml insulin, 10 µg/ml transferrin, 3×10^{-8} M sodium selenite, 160 µM L-proline, 200 µM ascorbic acid, 0.1 µM dexamethasone.

TGFβ3 (Peprotech, 100-36E) was used at 5 ng/ml. Cells were treated as indicated with the ROCK1 inhibitor Y27632 (10 µM, Sigma, Y0503), the TGFβ receptor type I kinase inhibitor SB431542 (5 µM, Sigma, S4317), and the p38 inhibitor SB203580 (10 µM, Calbiochem, 559389).

Cell Characterization: Images of ATDC5 cells and MSCs attached to each gel substrate and plastic were taken with a Zeiss Axiovert 40CFL microscope 24 hrs after seeding. Using ImageJ, the outline of each cell was drawn and analyzed for cell area and roundness ($4 \times \text{cell_area} / \pi \times \text{major_axis}^2$). Each image contained approximately 100 cells. Cell confluency in each image was calculated to be less than 35%. Average roundness and cell area were calculated for each image and found to be statistically indistinguishable through ANOVA analysis. Values given in Table 5.1 are the averages and standard deviations for all cells analyzed across 3 biological replicates for each substrate.

Gene	Sequence	
Sox9	Forward	TCGCCTTCCCCGGGTTTAGAGC
	Reverse	GGCGGCGGGCACTTAGCAGA
Col2 α 1	Forward	ACGAAGCGGCTGGCAACCTCA
	Reverse	CCCTCGGCCCTCATCTCTACATCA
Aggrecan	Forward	GTGAGGACCTGGTAGTGCGAGTGA
	Reverse	GAGCCTGGGCGATAGTGGAATATA
TGF β 1	Forward	AGCCCGAAGCGGACTACTAT
	Reverse	TCCCGAATGTCTGACGTATTG
Smad3	Forward	ACCAAGTGCATTACCATCC
	Reverse	CAGTAGATAACGTGAGGGAGCCC
L19	Forward	ACGGCTTGCTGCCTTCGCAT
	Reverse	AGGAACCTTCTCTCGTCTCCGGG
18S	Forward	GCGGCTTGGTGA CTCTAGATA
	Reverse	GAATCGAACCTGATTCCC

Table 2.1: Primers for SYBR-green detection of mouse sequences by quantitative RT-PCR analysis.

QPCR: RNA was isolated using RNeasy column purification (Qiagen, 74104). RNeasy lysis buffer was added to both gel and plastic conditions and RNA was isolated according to manufacturer's instructions, including an on-column DNase treatment. The concentration and purity of RNA was determined using a Nanodrop ND-1000 Spectrophotometer

(Thermo Scientific). Approximately 1 μ g of RNA was converted to cDNA in a reverse transcription (RT) reaction using the iScript cDNA Synthesis Kit (Bio-Rad, 170-8891). Quantitative PCR analysis of each sample was performed in a C1000 Thermal Cycler with CFX96 Real-Time System (Bio-Rad). Forward and reverse intron-spanning primers (Table 2.1) and iQ SYBR-Green Supermix (Bio-Rad, 170-8882) were used to amplify each cDNA of interest. Each sample was run in duplicate and all results were normalized

to the housekeeping genes 18S or L19. Fold changes in gene expression were calculated using the delta-delta Ct method (Livak and Schmittgen, 2001). Figures show the mean and standard deviation for a representative experiment, each of which was repeated independently at least three times. For statistical analysis, average expression and standard error of the mean were calculated for each condition from multiple biological replicates, each of which is an average of two technical replicates. ANOVA analysis followed by Student Newman Keuls test was used to evaluate statistical significance.

Alcian Blue Assay: ATDC5 cells cultured on plastic and gel substrates for 7 days were analyzed for proteoglycan production using an Alcian blue assay. Collagen II-coated plastic and gel substrates without seeded ATDC5s were used as negative controls. All substrates were rinsed with cold PBS, fixed for 30 minutes in 4% formalin, rinsed with deionized water, equilibrated in 3% glacial acetic acid for 30 minutes, stained with 0.1 % Alcian blue dissolved in 3% glacial acetic acid (pH 2.5) for 30 minutes with constant agitation, and rinsed with 3% glacial acetic acid 3 times for 30 minutes each. Images show the area on each substrate with the greatest concentration of staining and are representative of 3 or more biological replicates. Because gel substrates interfered with the traditional spectrophotometric analysis of Alcian blue staining, quantitative analysis was performed by thresholding across all substrates to select stained regions, from which pixel area was calculated. Values reflect mean fold change in stained area relative to cells grown on plastic. ANOVA analysis followed by the Student Newman Keuls test was used to evaluate statistical significance.

ELISA: Media was harvested from ATDC5 cells cultured on either gel or plastic substrates for 48 hours as indicated. TGF β 1 levels were analyzed using an ELISA kit (R&D Systems, MB100B) according to the manufacturer's instructions. The kit detects total TGF β 1 levels and does not distinguish between active and inactive ligands. All data was normalized to cell number and compared to a blank sample containing only media. Figures represent the average and standard deviation for three or more biological replicates. Spearman rank analysis was used to evaluate the significance of the observed trend.

Transfection and Luciferase Assay: For transient transfection and luciferase assays, cells were seeded into 6 well dishes and transfected at approximately 80% confluency with a total of 1 μ g of a (SBE)₄-luc reporter plasmid (Zawel *et al.*, 1998) in 100 μ l of pre-warmed OptiMEM with 5 μ l of FUGENE 6 Transfection Reagent (Roche, 11 814 443 001). All cells were cotransfected with an equivalent amount of total DNA including 0.5 μ g of pRK5- β Gal reporter construct, which constitutively expresses β -galactosidase (Feng *et al.*, 1995). The next day, media was changed prior to commencement of the indicated experimental conditions. At the completion of the experiment, cells were washed twice with PBS and lysed using 300 μ l of Reporter Lysis Buffer (Promega, E397A). Lysates were cleared by centrifugation and assayed for luciferase and β -gal activity according to the manufacturers' protocols (Promega and Tropix, respectively). Luciferase is expressed relative to β -galactosidase expression to normalize for technical variability. Figures represent averages and standard deviations of three biological replicates. Student's t test was used to evaluate statistical significance.

Smad3 Ablation: ATDC5 cells plated in T75 flasks were infected by adding media containing lentivirus constructs that express either a pLKO.1 puro Smad3 shRNA (Sigma, NM_016769.2-1430s1c1) or a non-targeting shRNA sequence (Sigma, SHC002), which was used as a negative control. Lentivirus was produced in the UCSF Lentiviral RNAi Core. The day after infection, cells were seeded on to either plastic or gel substrates for 8 h prior to addition of selection media containing 2 µg/ml of puromycin. Following selection, TGFβ was added as indicated.

Western Blot Analysis: ATDC5 cells were serum starved (50/50 DMEM/F12, 0.2% FBS) for 4 hours prior to treatment with TGFβ for 45 minutes. Whole cell lysates were collected in 1x RIPA buffer (10 mM Tris pH 8, 1 mM EDTA, 1 mM EGTA, 140 mM sodium chloride, 1% Triton X100, 0.1% sodium deoxycholate, 0.1% SDS) supplemented with, 5mM Na₃VO₄, 10mM NaPP_i, 100mM NaF, 500µM PMSF, and 5mg/ml eComplete Mini protease inhibitor tablet (Roche 11 836 153 001). Lysates were sonicated three times for 5 seconds each, clarified by centrifugation, and assessed for protein concentration using a Bradford assay. Protein was separated on 8.5% SDS-PAGE gels and transferred to nitrocellulose membranes. Blots were probed with the following primary and secondary antibodies: β-actin (Abcam, ab8226), Smad2/3 (Santa Cruz, sc8332), pSmad3 (a gift from Dr. E. Leof), p38 (Cell Signaling, 9218), pp38 (Cell Signaling, 9211), and anti-mouse and anti-rabbit secondary antibodies that were conjugated to 680 or 800CW IRDye fluorophores detected using a Licor infrared imaging system (Licor, 926-68020 and 926-32211). Blots shown are representative of multiple technical replicates of at least 2 independent experiments for each condition.

Immunofluorescence: Cells were cultured as indicated on collagen II-coated gel or glass substrates in 8 well Lab-Tek chamber slides (Nunc, 177402), with and without TGF β for 45 mins prior to harvest. Cells were washed in PBS twice, followed by fixation in 4% paraformaldehyde in PBS for 15 min at room temperature. After three PBS washes, cells were permeabilized in PBS with 0.5% Triton X-100 for 5 mins and washed again (3xPBS). Cells were blocked for 1 hour (PBS, 10% goat serum, and 0.5% Triton X-100) prior to overnight incubation with Smad2/3 antibody (Santa Cruz, sc8332) diluted 1:400 in PBS, 2% goat serum, and 3% Triton X-100 at 4°C in a humidifying chamber. After three PBS washes, cells were incubated with the secondary goat anti-rabbit Alexa Fluor 488 (Invitrogen, A11034) diluted 1:400 in PBS with 2% goat serum and 1.5% Triton X-100 for 1 hour at room temperature, followed by another three washes with PBS. Rhodamine phalloidin (Invitrogen, R415) was diluted to 1:800 in PBS and incubated with fixed cells for 20 min at room temperature. Finally, cells were washed with PBS three times and the well walls removed. For cells cultured on glass, the gasket was removed before adding Slowfade Gold mounting medium with DAPI (Invitrogen, S36939) and covering it with a coverslip. For cells cultured on gels, the gasket was left attached and mounting medium was added to each gel before applying the coverslip. Cells were visualized using an Olympus IX Widefield Microscope. Images were processed in Image J. The averages and standard deviations shown in the figure represent the percentage of cells with nuclear localized Smad2/3 in several images taken across 3 biological replicates for each substrate. ANOVA analysis followed by the Student Newman Keuls test was used to evaluate statistical significance.

CHAPTER 3

Development of Cell Culture Substrates that Mimic the Stiffness Articular Cartilage

Introduction

Physical cues are powerful drivers of cell behavior. Fluid flow, cyclic stretch, cell shape, topography, and ECM stiffness can direct cellular behavior in a manner that mirrors biochemical regulation (Assoian and Klein, 2008; Chen *et al.*, 2001; Engler *et al.*, 2006; Geiger *et al.*, 2009; Wang and Thampatty, 2006). Specifically, the physical cue of stiffness has been shown to regulate migration, through durotaxis, cell proliferation, differentiation, and disease state (Assoian and Klein, 2008; Engler *et al.*, 2006; Paszek *et al.*, 2005; Wells, 2008). Notably, the ECM stiffness of several tissues activates the differentiation of its native cell type (Engler *et al.*, 2006; Flanagan *et al.*, 2002; Georges and Janmey, 2005). For example, myocyte differentiation is induced by culture on a ~10 kPa substrate, which mimics the stiffness of muscle tissue (Georges and Janmey, 2005). Cartilage ECM stiffness is highly specified, affording it resilience under a variety of loads in the articulating joints. As with other tissues, cartilage ECM stiffness likely acts as a physical regulator to influence chondrocyte differentiation.

In studying a cellular mechanosensing mechanism, it is of the utmost importance to understand the mechanics of the tissue to be modeled. Refined understanding of the physical cue and the mechanics of the tissue to be studied is important to correctly interpret the results of cellular mechanosensing studies. Cartilage is a relatively simple tissue, its matrix composed of only a few major components lacking blood vessels or other complex architecture, and housing a single cell type (Hu and Athanasiou, 2003).

However, the mechanics of cartilage ECM are complex. It is viscoelastic and highly strain rate dependent; therefore its dynamic elastic modulus is 10-20 fold higher than its static equilibrium modulus (Kiviranta *et al.*, 2008; Knecht *et al.*, 2006; Setton *et al.*, 1999). As we wish to study the mechanisms involved in passive regulation of chondrogenic differentiation by the ECM in the absence of loading, the stiffness under static loading is the more appropriate parameter to model. Moreover, the stiffness is also affected by the length scale of the testing regimen. The stiffness measured at the micrometer scale is 10-fold greater than at the nanometer scale (Stolz *et al.*, 2009). The length scale at which a cell sense stiffness, while still under debate, is believed to be 10-100 μm (Buxboim *et al.*, 2010; Lin *et al.*, 2010). Therefore, we believe measurements of the mechanical properties of cartilage ECM at the microscale may represent the best representation of the forces felt by chondrocytes *in vivo* under static conditions. When the work described in this dissertation began, there were no studies of how substrate stiffness affected chondrocyte differentiation. The substrates normally used to study mechanosensing mechanisms were far too compliant to model the stiffness of articular cartilage. Therefore, a substrate was needed that spanned the stiffness range of cartilage (~0.5 MPa)(Kiviranta *et al.*, 2008).

In this chapter, I will describe the development of polyacrylamide (PA) substrates with stiffnesses in the MPa range in order to model the mechanical behavior of cartilage ECM and study the mechanisms through which stiffness primes the TGF β pathway to regulate chondrocyte differentiation.

Results

Piperazine diacrylamide PA gel properties

PA gels are an established substrate used in cellular mechanosensing studies. Normally, PA gels are crosslinked with bisacrylamide, but this gel composition can only reach a stiffness of 10 kPa (Griffith and Swartz, 2006), well below the MPa range required for modeling cartilage ECM (Kiviranta *et al.*, 2008). In order to model the stiffness of articular cartilage, gels that can obtain stiffnesses into the MPa range are required.

Piperazine diacrylamide (PDA) is a crosslinker normally used in SDS-PAGE gels to reduce pore size and increase the gel's mechanical strength without significantly affecting polymerization protocols (Wiersma *et al.*, 1994). Gels polymerized with PDA have been used to make gels with stiffnesses of up to 20 MPa (Wiersma *et al.*, 1994). PDA was therefore incorporated into the PA gels used in this study to achieve stiffnesses in the MPa range.

The common protocol for preparing PA gels for cellular mechanosensing studies calls for the gels to be polymerized as a very thin layer attached to a coverslip activated by aminopropyl trimethoxysilane (Damljanovic *et al.*, 2005). However, gels polymerized with PDA swell considerably after polymerization and will completely detach from their coverslip backing within a few hours. Coverslips aid in the manipulation of very compliant gels, but the gels produced with PDA are of such a robust stiffness that there is no need for a rigid support. Therefore, PDA gels were polymerized as a slab in 1mm thick vertical glass mold and cut to fit 6 well plates with a 3 cm biscuit cutter. PDA gels prepared in this manner were robust and easily manipulated with tweezers without a coverslip backing.

Identifying the stiffness of PDA polyacrylamide gels

The stiffnesses of PDA gels of various compositions were tested using several mechanical testing regimens. As expected the elastic moduli of the PDA gels increased with increasing crosslinker concentration (Figure 3.1). Similar results were obtained for both static (nanoindentation, AFM, unconfined compression) and dynamic (microindentation) loading on PDA gels suggesting that the gels were extremely elastic and strain rate had very little effect on its mechanical properties. This is in stark contrast with cartilage, which varies with the strain rate (Kiviranta *et al.*, 2008; Knecht *et al.*,

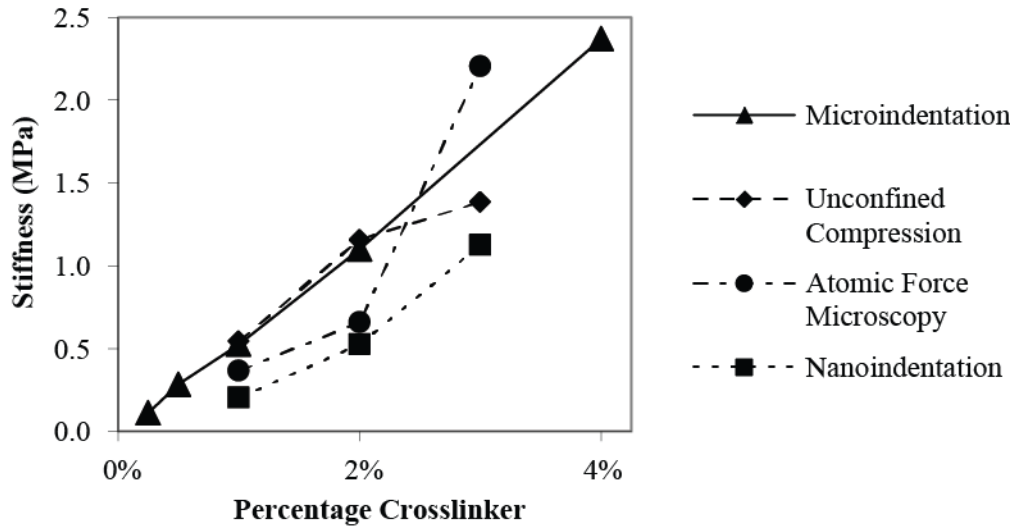


Figure 3.1: PA gel stiffness determined by several mechanical testing methods. PA gel stiffness was measured using microindentation, unconfined compression, atomic force microscopy, and nanoindentation. Increasing the crosslinker concentration increased PA gel stiffness.

2006). As all cellular differentiation studies will be done under static conditions the PA gel stiffness measured by a static testing regimen will be matched to the same property in articular cartilage.

Several testing regimens at different length scales were used to identify the stiffness of PDA gels. The stiffness measured by nanoindentation was selected as the most relevant because it is measured at the microscale, similar to the length scale at

which cells mechanosense their microenvironment (Buxboim *et al.*, 2010; Lin *et al.*, 2010). PDA gels with stiffnesses that fell within the range reported for articular cartilage as measured by nanoindentation were selected for cellular mechanosensing studies. It is important to note that PDA gel stiffness is affected by temperature and osmolarity of the surrounding solution (Damljanovic *et al.*, 2005).

Preparing PA gels for ligand attachment

PA gels, originally used to separate protein samples for western blots, are resistant to protein attachment. To facilitate cellular attachment, ligands must be covalently bonded to the surface of a PA gel. There are currently several methods to chemically bond ligands to the surface of PA gels. For a list of the most common methods see (Kadow *et al.*, 2007). Only a few were investigated in this dissertation. First, gels were polymerized with 2-acrylamido-2-methylpropane sulfonic acid (AMPSA), which is negatively charged. Incorporation of AMPSA should electrostatically attract proteins to the gel surface without requiring a conjugation reaction (de Rooij *et al.*, 2005; Kadow *et al.*, 2007). However, in our hands, cell attachment using this approach was poor (Figure 3.2).

A second method of protein conjugation investigated for this dissertation was the hydrazine method (Damljanovic *et al.*, 2005; Kadow *et al.*, 2007). Hydrazine converts acrylamide within the gel into hydrazide groups that react with aldehydes and ketones on oxidized collagen, forming a chemical bond. This method is relatively simple, requiring submersion of a prepolymerized gel slab in hydrazine for 4 hours. While the acrylamide groups on the surface of the gel were expected to convert to hydrazide groups, gels that

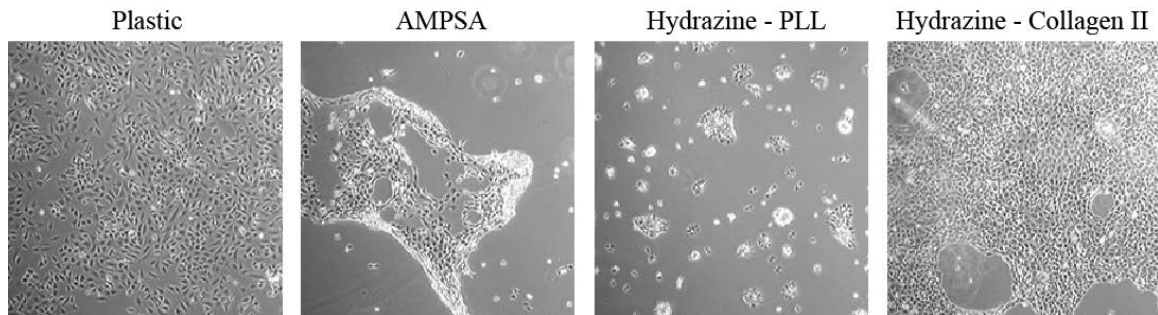


Figure 3.2: PA gel protein conjugation method comparison. Protein conjugation methods were compared to plastic controls. PA gels polymerized with AMPSA and PA gels treated with hydrazine and poly-L lysine had poor cell attachment compared to gels treated with hydrazine and collagen II.

were broken or cut after the hydrazine treatment revealed that the conversion occurred through the entire thickness of the gel. Although this method was robust and simple, it proved to be unreliable. Successful protein conjugation required several chemical reactions: conversion of acrylamide into hydrazide groups with hydrazine, oxidation of the ligand to form aldehydes and ketones, and reaction of the hydrazide groups with the oxidized ligand to form a covalent bond. If protein conjugation was unsuccessful, and cellular attachment was poor, there was no indication as to which of these reactions had failed, making the protocol difficult to troubleshoot. Moreover, hydrazine is highly flammable and toxic, requiring thorough rinsing to remove any trace of hydrazine before cell seeding.

The protein conjugation protocol we ultimately selected to facilitate cellular attachment is based on a method using N-succinimidyl ester of acrylaminohexanoic acid (N6) described in Reinhart-King *et al.* and adapted by the Weaver lab (Kadow *et al.*, 2007; Reinhart-King *et al.*, 2005). The selected protocol substituted acrylic acid n-hydroxysuccinimide ester (N2) for N6, as N2 is similar to N6 and commercially available. N2 polymerizes to the surface of the gel when combined with bisacrylamide and Irgacure and exposed to UV light. To improve reaction efficiency the concentrations

of N2 and Irgacure were increased to improve ligand binding and increase the speed of the reaction. The n-hydroxysuccinimide ester (NHS) group of N2 reacts with amine groups on proteins forming a covalent bond between the ligand and the gel under basic conditions. Therefore, this method requires no pretreatment of the ligand to prepare it for the conjugation reaction. With fewer reactions, this protocol is easier to troubleshoot and far more reliable. Moreover, as only a small amount of N2 solution is used on the surface of the gel, less rinsing is required to clean the gel before cell seeding.

Ligand Selection

As the N2 method allows almost any protein to be covalently bonded to the surface of the PDA gel, the attachment ligand had to be carefully selected to provide good attachment and optimize chondroinduction on the substrate. The most common protein used in mechanosensing studies is collagen I. However, collagen I has been shown to promote dedifferentiation in chondrocytes (Nehrer *et al.*, 1997; Veilleux *et al.*, 2004). Therefore, even though collagen I may be a common choice among mechanosensing studies, it was excluded for this study. Poly-L-lysine (PLL) is also a common cell attachment ligand; however, PA gels conjugated with (PLL) resulted in poor attachment (Figure 3.2). Because of its chondroinductive properties, collagen II was selected as the gel ligand. Collagen II is similar to collagen I, making it an easy substitute for many ligation reactions that call for collagen I. Exceptional cell attachment was achieved on gels conjugated with collagen II, comparable to that on tissue culture plastic (Figure 3.2).

Although cells will not attach to PA gels without a ligand present, we have found cells will adhere, although weakly, to gels that have been coated with collagen in the

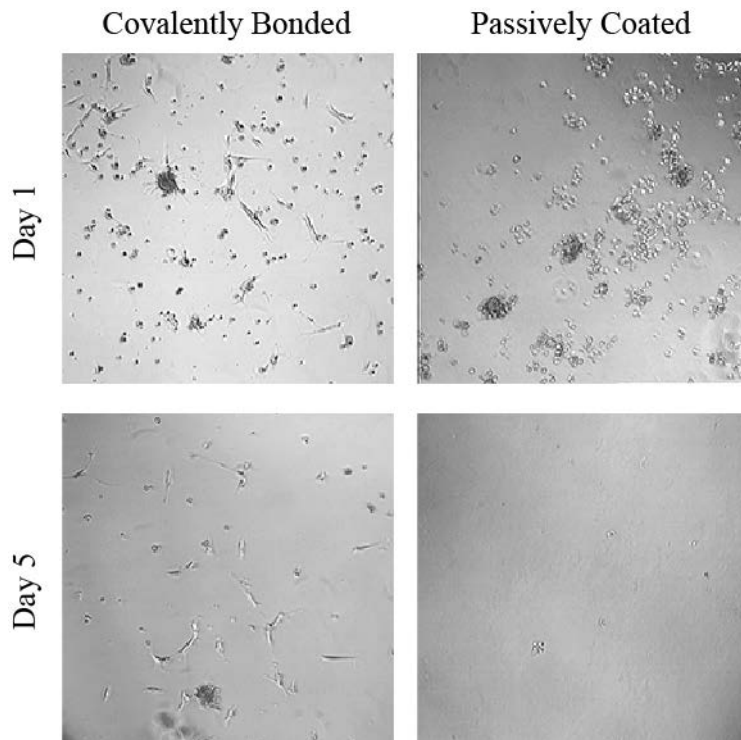


Figure 3.3: Passive protein coating allows weak and transient cell attachment to PA gels. Hydrazine-treated PA gels were coated with either oxidized collagen II (which allows formation of a covalent bond) or untreated collagen II (passively coated). ATDC5 cells adhered to both gels on day 1, but cells attached to the passively coated gel gradually detached by day 5.

absence of protein conjugation or AMPSA incorporation. In an experiment to troubleshoot protein conjugation methods, collagen II was added to a PA gel that had not been treated with hydrazine. The expected result was no cell attachment, however, cells did adhere at first and gradually detached over time (Figure 3.3). A similar result was seen on PA gels treated with FBS in the

absence of ligand coating or protein conjugation (data not shown). Therefore, it seems that ECM proteins in the FBS will weakly adhere to the PA gel and allow transient cell attachment. This also suggests that even with proper protein conjugation, treating gels with FBS prior to cell seeding may weaken cell attachment because of the availability of non-covalently linked proteins. Moreover, an overabundance of collagen II, that overwhelms the available N2 groups leaving excess weakly-adhered collagen, would have a similar negative effect on cellular attachment. Therefore, care should be taken in adjusting collagen II concentration for cell mechanosensing studies. It is important to note that along with inaccurate measurement, dissolving lyophilized proteins, especially

collagen, in solutions at room temperature can lead to loss of protein to the container and therefore inaccurate concentrations. To ensure accuracy of prepared solutions, add lyophilized collagen to solvents kept at 4°C.

Molecular biology methods applied to PDA gels

As a result of several noted complications in working with PDA gels, a few adjustments were made to adapt molecular biology methods to this cell culture system. PDA gels will absorb and retain cell culture media during culture. Even after thorough rinsing, PDA gels retain excess media, which leaches out during RNA or protein harvest. Media contamination is known to adversely affect RNA isolation, therefore, while RNA was successfully isolated from PDA gels using both QIAGEN RNeasy and Trizol Purelink protocols, care should be taken to rapidly harvest cells from gel substrates to minimize media contamination. For protein isolation, media contamination is not as detrimental, but lysate volume does increase on gel substrates from media leaching if cells are not isolated rapidly.

Alcian blue stains are also adversely affected by media retention in PDA gels, specifically because the phenyl red creates a background on gels substrates that makes comparisons with plastic controls difficult. Using a phenyl red-free media avoids this background issue, but a cell-free gel substrate should still be used as negative controls to identify the level of background staining. Moreover, Alcian blue is a pH sensitive dye that requires a pH of 2.5 to effectively stain proteoglycans. During the fixation in preparation for Alcian blue staining, gels will absorb and retain formaldehyde, which, with its high pH, will shield proteoglycans on the gel surface from being stained

effectively. Soaking gel substrates in glacial acetic acid (pH 2.5) for 30 mins after fixation but before Alcian blue staining will reduce the pH and eliminate the shielding effect, allowing accurate staining.

Spinfection, the process of using centrifugation to speed viral infection, has failed on gel substrates several times, possibly because the viral particles are absorbed into the gel without successful infection. It is advised that cells should be pre-infected on tissue culture plastic before seeding on gel substrates to achieve more efficient infection.

Due to the thickness of the PA gels, mounting for immunofluorescence imaging is cumbersome. Using a chamberslide with a 1mm thick gasket allows the gels to be mounted between a coverslip and glass slide, creating a compartment that securely mounts the gels and shields against drying. It is also important to note that the gels fluoresce when exposed to certain excitation wavelengths (particularly 540-560 nm). Therefore, an IgG control must be set up for each condition to allow comparison between gel substrates and plastic controls.

Discussion

In summary, we have developed a cell culture substrate that closely mimics the stiffness of articular cartilage by substituting piperazine diacrylamide for the normal crosslinker, bisacrylamide. Several ligation methods were explored and the N2 method was determined to be the most reliable. Collagen II was selected as the most appropriate ligand for cell mechanosensing studies in chondrocytes.

The PA gels developed in this chapter are versatile and mechanically robust, allowing mechanistic studies in the range reported for articular cartilage. However, there are several limitations to this culture system. First off, as PA gels resist protein coating, culture on these substrates hinges on successful protein conjugation methods which, as described previously can be very cumbersome. Moreover, PA gels require that cells be cultured in monolayer. The toxicity of unpolymerized acrylamide and the heat generated during polymerization makes embedding cells in PA gels impossible. 2D culture, while ideal for many molecular biology assays, is not necessarily representative of the 3D environment present in vivo (Baker and Chen, 2012; Janmey and Miller, 2011).

The following chapters will use these newly developed PA gels to study the mechanical properties and cellular mechanosensing mechanisms of articular cartilage. In Chapter 4, layered PA gels are used to model the stratified moduli of articular cartilage. In Chapters 5 and 6, ATDC5s, primary murine chondrocytes, and hMSCs are cultured on homogeneous PA gels to identify the mechanisms through which substrate stiffness and TGF β interact to direct chondrocyte differentiation and chondrogenesis.

CHAPTER 4

Depth-Dependent Modulus of Articular Cartilage Approaches Homogeneity with Osteoarthritis

Introduction

The unique structure and composition of articular cartilage affords it resilience under the multifaceted loads in the articulating joints. Negatively charged proteoglycans, enmeshed in a collagen network maintain positive fluid pressure by attracting solutes, affording cartilage resilience even after prolonged loading (Kwan *et al.*, 1984). This highly specified extracellular matrix is also inhomogeneous, consisting of layered variations in its composition and microstructure through its depth from the surface of articular cartilage to the bone cartilage interface (Matukas *et al.*, 1967). The mechanical behavior of cartilage is determined by its matrix composition and organization, and therefore these stratified microstructural zones provide the tissue with varying elastic moduli which increase through the depth of the tissue (Broom, 1984; Kempson *et al.*, 1970; Wilson *et al.*, 2007). Each zone affords cartilage resistance to a particular kind of loading, from shear stress by the collagen-rich superficial zone to sustained loads by the proteoglycan-rich deep zone (Kempson *et al.*, 1970; Klein *et al.*, 2003; Roth and Mow, 1980; Woo *et al.*, 1980). Therefore, stratification, in matrix composition and in elastic modulus, allows articular cartilage to function under variety of loads.

Osteoarthritis (OA), a disease that currently afflicts 50 million Americans, is characterized by pronounced structural change in articulating joints, including an

increased subchondral plate thickness and marked degradation of articular cartilage (Blaney Davidson *et al.*, 2007; Goldring and Goldring, 2007; Kleemann *et al.*, 2005; Wang *et al.*, 2011a). In studies of either osteoarthritic or enzymatically digested cartilage, the material properties, both elastic and viscoelastic, strongly correlate with the progression of the matrix degradation (Knecht *et al.*, 2006). Particularly, the change in the elastic modulus of cartilage has been reported to coincide with a loss of proteoglycan content within the extracellular matrix (ECM) (Kiviranta *et al.*, 2008; Kleemann *et al.*, 2005).

The degradation of cartilage matrix material properties with OA is usually determined by macroscopic testing or high resolution AFM-based indentation, both of which fall short of identifying changes in the stratified structure of cartilage ECM (Darling *et al.*, 2010; Imer *et al.*, 2009; Kleemann *et al.*, 2005; Knecht *et al.*, 2006; Li *et al.*, 2006; Stolz *et al.*, 2009). A few pioneering studies have successfully assessed the stratified modulus of healthy articular cartilage, primarily by optically tracking individual chondrocytes as the tissue is compressed (Chen *et al.*, 2001; Chen *et al.*, 2001; Guilak *et al.*, 1995; Schinagl *et al.*, 1997; Wang *et al.*, 2002; Wang *et al.*, 2001). Although these previous studies have shown that cartilage deformation and strain vary with depth, to our knowledge there is no testing method that allows the direct identification of the modulus of each layer of articular cartilage *in situ*. Moreover, the effects of OA on the depth-dependent moduli of articular cartilage remain to be described.

In order to further understand the stratified depth-dependent behavior of cartilage, we propose a new constitutive relationship, calibrated using a stratified gel system with known depth-dependent mechanical properties, to determine the modulus changes *in situ*

in multilayered materials. This approach will allow us to test our hypothesis that osteoarthritis diminishes the stratified material properties of cartilage ECM.

Results

Identifying the elastic modulus of intact stratified gels.

In order to model the elastic modulus of articular cartilage, polyacrylamide gels were developed that spanned a range of moduli from 0.2 to 1 MPa (Table 4.1). Homogeneous PA gels with this range of compositions have been used previously as standards for cartilage material properties (Hansma *et al.*, 2009; Li *et al.*, 2011). In order to determine if the elastic modulus of an underlying layer could be accurately measured by microindentation, four stratified gels were prepared; their composition is

Crosslinker Conc. (w/v)	Elastic Modulus (MPa)
0.5%	0.21 (+/- 0.004)
1%	0.42 (+/- 0.01)
2%	0.89 (+/- 0.01)
4%	2.00 (+/- 0.03)

Table 4.1: Elastic moduli of homogeneous polyacrylamide gels. The elastic moduli of homogeneous polyacrylamide gels were determined by the TDI to be used as standards in stratified gel measurements.

described in Table 4.2. The superficial layer was always prepared with a crosslinker

	Crosslinker Conc. (w/v)	
	Top Layer	Bottom Layer
Gel A	0.5%	0.5%
Gel B	0.5%	1%
Gel C	0.5%	2%
Gel D	0.5%	4%

Table 4.2: Composition of stratified polyacrylamide gels. Stratified polyacrylamide gels were assembled from gels with identical compositions to the homogenous gel standards.

concentration at or below that of the underlying layer, producing a compliant superficial layer over a stiffer underlying layer (Figure 4.1A). A typical force displacement curve of a stratified gel is represented in Figure 4.1B, whereas a representative force displacement curve of a

homogeneous gel is shown in the inset. The stratified gels appear to behave like two springs in series, with the apparent modulus (proportional to the slope of the loading curve) shifting from that of the compliant superficial gel to that of the stiffer underlying

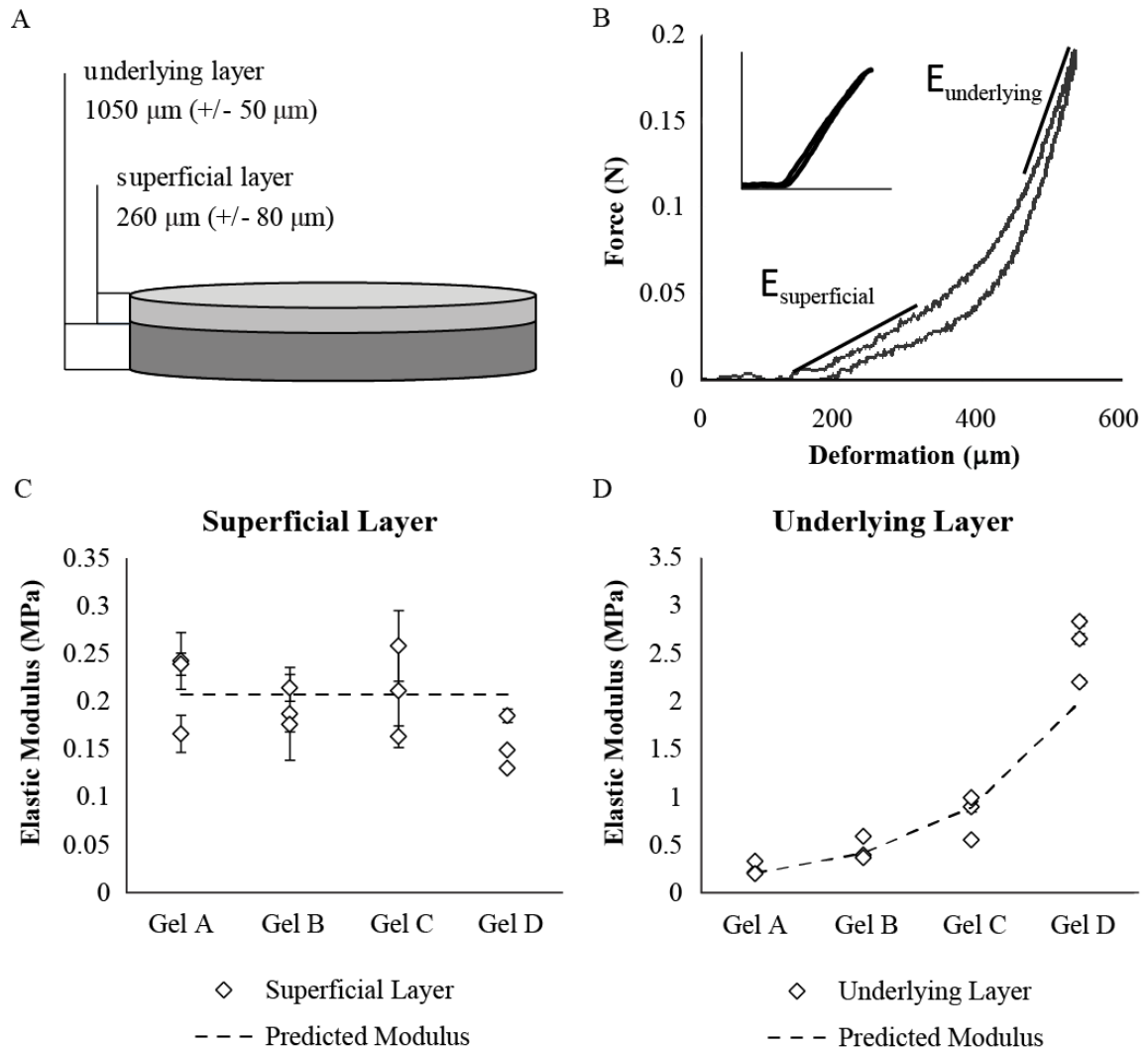


Figure 4.1: Superficial and underlying moduli of stratified gels. Stratified gels were assembled from two homogenous polyacrylamide gels, polymerized in series, with a thin superficial layer ($\sim 260 \mu\text{m}$) and a thick underlying layer ($\sim 1050 \mu\text{m}$) (A). In a representative force deformation curve of a stratified gel, two distinct slopes can be identified that correlate with the expected modulus of the superficial ($E_{\text{superficial}}$) and underlying ($E_{\text{underlying}}$) gel (B). This pattern of loading is distinct from that of a homogeneous gel (inset graph). Analyzing the four gels described in Table 4.2, the superficial (C) and underlying (D) moduli were statistically indistinguishable from the modulus of a similarly composed homogenous gel (predicted modulus). The stiffness of the underlying gel increased with increasing crosslinker concentration as expected ($p < 0.001$, Spearman rank correlation test). Each data point represents the average of five measurements taken at one site. Error bars demonstrate the standard deviation among those five measurements.

gel with increasing displacement. Therefore, within the loading curve, the slopes at initial contact and at peak force should correspond to the elastic moduli of the superficial and underlying gels, respectively.

Analysis of the loading curves of stratified gels revealed that the moduli calculated from the two distinct slopes corresponded to the expected moduli for each gel layer. In Figure 4.1C, the moduli of stratified gel superficial layers (0.2 MPa) closely matched the modulus of a corresponding homogenous gel (0.21 MPa) (Table 4.1), independent of the modulus of the underlying gel. We next tested if the modulus of the underlying layer could be accurately measured by microindentation. The measured moduli of the underlying gels increased, as expected with increasing crosslinker concentration. Moduli acquired for the underlying gel were statistically indistinguishable from the moduli of similarly composed homogeneous gels (Figure 4.1D, Table 4.1 & 4.2). Gel 1, assembled as a negative control from a superficial and underlying gel with identical crosslinker concentrations (0.5% w/v), behaved as a homogeneous gel with statistically indistinguishable superficial and underlying moduli (0.2 and 0.21 MPa, respectively). The ability to accurately derive the superficial and underlying moduli of a stratified material from its loading curve suggests the loading behavior can be described mathematically.

Developing a model for the loading of stratified moduli.

As the indenter is a flat-ended cylindrical punch, the relationship between load and displacement ($F - x$) for a homogenous material is given by

$$F = \frac{2Eax}{1 - \rho^2}, \quad (\text{Equation 1})$$

where E is the elastic modulus, a is the radius of the indenter, and ρ is Poisson's ratio, assumed to be 0.5 for this study (Sneddon, 1965). If stratified gels behave as two springs in series, the modulus in Eq. (1) can be replaced with an apparent modulus, as with two springs in series, given by

$$E_{app} = \left(\frac{1}{E_1} + \frac{1}{E_2} \right)^{-1}, \quad (\text{Equation 2})$$

where E_1 and E_2 are the individual moduli of the superficial and underlying gels, respectively (Oyen *et al.*, 2004). As seen from the example loading curves, however, the apparent modulus is not a constant, but changes with displacement. By applying a depth fraction X_i (Herakovich, 1997; Oyen *et al.*, 2004) to weight the moduli with displacement from initial loading through the depth of the superficial gel (t), we can define the function E_{app} as

$$E_{app}(x) = \left(\frac{X_1}{E_1} + \frac{X_2}{E_2} \right)^{-1} = \left[\frac{1}{E_1} \frac{t-x}{t} + \frac{1}{E_2} \frac{x}{t} \right]^{-1}. \quad (\text{Equation 3})$$

With Eq. (3), at a depth of initial contact ($x = 0$), E_{app} is defined only by E_1 , the modulus of the superficial gel. When displacement reaches the thickness of the superficial gel ($x = t$) E_{app} is defined only by E_2 , the modulus of the underlying gel. At displacements greater than the thickness of the superficial gel, the function is no longer valid, and E_{app} is defined solely by the modulus of the underlying gel (E_2). This equation therefore agrees with our earlier observations that the slope of the loading curve defines the superficial and underlying moduli at initial contact ($x = 0$) and at peak force ($x \geq t$), respectively. Eq. (3) simplifies to Eq. (4) given by

$$E_{app}(x) = \frac{E_1 E_2 t}{E_2 t + (E_1 - E_2)x} \quad \text{for } x \leq t,$$

$$E_{app}(x) = E_2 \quad \text{for } x > t.$$

(Equation 4)

It should be noted that if $E_1 = E_2$, for $x \leq t$, Eq. (4) will reduce to a single modulus as expected for a homogenous material. Eq. (4) should describe the slope of Eq. (1) such that

$$F(x) = \alpha \int E_{app}(x), \text{ where}$$

$$\alpha = \frac{2a}{1 - \rho^2}.$$

(Equation 5)

Therefore the loading curve of a stratified material can be described by the function

$$F_1(x) = \frac{\alpha E_1 E_2 t}{E_1 - E_2} (\ln(E_2 t + (E_1 - E_2)x) - \ln(E_2 t)),$$

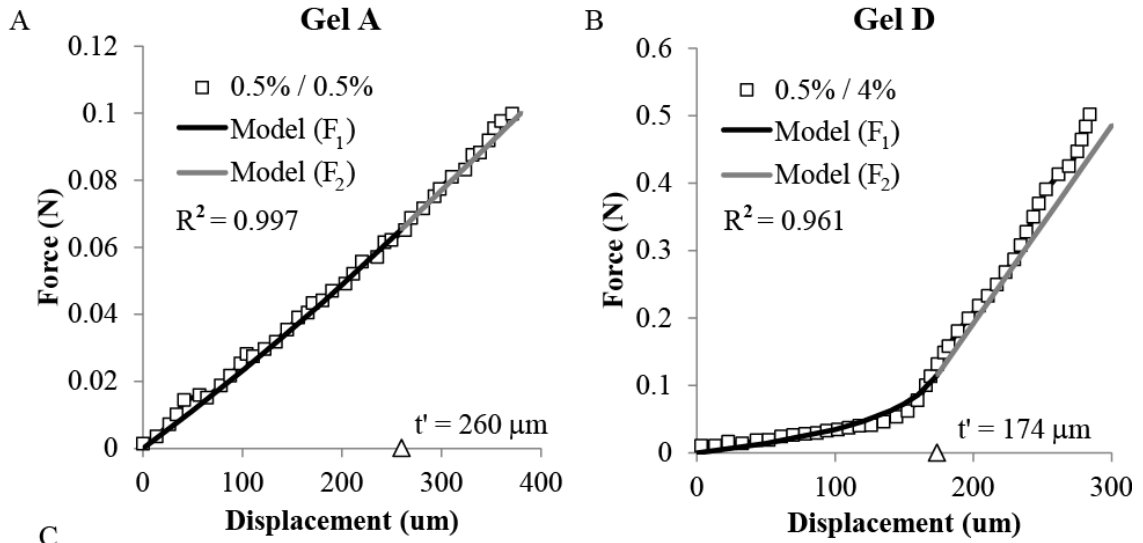
$$F_2(x) = \alpha E_2 x \quad \text{for } x > t.$$

(Equation 6)

$F_1(x)$ of Eq. (6) remains valid from initial contact through the thickness of the superficial layer. As E_2 approaches E_1 , $F_1(x)$ approaches a linear function representing an almost homogenous material. However, when $E_1 = E_2$, because of the denominator in the first term of the equation, $F_1(x)$ of Eq. (6) is no longer valid.

Comparing the model to experimental data for stratified gels.

If the stratified gels behave as two springs in series weighted by depth, Eq. (6) should describe the loading curves of each of the experimental gels. A representative loading curve from each of the four stratified gels was compared to the model generated by Eq. (6) (Figure 4.2). The parameters E_1 and E_2 were set to the moduli determined in



Name	Composition		E_1 (MPa)	E_2 (MPa)	t' (μm)	t (μm)	R^2
	Superficial Gel	Underlying Gel					
Gel A	0.5%	0.5%	0.166	0.216	260	340	0.997
Gel B	0.5%	1%	0.214	0.591	349	240	0.998
Gel C	0.5%	2%	0.163	0.995	316	320	0.991
Gel D	0.5%	4%	0.185	2.200	174	180	0.961

Figure 4.2: Model describes loading curves of experimental gel data. Model-generated loading curves, derived using Eq. (6) and the elastic moduli of each layer determined in Figure 4.1, are graphed with representative loading curves for Gel A (A) and Gel D (B) for comparison. All model-generated loading curves significantly predicted loading behavior of stratified gels (C) ($R^2 > 0.961$). The model generated an apparent thickness of the superficial gel, t' , which agreed well with the experimentally measured thickness of the superficial gel, t .

Figure 4.1 from the slope of the loading curves. Two example loading curves graphed with model generated data are shown in Figure 4.2A and B. The apparent thickness of the superficial gel, t' , was generated within the model to produce a line of best-fit with the experimental data (Figure 4.2C). The apparent thickness for each gel approximated the actual superficial gel thicknesses measured experimentally with a caliper. Under

regression analysis, all experimental data closely matched that of the model, with all R^2 values at or above 0.961 (Figure 4.2C).

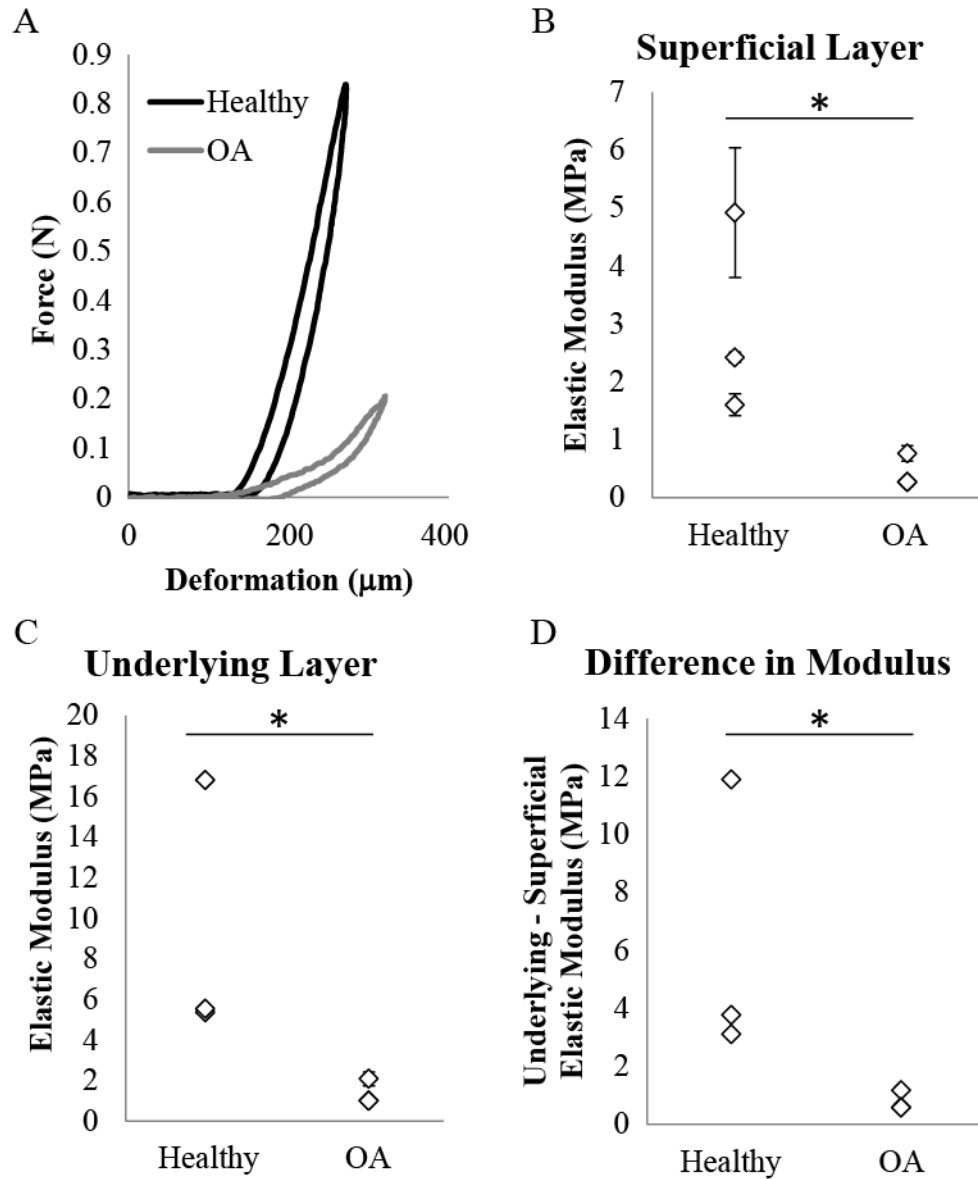


Figure 4.3: The stratified moduli of articular cartilage approach homogeneity with OA. Force displacement curves of human articular cartilage are bimodal, resembling that of a stratified gel (A). Both the superficial and underlying moduli of articular cartilage are significantly decreased with osteoarthritis (B, C). The difference in moduli between the superficial and underlying layers of cartilage decreases on average from 6 to 0.8 MPa with osteoarthritis indicating that the diseased tissue approaches homogeneity (D) (* $p < 0.05$). Each point represents the average of five measurements taken at one site.

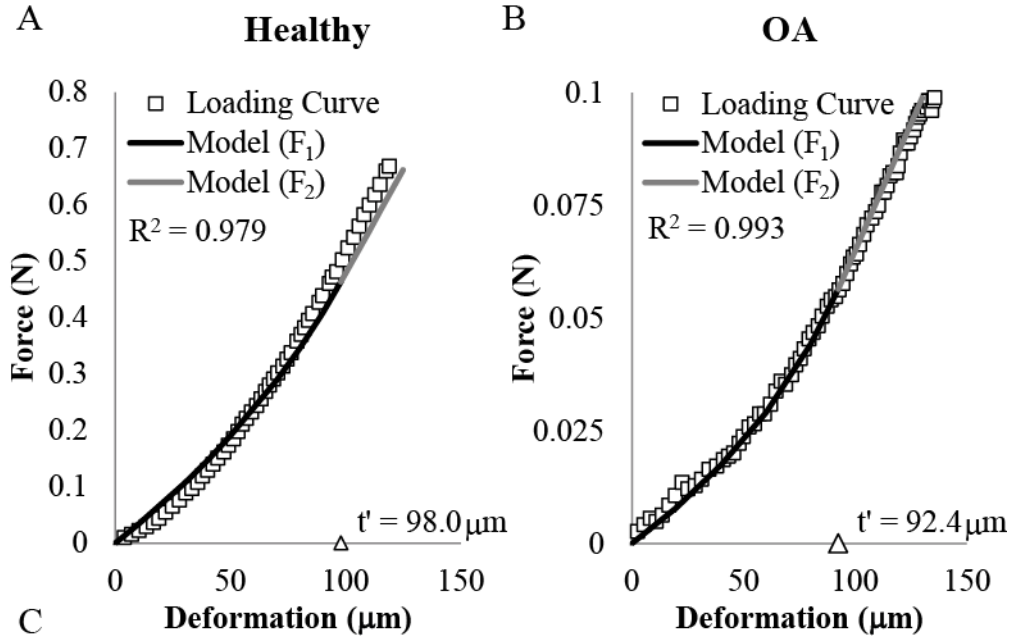
Stratified moduli of articular cartilage approach homogeneity with OA.

To determine the effect of osteoarthritis on the stratified material properties of intact articular cartilage, the methods developed to assess stratified gels were applied to human tissue. In applying this model, we focus on the stratified elastic moduli of cartilage while assuming all other depth-dependent material properties are constant. Several measurements were taken on the articular cartilage from the tibial plateau and femoral condyles of young healthy or older osteoarthritic donors. Representative force displacement curves of young and osteoarthritic cartilage can be seen in Figure 4.3A. Osteoarthritis dramatically reduces the moduli of articular cartilage at each layer. The average moduli of the superficial and underlying layers decrease from 3 to 0.4 MPa, and 9 to 1.2 MPa, respectively (Figure 4.3B, 4.3C). Interestingly, these changes in superficial and underlying modulus result in a more homogeneous architecture in the osteoarthritic tissue. With the disease, the difference between superficial and underlying moduli of cartilage decreases an order of magnitude from a 6 MPa average difference between the stratified moduli in healthy cartilage to a 0.8 MPa average difference in OA cartilage (Figure 4.3D).

The model generated from stratified gels predicts the loading behavior of articular cartilage.

Using the experimentally derived moduli for the superficial and underlying layers, the model generated from stratified gels was applied to articular cartilage. Curve-fitting software was used to fit the model to a single loading curve for each articular cartilage sample. Example experimental loading curves with model generated data for both healthy and osteoarthritic cartilage are graphed in Figure 4.4A and 4.4B. As all

measurements were nondestructive, the thickness of the superficial layer could not be determined experimentally. Therefore the curve-fitting software generated an apparent thickness, t' , that generated the best fit with the experimental data given the superficial and underlying moduli. All model generated curves fit the experimental data with an R^2 greater than 0.977 (Figure 4.4C).



Sample	Site	E_1 (MPa)	E_2 (MPa)	t' (μm)	R^2
Healthy	1	4.92	16.8	35.9	0.986
	2	1.60	5.35	43.2	0.980
	3	2.42	5.51	98.0	0.979
OA	1	0.772	1.92	25.9	0.977
	2	0.275	0.846	92.4	0.993
	3	0.276	0.832	154.8	0.994

Figure 4.4: Applying the stratified gel model to articular cartilage. Using Eq. (6) and the experimentally derived superficial and underlying modulus, curve-fitting software was able to generate a curve that closely approximated the loading curve for healthy (A) and osteoarthritic (B) cartilage. All model-generated loading curves significantly predicted loading behavior of cartilage samples (C) ($R^2 > 0.977$). The loading sites presented in A and B are bolded in the chart.

Discussion

We have developed a novel analytical model that allows quantification of stratified material properties in an intact sample. Using reference point microindentation, we were able to detect the distinct modulus of each layer of an intact stratified polyacrylamide gel. Modeling the stratified gel as two springs in series weighted by depth, we accurately predicted the experimental loading behavior of stratified gels. Applying this model to intact human cartilage samples *in situ*, superficial and underlying moduli were determined. Although others have successfully measured depth-dependent mechanical properties of articular cartilage in osteochondral cores (Chen *et al.*, 2001; Chen *et al.*, 2001; Guilak *et al.*, 1995; Klein *et al.*, 2007; Schinagl *et al.*, 1997; Schinagl *et al.*, 1996; Wang *et al.*, 2002; Wang *et al.*, 2001), to our knowledge, this is the first measurement of the stratified moduli of articular cartilage in an intact sample. Moreover, comparison between young cadaveric cartilage and severely degraded cartilage suggests that osteoarthritis has marked effects on the stratified material properties of articular cartilage. An overall reduction in modulus with disease is observed in both the superficial and underlying layers. This softening also dramatically diminishes the difference between the moduli of the superficial and underlying layers, which results in a homogeneous tissue lacking in the characteristic depth-dependent material properties of healthy cartilage.

While it is well known that the depth-dependent material properties of cartilage are integral to its function (Broom, 1984; Klein *et al.*, 2003; Roth and Mow, 1980; Woo *et al.*, 1980), compared to other mechanical assessments, relatively few studies have explored the depth-dependent material properties of articular cartilage (Chen *et al.*, 2001;

Chen *et al.*, 2001; Guilak *et al.*, 1995; Klein *et al.*, 2007; Schinagl *et al.*, 1997; Wang *et al.*, 2002; Wang *et al.*, 2001). The most common method requires microscopic imaging to track the displacement of fluorescently labeled chondrocytes in osteochondral cores under confined compression (Chen *et al.*, 2001; Klein *et al.*, 2007; Schinagl *et al.*, 1997; Wang *et al.*, 2002). This method, while allowing direct measurement of displacement under load through the entire depth of the sample, has drawbacks in requiring machining of samples and the introduction of non-physiologic boundary conditions at the imaging site. Our method demonstrates that microindentation can successfully assess stratified material properties *in situ*, preserving the architecture of the sample for further studies.

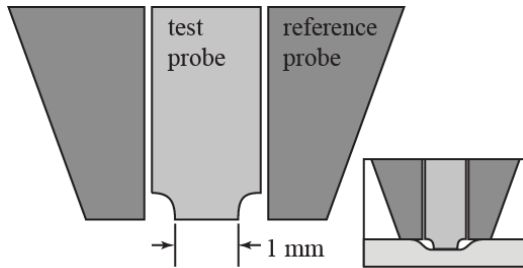
Our two layer model is just an approximation of the gradual change in modulus through the depth of the tissue. In order to apply this simple model, we assume that cartilage is composed of two layers of otherwise homogeneous, isotropic matrix. This ignores the inhomogeneity of the matrix and contributions from viscoelastic properties, fluid flow, time and shear rate dependency among other properties that add to the complexity of cartilage matrix (Huang *et al.*, 2003; Mak *et al.*, 1987; Mow *et al.*, 1989; Wu and Herzog, 2002). Indeed while we focus here on the modulus of cartilage matrix, the permeability, fixed charge density, and bulk modulus have all been shown to vary with depth (Chen *et al.*, 2001; Wang *et al.*, 2001). Nevertheless, our model clearly reveals a novel effect of OA on cartilage ECM: its loss of depth-dependent differences in modulus with disease.

Our results agree with previous studies that the stratified moduli of articular cartilage increases with tissue depth (Chen *et al.*, 2001; Klein *et al.*, 2007; Schinagl *et al.*, 1997; Wang *et al.*, 2001). Many of these studies used bovine articular cartilage and

reported more compliant superficial and underlying moduli than those reported here. Among the studies of depth dependent material properties, only one, to our knowledge, has reported the stratified moduli of human articular cartilage. Chen et al. reported the moduli of the superficial and underlying layers of human femoral head articular cartilage to be 1.16 and 7.75 MPa, respectively (Chen *et al.*, 2001), which closely match the moduli determined in our study (2.98 and 9.22 MPa, respectively). The differences may be attributed to the differences in loading regimen and variation between hip and knee cartilage (Hu and Athanasiou, 2003).

Our observation that osteoarthritis dramatically affects the stratified moduli and architecture of articular cartilage appears novel. These results suggest the need for additional research into this area to fully explore how the progression of osteoarthritis damages not only the macroscopic properties of cartilage, but the discrete properties of each layer. Clinically, the most recognizable marker of early OA is fibrillation of the superficial layer of cartilage. Nevertheless, in a composition-based finite element model, Saarakkala et al. demonstrated that in early OA, along with changes the superficial layer, the composition of the underlying layers of cartilage is also significantly affected (Saarakkala *et al.*, 2010). A significant loss of proteoglycans in the normally proteoglycan-rich underlying layers of articular cartilage accompanies early OA. This loss in proteoglycan content may be the cause of the dramatic loss in underlying layer modulus of osteoarthritic cartilage, ultimately driving the tissue toward homogeneity. In their analysis of the depth-dependent moduli, Wang et al. found that stratified moduli produce more stable strains in the deep zone of articular cartilage (compared with a homogeneous model) (Wang *et al.*, 2001). Therefore, in approaching homogeneity,

osteoarthritic cartilage may be exacerbating damage to the underlying layer. In its ability to assess intact cartilage, the reference point microindentation may represent a new method to non-destructively assess the material properties of articular cartilage for early diagnosis of OA.



Supplemental Figure 4.1: Type V Probe Assembly. The 1 mm diameter test probe is surrounded by a reference probe which rests on the surface of the material to be tested while the test probe indents.

CHAPTER 5

ECM Stiffness Primes the TGF β Pathway to Promote Chondrocyte Differentiation

Introduction

The extracellular microenvironment is rich in physical cues that, like biochemical cues, are powerful regulators of cell behavior. Cells respond to physical cues, such as topography, mechanical stimulation, and extracellular matrix (ECM) stiffness, with changes in cell proliferation, migration, apoptosis and differentiation (Assoian and Klein, 2008; Chen *et al.*, 1997; Engler *et al.*, 2006; Geiger *et al.*, 2009; Wang and Thampatty, 2006). The importance of ECM stiffness in cell fate selection is apparent in mesenchymal stem cells, which select a neural lineage when cultured on a compliant matrix (1 kPa), but differentiate into myotubes on a stiffer matrix (10 kPa) (Engler *et al.*, 2006). Therefore, just as morphogen gradients define boundaries and prime cells for lineage selection and differentiation, ECM stiffness refines cellular behavior to match the physical microenvironment. Though cells encounter biochemical and physical cues simultaneously, the mechanisms by which this information is assimilated to direct cellular responses remain unclear.

Cells maintain homeostasis between ECM stiffness and cytoskeletal tension through a tightly controlled hierarchical mechanotransduction pathway. Upon integrin binding to ECM ligands and the generation of internal cell tension, cells develop focal adhesions, a highly ordered array of proteins including focal adhesion kinase (FAK), talin, vinculin, and α -actinin (Geiger *et al.*, 2009; Kanchanawong *et al.*, 2010; Miranti and Brugge, 2002). These proteins interact with small GTP-ases (i.e. Rho, Rac) and

other signaling pathways, facilitating changes in cytoskeletal organization, actinomyosin contractility, and cell shape with even small changes in matrix compliance (Geiger *et al.*, 2009; Paszek *et al.*, 2005). Accordingly, distortion of normal ECM stiffness has been implicated in many diseases, including cancer and liver fibrosis (Butcher *et al.*, 2009; Li *et al.*, 2007b; Paszek *et al.*, 2005).

Cells integrate their response to physical and biochemical cues to guide cellular decision-making. Physical cues including substrate stiffness, cell shape, or cytoskeletal tension can radically alter the cellular response to growth factors (Gao *et al.*, 2010; Leight *et al.*, 2012; Park *et al.*, 2011; Wang *et al.*, 2011b). For example, insufficient cytoskeletal tension impairs BMP-induced-osteogenesis (Wang *et al.*, 2011b). Wang *et al.* recently showed that BMP signaling is sensitive to the activity of Rho, which is an integral part of mechanotransduction pathways. Among the many effectors shared by biochemical and mechanotransduction pathways, integrins are a prime example of molecules that functionally interact with the ECM and the cytoskeleton as well as with growth factors and their receptors (Miranti and Brugge, 2002; Munger and Sheppard, 2011). ECM stiffness and TGF β signaling can each direct the localization and activity of the transcriptional coregulator TAZ (Dupont *et al.*, 2011; Varelas *et al.*, 2008). Nonetheless, the molecular mechanisms by which cells generate an integrated response to biochemical and physical cues are not well-defined.

As a tissue with a primarily mechanical function, cushioning joint surfaces, cartilage is an ideal model for exploring the interaction between physical and biochemical cues. From development – in which cellular condensations drive mesenchymal precursors to select a chondrogenic lineage, to disease – in which osteoarthritis (OA) causes the

coupled degeneration of cartilage physical and biochemical properties, this tissue is replete with examples of intersecting physical and biochemical cues (Aigner *et al.*, 2002; Henderson and Carter, 2002; Setton *et al.*, 1999; Shieh and Athanasiou, 2003). Physical properties of cartilage matrix are carefully defined spatially and temporally, facilitating the mechanical and biological functions of this tissue. The stiffness of cartilage ECM varies with development (up to 10-fold increase from fetal to adult cartilage (Williamson *et al.*, 2001)), location (5-fold increase through tissue depth and up to 3-fold increase from pericellular to interterritorial matrix (Akizuki *et al.*, 1986; Darling *et al.*, 2010; Setton *et al.*, 1999)), and disease (2-fold decrease in late stage OA (Kleemann *et al.*, 2005)). In addition to a mechanical role at the tissue level, we hypothesize that, at a cellular level, the stiffness of cartilage ECM plays a key role in directing chondrocyte differentiation and homeostasis, possibly by regulating other signaling pathways that control chondrogenesis.

The growth factor TGF β plays a major role in the regulation of chondrogenesis. TGF β induces chondrocyte lineage selection and cartilage matrix synthesis while inhibiting terminal chondrocyte differentiation and hypertrophy (Blaney Davidson *et al.*, 2007; Derynck *et al.*, 2008). The TGF β pathway is regulated at multiple hierarchical levels, several of which intersect with the mechanotransduction pathway. The conversion of the TGF β ligand from a latent to an active form can occur by proteolytic cleavage, integrin-mediated activation, and by cell-generated tension (Annes *et al.*, 2003; Munger *et al.*, 1999; Wipff *et al.*, 2007). Once activated, the ligands signal through a heterotetrameric complex consisting of two type I and two type II serine/threonine kinase receptors, the availability and clustering of which is also tightly controlled (Massague,

1998). Signaling within the cell can be relayed through many different pathways, including Rho/ROCK and MAPK pathways, but the 'canonical' effectors of TGF β signaling are the R-Smads 2 and 3 and the common mediator Smad4 (Wrana, 2000). Even before phosphorylation by TGF β receptors, localization and stability of Smad2 and Smad3 are regulated through interactions with multiple proteins, including microtubules, filamin and, ubiquitin ligases (Dong *et al.*, 2000; Lin *et al.*, 2000; Sasaki *et al.*, 2001; Zhang *et al.*, 2001). The activated T β RI phosphorylates Smad2 and Smad3 on the C terminal domain, causing heteromerization with Smad4 and preferential retention in the nucleus where Smads act as transcription factors. For example in chondrocytes, phosphorylated Smad3 recruits CBP to activate Sox9-mediated transcription of Col2 α 1 (Furumatsu *et al.*, 2005).

TGF β and mechanotransduction share many effectors and regulate many of the same cellular processes. However, the mechanisms by which signaling between these two pathways is integrated are not well-defined in chondrocytes or other cell types. While a recent study highlights this integration in epithelial mesenchymal transition in the context of cancer (Leight *et al.*, 2012), these mechanisms may operate in other diseases where both ECM stiffness and TGF β have already been implicated individually, such as liver fibrosis and cancer (Butcher *et al.*, 2009; Hinz, 2009; Ingber, 2003; Li *et al.*, 2007b; Paszek *et al.*, 2005; Tomasek *et al.*, 2002; Wells and Discher, 2008). In cartilage, understanding the interaction between ECM stiffness and TGF β may elucidate mechanisms that self-promote chondrocyte differentiation in development, or those that spiral out of control in OA. Therefore, using chondrocytes as an experimental model, we

explore the mechanisms by which cells integrate the physical and biochemical cues provided by ECM stiffness and TGF β respectively.

Results

Chondrocyte differentiation is tuned to an optimal ECM stiffness

To determine if chondrocyte differentiation is sensitive to the stiffness of the extracellular microenvironment, primary murine chondrocytes and ATDC5 chondroprogenitor cells were differentiated for 2 and 7 days on collagen II-coated polyacrylamide substrates with stiffnesses that span the range reported for articular cartilage (0.2 MPa to 1.1 MPa) (Table 5.1) (Hansma *et al.*, 2009; Kiviranta *et al.*, 2008).

Substrate stiffness strongly regulated expression of multiple markers of chondrocyte differentiation, including the lineage-specific transcription factor Sox9 and genes encoding the major constituents of cartilage matrix, Col2 α 1 and aggrecan. Specifically, in primary murine chondrocytes cultured on the 0.5 MPa gel substrates with a stiffness most similar to healthy articular cartilage, Sox9, Col2 α 1, and aggrecan are

Material	Substrate Name	Stiffness (MPa)	Composition		Collagen Density ($\mu\text{g}/\text{cm}^2$)	Cell Characterization	
			Acrylamide (% Wt)	Piperazine Diacrylamide (% Wt)		Average Cell Area (μm^2)	Average Roundness (0 – 1)
Polyacrylamide Gels	0.2 MPa	0.190 [§] +/- 0.026	30	1	1.34 +/- 0.72	1062 +/- 629	0.67 +/- 0.16
	0.5 MPa	0.526 [§] +/- 0.033	30	2	1.81 +/- 1.02	1041 +/- 637	0.66 +/- 0.16
	1.1 MPa	1.107 [§] +/- 0.083	30	3	2.05 +/- 0.57	1137 +/- 820	0.66 +/- 0.17
Tissue Culture Plastic	Plastic	10 ⁶	N/A	N/A	1.17 +/- 0.12	1113 +/- 637	0.63 +/- 0.16
Articular Cartilage	N/A	0.2 – 1 [‡]	[§] Hansma <i>et al.</i> , 2009; [‡] Kiviranta <i>et al.</i> , 2008				

Table 5.1: Physical characteristics of experimental substrates. Polyacrylamide gel substrates are referred to in the manuscript by their average stiffness, measured previously by nanoindentation (Hansma *et al.*, 2009). These values span the stiffness range reported for articular cartilage, also measured by nanoindentation (Kiviranta *et al.*, 2008). Collagen density between substrates was found to be statistically indistinguishable. ATDC5 cell morphology was also found to be statistically indistinguishable, given by average cell area and roundness (1 – 0 where 1 = circular)

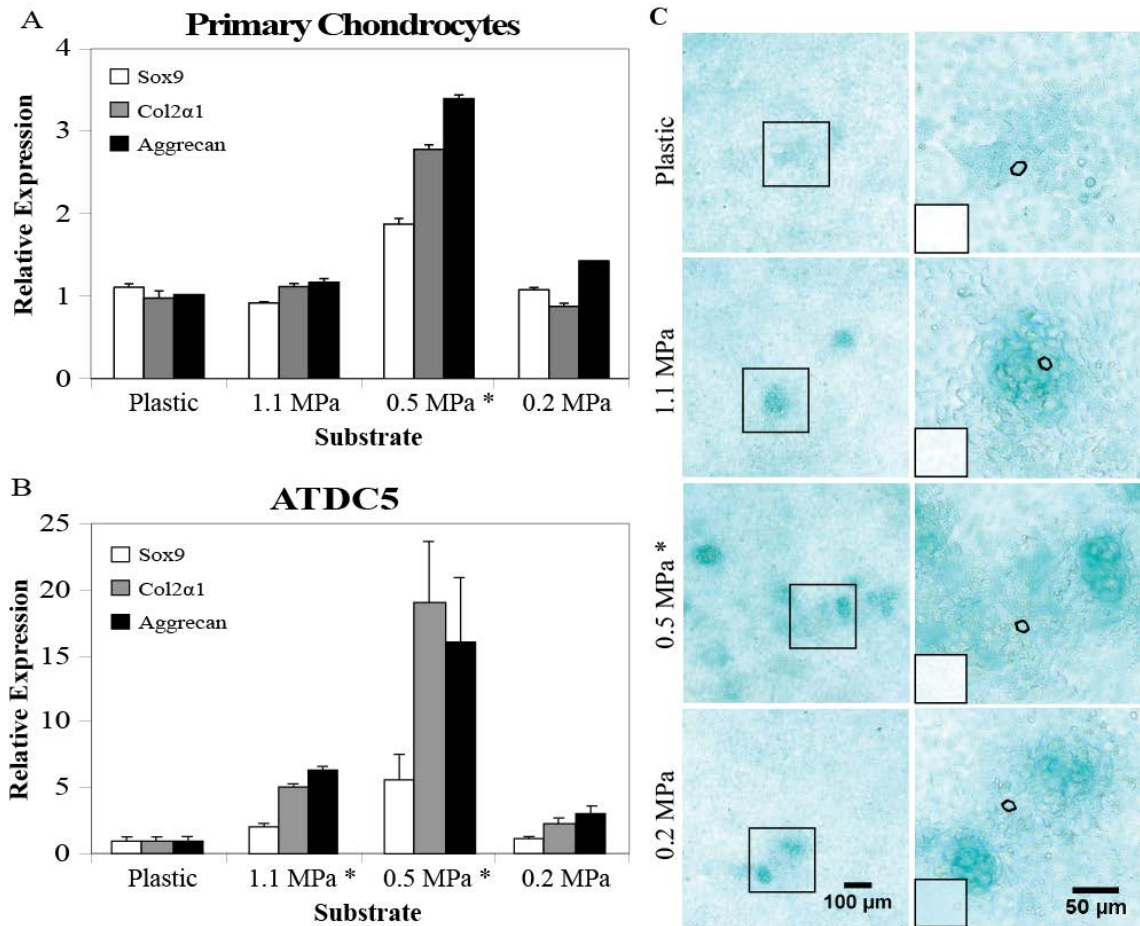


Figure 5.1: Chondrocyte differentiation is stiffness-sensitive. Primary murine chondrocytes (A) and ATDC5 cells (B) cultured in differentiation media on plastic or polyacrylamide gels of the indicated stiffness demonstrate the greatest increase in Sox9, Col2 α 1, and aggrecan gene expression on 0.5 MPa substrates, similar to the stiffness of articular cartilage. Alcian blue staining of proteoglycan production, a functional measure of chondrocyte differentiation, reveals a significant 3.1-fold increase in stained area for ATDC5 cells grown on 0.5 MPa substrates relative to cells grown on plastic (C). The right panels are high-magnification images of regions outlined in the left panels. Staining localizes to regions between cells (a single cell perimeter is marked by a dotted line). The small box to the bottom left of each image shows background Alcian blue staining of control cell-free substrates (* $p < 0.05$)

induced 2, 2.5, and 3-fold, respectively, relative to the plastic control (Figure 5.1A).

Moreover, the induction of these genes is much lower on substrates with a stiffness below 0.5 MPa, demonstrating the specificity of stiffness-induced chondrocyte gene expression.

This stiffness-specific induction was even more robust in ATDC5 cells, with Sox9, Col2 α 1, and aggrecan mRNA expression induced to 6, 19, and 16-fold, respectively, on 0.5 MPa substrates relative to plastic controls (Figure 5.1B). These

changes in chondrocyte gene expression are accompanied by a stiffness-sensitive production of proteoglycan, as detected by Alcian blue staining, which is also maximal on the 0.5 MPa gel (Figure 5.1C). Therefore, chondrocyte differentiation is carefully tuned to the stiffness of the extracellular matrix, such that maximal differentiation occurs on substrates that mimic the stiffness of native healthy articular cartilage.

Potent chondroinductive synergy between ECM stiffness and TGF β

The cellular microenvironment is rich in both biochemical and physical cues that can potently regulate differentiation and cell behavior. Therefore, we evaluated the effect of substrate stiffness on chondrogenic differentiation in the presence or absence of TGF β , a potent biochemical agonist of chondrocyte differentiation (Blaney Davidson *et al.*, 2007; Derynck *et al.*, 2008). TGF β induces the expression of Col2 α 1 and aggrecan in differentiating ATDC5 cells grown for 7 days on plastic substrates (Figures 5.2A-C). Interestingly, ATDC5 cells exhibit an equivalent chondroinductive response to a 0.5 MPa substrate and to TGF β (Figure 5.2A-C). Even these responses, however, pale in

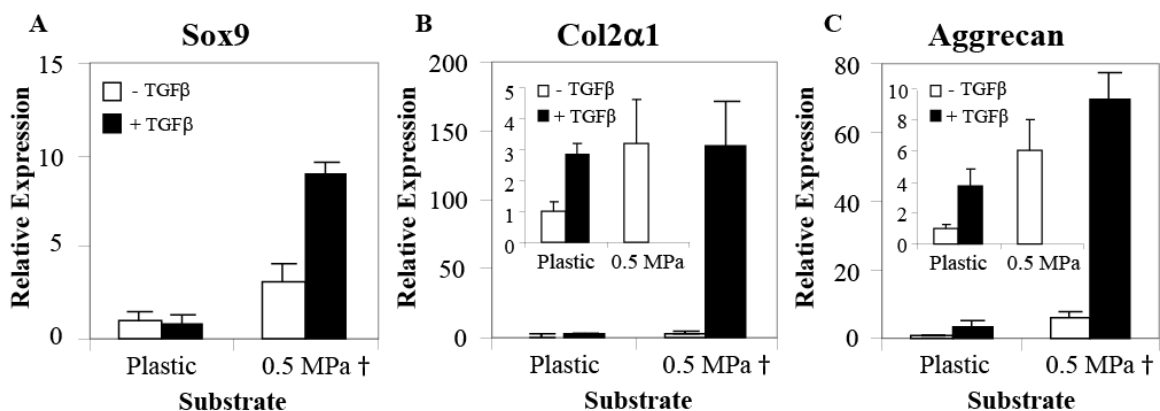


Figure 5.2: Substrate stiffness and TGF β synergize to induce chondrogenic differentiation. Sox9 (A), Col2 α 1 (B), and aggrecan (C) mRNA expression is greatly induced by TGF β (5 ng/ml) in ATDC5 cells differentiated for 7 days on 0.5 MPa substrates, relative to cells grown on plastic or in the absence of TGF β († p < 0.01).

comparison to the strong synergistic induction of Sox9, Col2 α 1, and aggrecan expression (9, 140, and 70-fold, respectively) in TGF β -treated ATDC5 cells differentiated for 7 days on 0.5 MPa substrates (Figures 5.2A-C). This powerful chondroinductive synergy demonstrates that the cellular response to TGF β is highly dependent on the physical microenvironment.

Mechanosensitive chondroinduction is mediated by ROCK signaling

The potent chondroinductive response of ATDC5 cells to substrate stiffness provides a tractable in vitro model system to explore the mechanisms of stiffness-induced chondrocyte differentiation. Cells respond to substrate stiffness by increasing internal cellular tension through stress fiber formation and cell spreading (Discher *et al.*, 2005). Although ATDC5 morphology and cell spread area do not vary significantly across the substrate stiffnesses tested (Table 5.1), stress fiber formation in primary murine chondrocytes and ATDC5 cells increases with substrate stiffness (Figures 5.3A, 5.3B). This suggests that 0.5 MPa substrates induce chondrocyte differentiation through an alteration in internal cell tension. As key components of the cellular mechanosensory apparatus, Rho and ROCK participate in stiffness sensing in part through stress fiber formation (Amano *et al.*, 1997; Maekawa *et al.*, 1999). ROCK activity increases with substrate stiffness, such that cells cultured on stiffer substrates (i.e. plastic) generate higher ROCK activity than cells cultured on more compliant substrates (Huang and Ingber, 2005). To determine if the chondroinductive effect of substrate stiffness occurred through these established mechanisms, primary murine chondrocytes and ATDC5 cells were treated with the ROCK inhibitor Y27632. On plastic, inhibition of ROCK enhances

the expression of chondrocyte differentiation marker genes after 48 hrs of culture (Figure 5.3C). However, on a substrate that mimics the stiffness of articular cartilage, ROCK inhibition completely represses the induction of Col2 α 1 mRNA. Similar results are seen in Sox9 and Aggrecan expression. This observation affirms the key role for ROCK in the ability of chondrocytes to sense and respond to ECM stiffness.

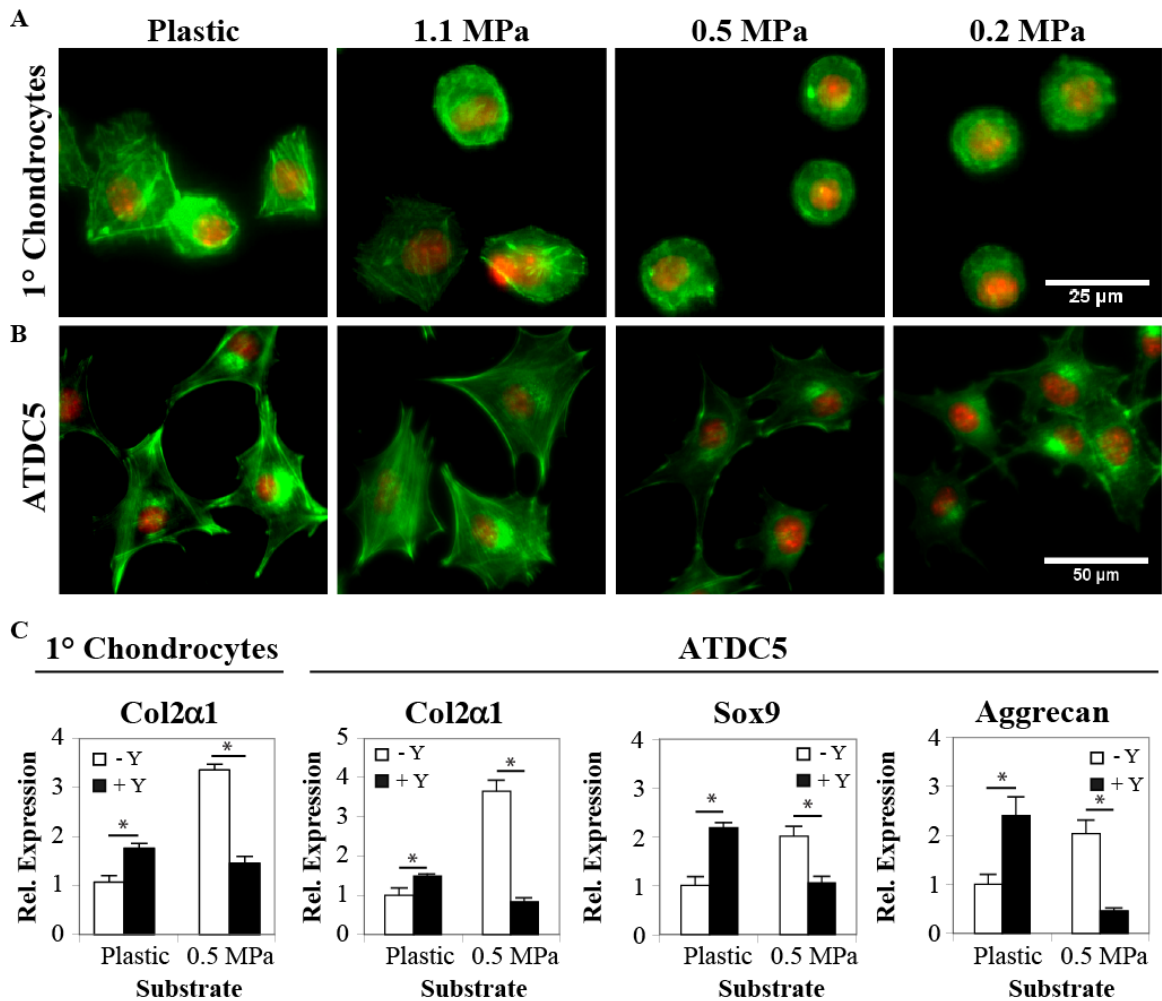


Figure 5.3: Mechanosensitive chondroinduction is mediated by ROCK signaling. Stress fibers, visualized by rhodamine phalloidin (green), are visible in primary chondrocytes (A) and ATDC5 cells (B) with greater frequency and intensity on substrates with stiffnesses of 1.1 MPa or greater. Nuclei are stained with DAPI (red). ROCK inhibition with Y27632 (Y, 10 μ M) induces Col2 α 1 in primary chondrocytes and ATDC5 cells differentiated for 24 hrs on plastic, but represses induction in cells differentiated on 0.5 MPa substrates (C). Similar results are seen for Sox9 and aggrecan expression (* $p < 0.05$).

Mechanosensitive TGF β 1 expression promotes chondrogenic differentiation

The effect of ECM stiffness on primary murine chondrocyte and ATDC5 gene expression is apparent within 24h, when Col2 α 1 mRNA levels are increased in cells grown on 0.5 MPa substrates relative to those grown on plastic (Figure 5.3C). At this time, TGF β 1 mRNA expression is increased by 3-fold in primary murine chondrocytes and ATDC5 cells cultured on a 0.5 MPa substrate, a finding confirmed by ELISA analysis of TGF β 1 protein levels in ATDC5 conditioned media (Figure 5.4A-C). Although others have shown that TGF β 1 mRNA and protein expression are regulated in response to exogenous physical stimuli (Li *et al.*, 2010b; Sakai *et al.*, 1998; Streuli *et al.*, 1993); to our knowledge, this is the first report that substrate stiffness can regulate expression of a TGF β ligand.

ssessed the stiffness-specificity of the induction of TGF β 1 mRNA and protein. Levels of both TGF β 1 mRNA and protein increased with substrate compliance (Figure 5.4C and data not shown). The ROCK inhibitor Y27632 increased TGF β 1 expression in cells cultured on plastic but had no effect on cells grown on 0.5 MPa substrates (Figure 5.4D), suggesting that TGF β 1 expression is induced on compliant substrates due to reduced ROCK activity. This stiffness-dependent pattern of TGF β 1 gene expression is distinct from that of chondrocyte differentiation genes that is induced specifically on 0.5 MPa substrates.

To determine if the stiffness-sensitive increase in autocrine TGF β 1 expression is required for the chondroinductive effects of the 0.5 MPa substrate, ATDC5 cells were treated with a T β RI-inhibitor (SB431542), which acts downstream of the TGF β 1 ligand. While baseline levels of Col2 α 1 in ATDC5 cells cultured on plastic were not sensitive to

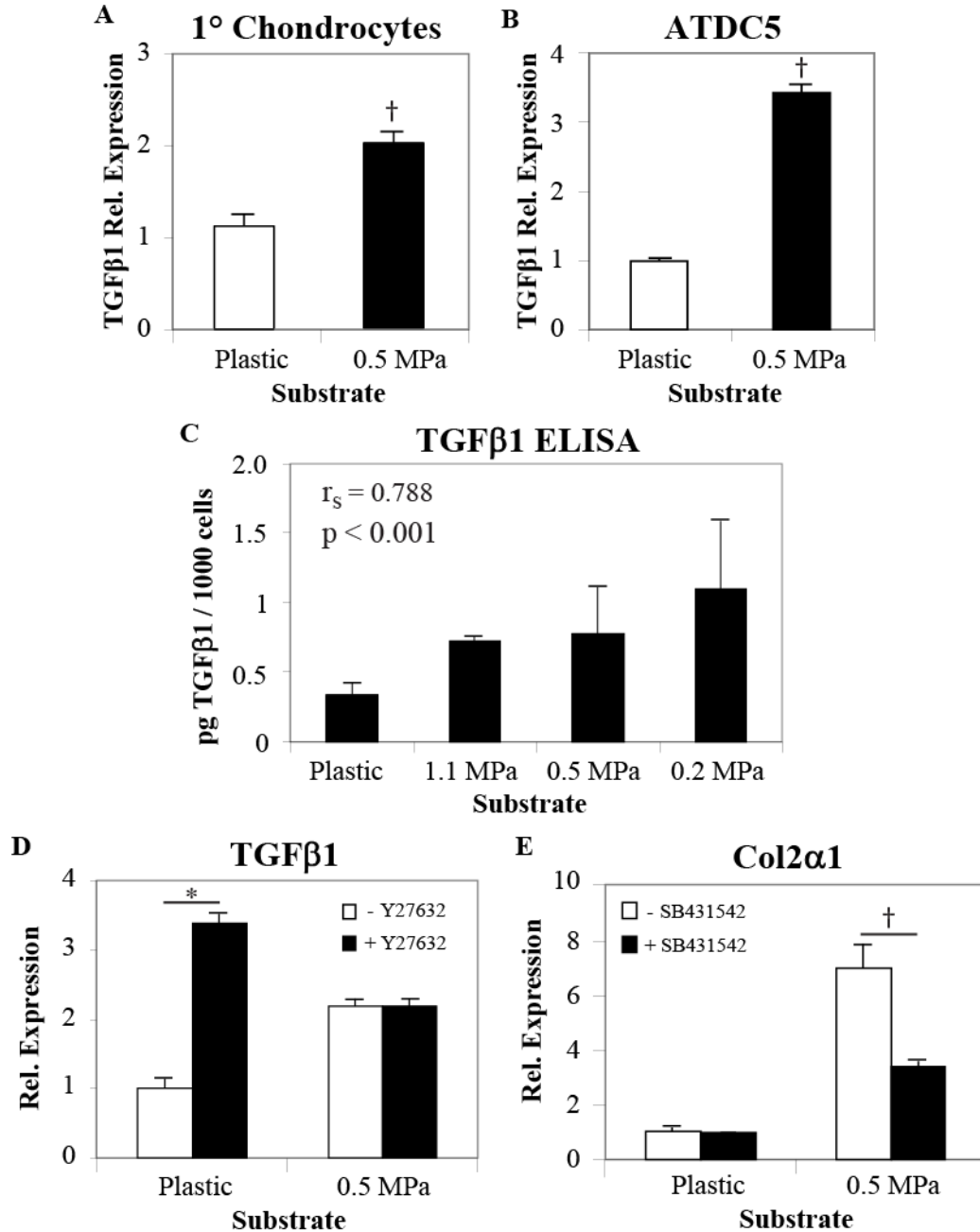


Figure 5.4: Mechanosensitive, ROCK-dependent induction of TGFβ1 is required for chondroinduction. Within 48 hrs, TGFβ1 mRNA is induced in primary chondrocytes (A) and ATDC5 cells (B) in a stiffness-dependent manner. TGFβ1 protein produced by ATDC5 cells, as assessed in media by an ELISA assay, increases with decreasing substrate stiffness (C). The expression of TGFβ1 mRNA in ATDC5 cells is increased by ROCK inhibition with Y27632 (10 μM) on plastic but is unaffected on 0.5 MPa substrates (D). Induction of Col2α1 mRNA in ATDC5 cells cultured on a 0.5 MPa gel is impaired by 24 hr exposure to SB431542 (5 μM), a chemical antagonist of the TGFβ type I receptor (E), (* p < 0.05, † p < 0.01).

the inhibitor, the induction of Col2 α 1 on 0.5 MPa substrates was diminished by the T β RI-inhibitor (Figure 5.4E). Therefore, the chondroinductive response to substrate stiffness requires a mechanosensitive induction of autocrine TGF β 1. However, this mechanism alone does not fully explain why chondrocyte gene expression is optimal on the 0.5 MPa stiffness since, on more compliant substrates, TGF- β 1 is induced but chondrogenic genes are not.

Mechanosensitive regulation of Smad3 stability, phosphorylation, and translocation

We next examined the effect of substrate stiffness on Smad3, a key effector of TGF β signaling that is phosphorylated upon ligand activation of the TGF β receptor complex (Wrana, 2000). Although no significant stiffness-dependent changes in Smad3 mRNA levels were detected (Supplemental Figure 5.1), Smad3 protein levels were consistently elevated in ATDC5 cells grown on 0.5 MPa substrates (Figure 5.5A). Furthermore, even in the absence of exogenously-added TGF β , Smad3 phosphorylation on the C-terminal SSXS domain was increased on 0.5 MPa substrates relative to that observed on either stiffer or more compliant substrates (Figure 5.5A). In ATDC5 chondroprogenitor cells, this stiffness-specific increase in Smad3 phosphorylation mirrored the maximal increases in chondrogenic gene expression on 0.5 MPa substrates (Figure 5.1A). From this result, it appears that on overly compliant substrates, even in the presence of increased autocrine TGF β 1 expression (Figure 5.4C), the lack of chondroinduction, may be due to other mechanisms, such as those limiting ligand-mediated activation of the downstream effector Smad3.

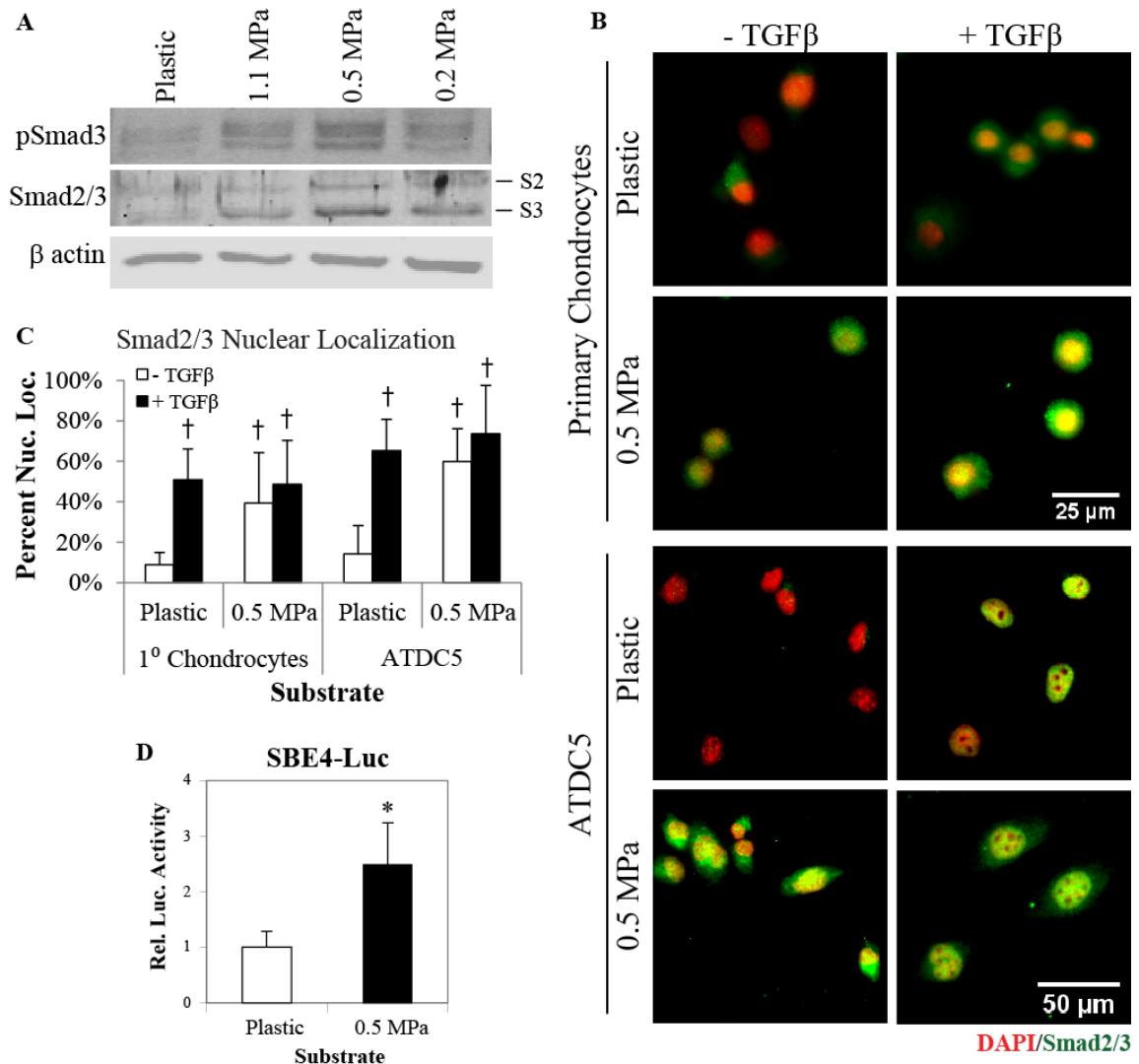


Figure 5.5: Smad3 phosphorylation, localization and transcriptional activity are sensitive to ECM stiffness. Western analysis of whole cell lysates from ATDC5 cells cultured as indicated for 24 hrs reveals that C-terminal Smad3 phosphorylation (top panel) and total protein (middle panel) are increased specifically on a 0.5 MPa substrate, whereas β -actin levels (lower panel) remain unchanged (A). Immunofluorescence microscopy allows visualization of stiffness and TGF β -sensitive Smad2/3 localization (green) relative to DAPI-stained nuclei (red) (B). Relative to cells grown on plastic, a greater percentage of primary chondrocytes and ATDC5 cells have nuclear Smad2/3 when grown on 0.5 MPa substrates, particularly in the absence added TGF β (C). In transiently transfected ATDC5 cells grown for 48hrs on 0.5 MPa substrates, the activity of the TGF β -responsive SBE-luciferase promoter reporter construct is increased relative to cells grown on plastic (D). Luciferase activity is normalized to expression of β -galactosidase from a cotransfected control construct (* $p < 0.05$, † $p < 0.01$).

Consistent with its increased phosphorylation, Smad3 preferentially localizes to the nucleus of primary murine chondrocytes and ATDC5 cells grown on 0.5 MPa substrates. Nuclear Smad3 localization is as frequent in cells grown on 0.5 MPa substrates in the absence of exogenously-added TGF β as in TGF β -treated cells grown on plastic (Figures 5.5B, 5.5C). To determine if this stiffness-dependent increase in nuclear Smad3 is sufficient to induce transactivation, we assessed the effect of substrate stiffness on the activation of a classical Smad3-responsive promoter-reporter construct, SBE-luciferase (Figure 5.5D). Transactivation of SBE-luciferase is increased in ATDC5 cells grown on 0.5 MPa substrates relative to those grown on plastic. Together these findings suggest that the TGF β pathway exhibits stiffness-sensitive regulation at multiple levels, including post-transcriptional control of Smad3 levels, phosphorylation, localization, and transactivation - all of which are maximal in chondroprogenitor cells grown on 0.5 MPa substrates that mimic the stiffness of healthy articular cartilage.

Synergistic response to TGF β and substrate stiffness requires p38 MAPK, but not Smad3

The potent synergistic response of ATDC5 cells to substrate stiffness and exogenously-added TGF β seen in Figure 5.2 provides an ideal model system in which to study the molecular mechanisms by which cells integrate signaling from physical and biochemical cues. Therefore, we sought to determine which of the downstream effectors of TGF β participate in the chondroinductive synergy between exogenously-added TGF β and substrate stiffness. As in Figure 5.5A, Smad3 and phospho-Smad3 levels are increased in ATDC5 cells grown on 0.5 MPa substrates relative to those grown on plastic

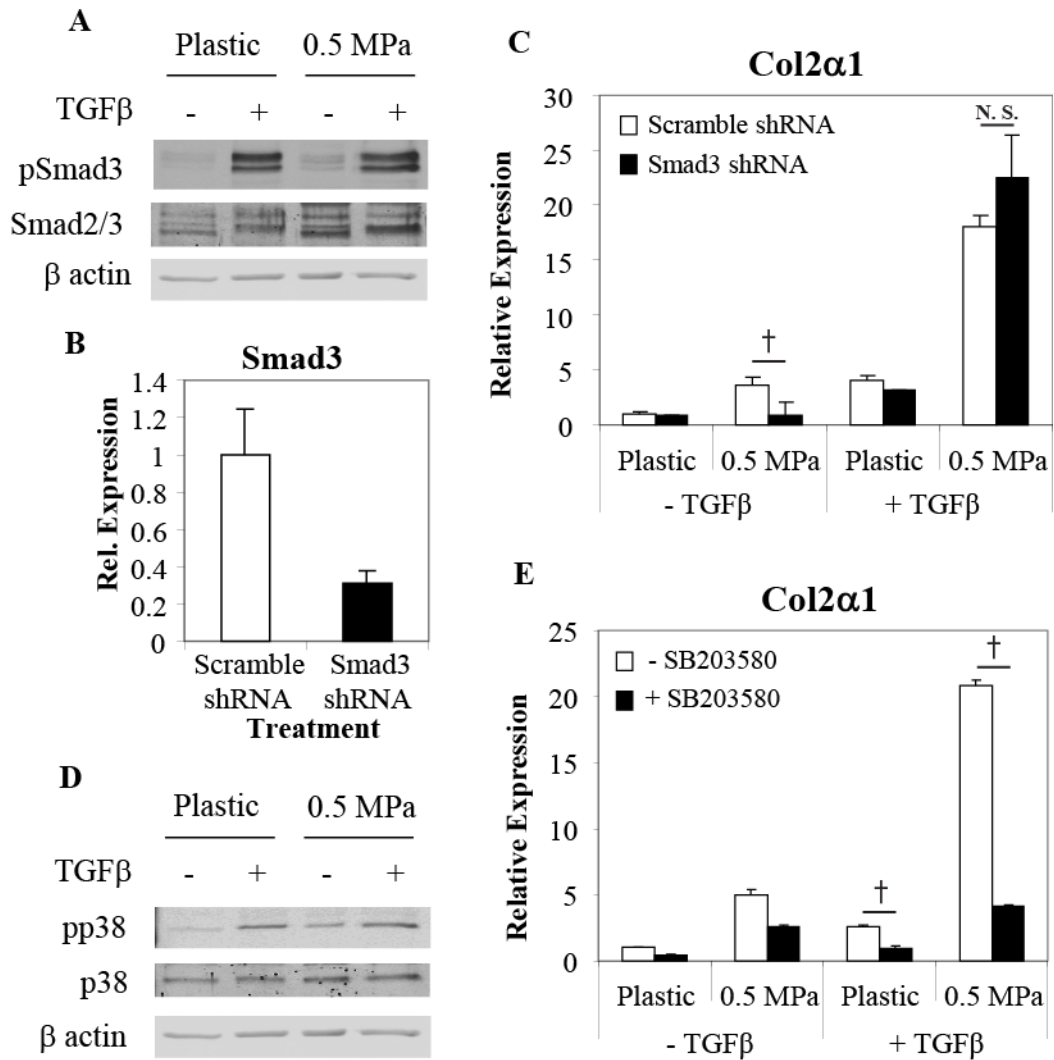


Figure 5.6: Synergy between TGF β and ECM stiffness requires p38 MAPK, but not Smad3. Western analysis reveals no substrate stiffness-dependent effect on TGF β -inducible Smad3 phosphorylation (top panel, A). Smad3 shRNA treatment achieves 70% reduction of Smad3 mRNA, relative to ATDC5 cells expressing a scrambled shRNA (B). shSmad3 impairs the stiffness-sensitive induction of Col2 α 1 mRNA, but not the synergistic induction of Col2 α 1 by TGF β (5 ng/ml, 24 hrs) and a 0.5 MPa substrate (C). Western analysis of phospho-p38 and p38 total protein reveals increased p38 phosphorylation in ATDCs cultured for 24 hrs on a 0.5 MPa substrate or in the presence of TGF β (5 ng/ml, 45 mins) (D). Synergistic induction of Col2 α 1 mRNA by a 0.5 MPa substrate and TGF β is greatly reduced upon inhibition of p38 activity by SB203580 (10 μ M) prior to a 1 hr TGF β treatment (E), (\dagger $p < 0.01$).

(Figure 5.6A). The addition of TGF β to cells grown on 0.5 MPa substrates increased the level of Smad3 phosphorylation to a similar level regardless of substrate stiffness, suggesting that factors in addition to elevated TGF β 1, as in Figure 5.4C, are required for synergy. In Smad3 shRNA expressing cells (Figure 5.6B), induction of Col2 α 1 by stiffness alone is impaired (Figure 5.6C). However, even with a 70% reduction in Smad3 levels, Col2 α 1 expression in ATDC5 cells is still synergistically induced by exogenously-added TGF β in ATDC5 cells grown on a 0.5 MPa substrate (Figure 6C). In these conditions, Smad2 mRNA expression is not increased to compensate for the decreased expression of Smad3 (data not shown). Synergy was also unaffected in Smad3^{fl/fl} primary articular chondrocytes infected with CRE adenovirus (data not shown). Therefore, the cooperative induction of chondrogenic gene expression between TGF β and 0.5 MPa substrates occurs through a Smad3-independent pathway.

As a first step in examining the role of another well-known target of TGF β signaling in the synergistic induction of Col2 α 1, we evaluated the effect of substrate stiffness and TGF β on p38 MAPK phosphorylation. TGF β rapidly activates the p38 pathway through the MAPKKK TAK1 activation of MKK3/6 (Derynck and Zhang, 2003; Moriguchi *et al.*, 1996). Phospho-p38 was increased on 0.5 MPa substrates relative to plastic (Figure 5.6D). TGF β induced p38-phosphorylation in ATDC5 cells grown on plastic and on 0.5 MPa substrates, but not in a synergistic manner. Nonetheless, p38 is critically involved in synergy since the p38 inhibitor, SB203580, strongly repressed the Col2 α 1 induction in response to exogenously-added TGF β in ATDC5 cells grown on a 0.5 MPa substrate. While the p38 inhibitor caused a 2.5-fold repression of Col2 α 1 expression on 0.5 MPa gels alone, it was responsible for a 5-fold

repression of the synergistic response (Figure 5.6E). This suggests that p38 participates in the chondroinductive effects of substrate stiffness, and is essential for the integration of physical and biochemical cues that robustly promotes chondrogenic differentiation on substrates that mimic the stiffness of healthy articular cartilage.

Discussion

We elucidate mechanisms by which physical cues provided by a discrete ECM stiffness specifically increase the efficiency of chondrocyte differentiation by coordinated multilevel regulation of the TGF β pathway (Figure 5.7). A cartilage-like substrate stiffness both enhances chondrocyte gene expression and primes cells for a robust response to the chondroinductive biochemical cue TGF β . In this way, the convergence of chondroinductive physical and biochemical cues drives a more potent response than either cue alone, thereby establishing a microenvironment that the cells interpret as ideal for chondrocyte differentiation. Through ROCK signaling, ECM stiffness regulates chondrocyte differentiation by promoting autocrine TGF β 1 expression on compliant substrates. Stiffness-sensitive chondrocyte differentiation requires Smad3, the phosphorylation of which is maximal on the same discrete stiffness that optimally induces chondrocyte gene expression. In addition to regulating TGF β ligand expression and Smad3 phosphorylation, localization, and transactivation, cells respond to exogenously-added TGF β on a cartilage-like stiffness with a p38 MAPK-dependent synergistic induction of chondrocyte gene expression. Therefore, by ECM stiffness-dependent calibration of the TGF β pathway, chondrocytes integrate physical and biochemical cues to efficiently promote cell differentiation.

We find that the cellular response to ECM stiffness targets the TGF β pathway at several hierarchical levels. Cellular mechanosensing of ECM stiffness requires the development of cytoskeletal tension and focal adhesions and the activation of Rho/ROCK (Assoian and Klein, 2008; Geiger *et al.*, 2009; Kanchanawong *et al.*, 2010; Miranti and Brugge, 2002), a pathway previously implicated in chondrocyte differentiation (Wang *et*

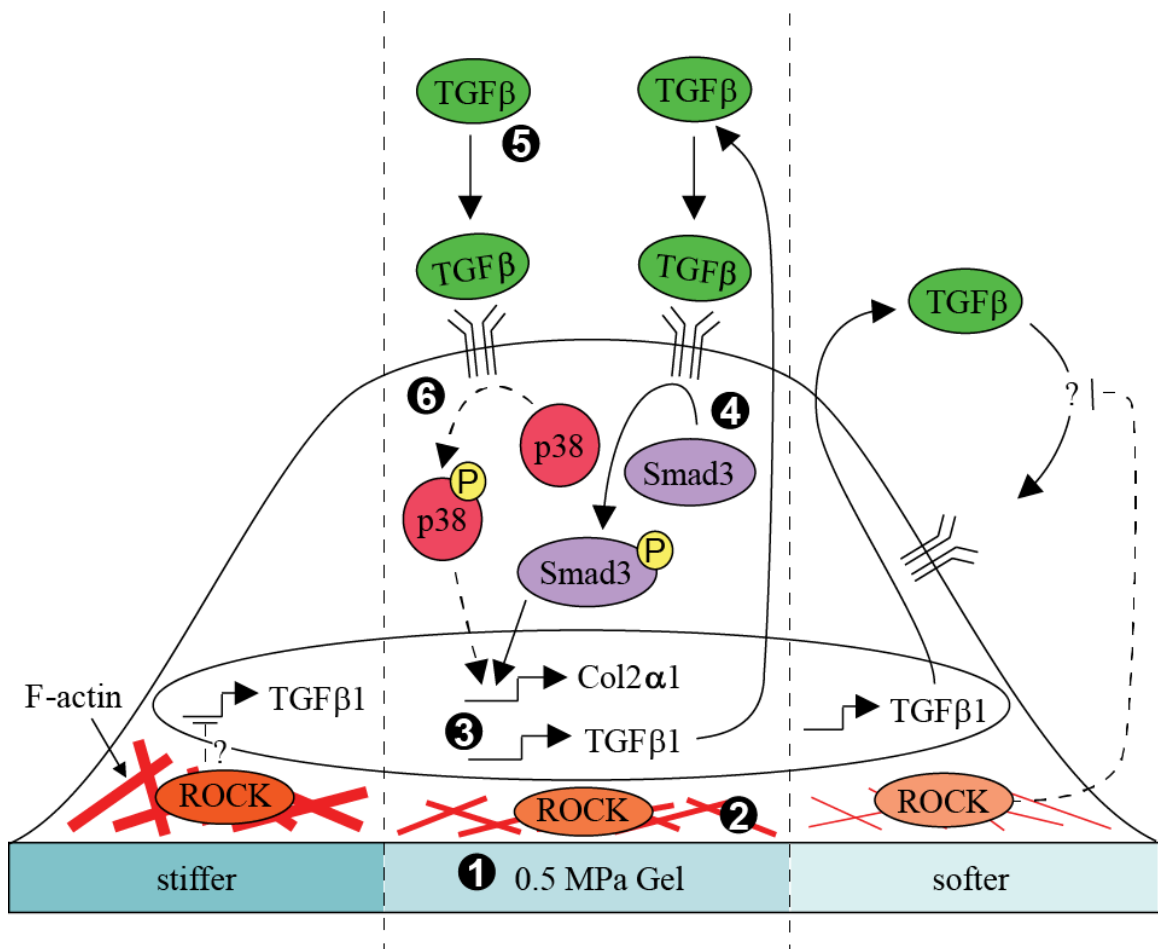


Figure 5.7: Schematic of the mechanism of chondrocyte integration of cues provided by ECM stiffness and TGFβ. (1) Chondrocyte differentiation is specifically induced on 0.5 MPa substrates. (2) This response is mediated through the ROCK pathway. (3) Autocrine TGFβ1 expression is required for chondroinduction, the expression of which is inhibited on stiffer substrates through a ROCK dependent mechanism. (4) While Smad3 phosphorylation and nuclear localization is increased on 0.5 MPa substrates, softer substrates that express autocrine TGFβ fail to activate this downstream effector. (5) Exogenously-added TGFβ elicits a synergistic response in combination with 0.5 MPa substrates. (6) This synergistic interaction acts through a p38-MAPK dependent mechanism, possibly through TGFβ activation of TAK1.

al., 2004; Woods and Beier, 2006). The role of Rho/ROCK signaling in chondrogenesis is complex, such that the effect of ROCK inhibition on chondrogenic differentiation is influenced by the cell type and the dimensionality of culture, among other factors (Clancy *et al.*, 1997; Kumar and Lassar, 2009; Nofal and Knudson, 2002; Woods and Beier, 2006; Woods *et al.*, 2005). Like Woods *et al.* we find that chondrocyte

differentiation is ROCK-dependent, such that inhibition of ROCK signaling enhances differentiation of cells grown on plastic but inhibits differentiation in cells grown on more compliant substrates (Figure 5.3C). Our results suggest that there is an optimal level of ROCK activity on 0.5 MPa substrates that activates chondroinduction, in part, through the induction of TGF β 1 expression on compliant substrates. To our knowledge, this is the first report to show that expression of a component of the TGF β pathway occurs in a stiffness-dependent manner. Although the transcriptional mechanisms by which ECM stiffness regulates TGF β 1 expression remain to be explored, other physical stimuli have been shown to regulate TGF β 1 expression and activity. TGF β 1 mRNA expression is induced by shear fluid flow, in vitro compressive loading, or culture on floating substrates (Li *et al.*, 2010b; Sakai *et al.*, 1998; Streuli *et al.*, 1993). Myocyte stretch induces the release of activated TGF β 1 from the latency associated peptide on stiff substrate (Hinz, 2009; Wells and Discher, 2008). Future studies will test the hypothesis that this combination of regulatory mechanisms - ECM stiffness-sensitive induction of TGF β 1 transcription on compliant substrates and post-translational TGF β 1 activation on stiff substrates - contributes to the potent stiffness-specific chondroinduction in ATDC5 cells and primary chondrocytes (0.5 MPa).

This hierarchical regulation continues inside the cell, where ECM stiffness targets the key TGF β effector, Smad3. ATDC5 cells grown on the chondroinductive 0.5 MPa substrates exhibit a specific increase in Smad3 phosphorylation. Phosphorylated Smad3 translocates to the nucleus where it can bind to Sox9 and enhance CBP recruitment to the Col2 α 1 promoter, where they cooperatively induce Col2 α 1 transcription (Furumatsu *et al.*, 2005). We found that the stiffness-specific phosphorylation and nuclear localization

of Smad3 correlates with and is required for the increased Col2 α 1 expression on 0.5 MPa substrates. Although several mechanisms may contribute to these observations, our data strongly suggests that autocrine TGF β 1 activity is significantly responsible for the stiffness-specific increase in Smad3 phosphorylation and the resulting induction of Col2 α 1. Treatment with either a TGF β receptor inhibitor or shSmad3 completely ablates the induction of Col2 α 1 gene expression on 0.5 MPa substrates. Though collagen II has also been shown to induce phosphorylation of Smad2/3 in the absence of exogenous TGF β (Garamszegi *et al.*, 2010), collagen II density did not vary greatly with substrate stiffness in our experiments.

Numerous links between Smad signaling and effectors of the mechanosensing pathway have been identified. Cytoskeletal tension, generated by either ECM stiffness or cell spreading, is sufficient to control the localization of YAP/TAZ (Dupont *et al.*, 2011), transcriptional coregulators that can direct nuclear localization of Smad2/3 (Varelas *et al.*, 2008). Whether tension-inducible YAP/TAZ translocation contributes to the stiffness-sensitive nuclear localization of Smad3 observed here remains unknown. More recently, Wang *et al.* showed that BMP-inducible nuclear translocation of Smad1/5/8 requires sufficient ROCK-dependent cytoskeletal tension (Wang *et al.*, 2011b). ROCK can also enhance the activity of both Smad3 and Sox9 by phosphorylation of the Smad3 linker region or Sox9 on serine 181 (Haudenschild *et al.*, 2010; Kamaraju and Roberts, 2005). Though the role of ROCK-inducible Sox9 phosphorylation in the chondroinductive synergy between ECM stiffness and TGF β remains unclear, this synergistic response does require p38 MAPK and functions even with very little Smad3. This is consistent with prior studies showing that TAK1, the upstream activator of p38

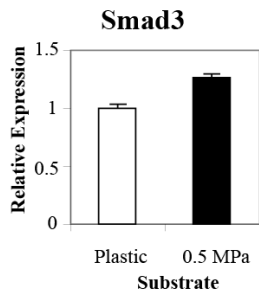
MAPK, regulates collagen II synthesis in chondrocytes independently of Smad3 signaling (Qiao *et al.*, 2005). ECM stiffness may also cause differential utilization of downstream TGF β receptors or effectors (Blaney Davidson *et al.*, 2009; van der Kraan *et al.*, 2009), or it may prime chromatin for a more potent TGF β -inducible transactivation (Mullen *et al.*), mechanisms shown to calibrate the cellular response to TGF β in osteoarthritic chondrocytes or in differentiating stem cells, respectively. Additional studies are needed to further investigate the synergistic response of chondrocytes to ECM stiffness and TGF β , work that will elucidate new mechanisms by which cells integrate physical and biochemical cues to refine and coordinate cell behavior, a paradigm that has relevance for cartilage and many other tissues. Nonetheless, the current work illustrates that cells respond to a chondroinductive physical cue (a cartilage-like substrate stiffness) by strategically targeting the activity of a powerful chondroinductive biochemical pathway (TGF β) at multiple hierarchical levels.

The range of stiffnesses present in cartilage varies spatially and temporally, such that each may have unique instructive roles. Consistent with the stiffness of adult articular cartilage, precommitted chondrocytes (ATDC5 chondroprogenitors or primary chondrocytes) showed maximal chondrocyte gene expression on 0.5 MPa substrates. More compliant matrices may be more chondroinductive during lineage selection as induction of chondrogenic gene expression in MSCs occurs on compliant 1 kPa substrates (Park *et al.*, 2011). Indeed, osteogenic differentiation in MSCs has been reported on a 25 kPa substrate, which is much softer than fully mineralized bone matrix (Engler *et al.*, 2006). This relationship between ECM stiffness and chondrocyte differentiation may be particularly important for understanding osteoarthritis, in which

the degradation of cartilage ECM stiffness coincides with the loss of chondrocyte homeostasis through mechanisms that are coupled but unclear. Since TGF β signaling through the p38 MAPK pathway is important *in vitro* and *in vivo* for chondrocyte maturation, proliferation and survival (Gunnell *et al.*, 2010; Li *et al.*, 2010a; Seto *et al.*, 2004), our finding that p38 MAPK is important for of synergy between TGF β and substrate stiffness suggests that coordinated signaling between biochemical and physical cues may be important for the maintenance of chondrocyte homeostasis. The ability of ECM stiffness to modulate the cellular response to TGF β , in particular, may elucidate the differential effects of this growth factor on chondrocytes, such that it can either promote or deter this degenerative cascade in a way that is highly sensitive to the cellular microenvironment (Blaney Davidson *et al.*, 2007).

Within and beyond cartilage, the interaction between TGF β and ECM stiffness may form a feedback loop to promote and maintain cellular homeostasis and ECM composition. TGF β plays a primary role in regulating ECM composition and stiffness in several tissues including bone, dentin, and skin (Arany *et al.*, 2006; Balooch *et al.*, 2005; Chang *et al.*, 2010; Saeki *et al.*, 2007). Therefore, disruption of TGF β signaling impairs ECM stiffness, and, as we show here, disruption of ECM stiffness alters the level of and cellular response to TGF β signaling. Indeed, in several other diseases, including breast cancer and liver fibrosis, the pathological phenotype is accompanied and perpetuated by non-physiologic stiffnesses and abnormal TGF β signaling (Butcher *et al.*, 2009; Hinz, 2009; Ingber, 2003; Li *et al.*, 2007b; Paszek *et al.*, 2005; Tomasek *et al.*, 2002; Wells and Discher, 2008). A deeper understanding of the interactions between physical and biochemical cues, particularly the mechanisms by which cells integrate cues provided by

ECM stiffness and TGF β , may elucidate mechanisms of disease and reveal novel therapeutic targets.



Supplemental Figure 5.1: Smad3 mRNA expression is relatively unaffected by substrate

CHAPTER 6

ECM Stiffness Regulates Chondrogenesis in Mesenchymal Stem Cells

Introduction

The previous chapter demonstrates that substrate stiffness primes the TGF β pathway to induce chondrocyte differentiation in mature chondrocytes. A discrete stiffness, similar to that reported for articular cartilage, induces chondrocyte specific gene expression and synergizes with exogenously added TGF β . Chondroinduction on a discrete, cartilage-like stiffness requires autocrine induction of TGF β 1, and in the absence of exogenously added TGF β , specifically induces Smad3 phosphorylation, nuclear localization, and transcriptional activity. However, it is still unknown whether these mechanisms, identified in a mature phenotype, are also present in MSCs undergoing chondroinduction.

Both TGF β and mechanical cues have been identified as powerful regulators of chondrogenesis in MSCs. TGF β is required for chondroinduction of MSCs (Bian *et al.*, 2011; Tuli *et al.*, 2003). In vivo, TGF β induces ectopic Sox9 expression and chondrocyte lineage selection (Kawakami *et al.*, 2006) most likely through Smad3-enhanced Sox9 transcriptional activity (Furumatsu *et al.*, 2005). Culture in compliant 3D formats activates chondrogenesis, marked by a loss of actin stress fibers and the generation of a rounded morphology (Benya *et al.*, 1988; Benya and Shaffer, 1982; Brown and Benya, 1988; von der Mark *et al.*, 1977). Moreover, Sox9 expression in MSC is regulated by the actin cytoskeleton and Rho/ROCK signaling (Woods *et al.*, 2005). Mechanical load-

induced chondrogenesis in hMSCs requires autocrine TGF β expression (Li *et al.*, 2010b), mirroring the autocrine TGF β expression induced by cartilage-like substrates in Chapter 5. Therefore, mechanisms similar to those described for mature chondrocytes may regulate stiffness-sensitive chondrogenesis in MSCs.

When work for this dissertation began, there was little known about the specific stiffness required to induce chondrogenesis in MSCs. In other tissues, both precursor and mature cell types are induced by a similar stiffness. Substrates of the same stiffness (~10 kPa) induce myotube formation in myoblasts and myogenic gene expression in both MSCs (Engler *et al.*, 2006; Georges and Janmey, 2005). Similar results were seen in neurite branching and MSC neurogenesis on extremely compliant substrates (~1 kPa) (Engler *et al.*, 2006; Flanagan *et al.*, 2002). Therefore, the 0.5 MPa substrates used in Chapter 5 may similarly induce chondrogenesis in MSCs. In this chapter we will determine whether substrate stiffness primes the TGF β pathway to induce chondrogenesis in MSCs.

Results

ECM Stiffness Regulates Chondrogenic Gene Expression

As demonstrated in Chapter 5, ECM stiffness regulates chondrocyte-specific gene expression in ATDC5s and primary chondrocytes. To determine whether ECM stiffness

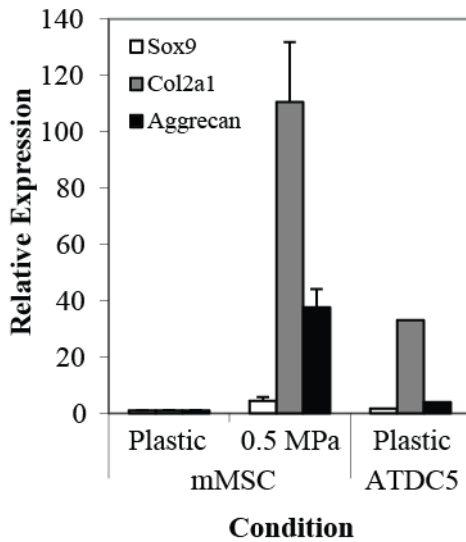


Figure 6.1: Chondrogenic gene expression in murine MSCs is stiffness-sensitive. Murine MSCs were cultured for 7 days in chondrogenic media supplemented with 5ng/ml TGF β . On a 0.5 MPa substrate, hMSCs induce Sox9, Col2 α 1, and Aggrecan gene expression 4, 110, and 37-fold above plastic controls. Chondroinduction in MSCs also exceeds levels in ATDC5s treated with TGF β for 8 days.

regulates chondrogenic gene expression, MSCs were cultured on several substrates with a stiffness range that spanned that reported for cartilage. First, mouse MSCs (mMSCs) cultured on a 0.5 MPa substrate for 7 days in chondrogenic media supplemented with TGF β induced Sox9, Col2 α 1, and Aggrecan expression 4, 110, and 37-fold above plastic controls, respectively (Figure 6.1).

While this induction in chondrogenic gene expression on 0.5 MPa substrates seems high, it is compared to the induction levels of mMSCs cultured on plastic that may be expressing little to no chondrocyte specific gene expression.

Comparing Sox9, Col2 α 1, and Aggrecan

expression levels in mMSCs to those in ATDC5 cells cultured in the presence of TGF β for 8 days we find culture on a 0.5 MPa gel induces comparable expression levels for these chondrogenic genes (Figure 6.1).

Human MSCs (hMSCs) also exhibit stiffness sensitive expression of Sox9. Compared to expression levels on plastic or overly compliant substrates, Sox9 expression

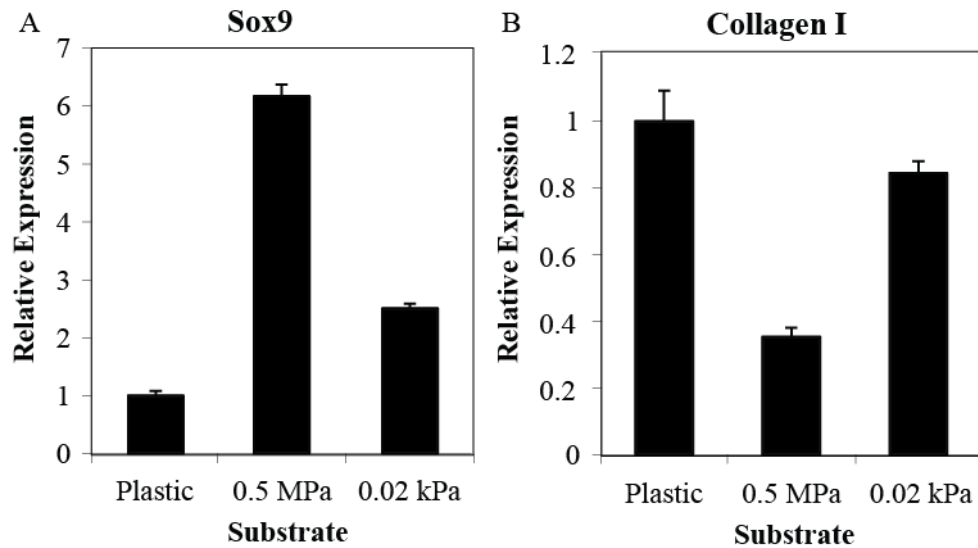


Figure 6.2: hMSC gene expression is stiffness-sensitive. hMSCs cultured in chondrogenic media for 7 days demonstrate the greatest increase in Sox9 gene expression on 0.5 MPa substrates, similar to the stiffness of articular cartilage (A). Collagen I gene expression in hMSCs is markedly knocked down specifically on 0.5 MPa substrates (B).

is induced 6-fold on 0.5 MPa substrates in hMSCs culture in chondrogenic media for 5 days (Figure 6.2A). Moreover, in hMSCs cultured on 0.5 MPa substrates there is a 65% knockdown in Collagen I expression, consistent with chondroinduction (Benya and Shaffer, 1982; von der Mark *et al.*, 1977)(Figure 6.2B). While this data is preliminary, it indicates that hMSCs are driven toward chondrocyte lineage selection on cartilage-like substrates.

Although hMSCs on 0.5 MPa gels induce Sox9 gene expression, Col2 α 1 and Aggrecan expression remains low. Aggrecan expression in hMSCs is repressed to the greatest extent on the 0.5 MPa substrate and appears to decrease with TGF β exposure time on all substrates (Figure 6.3A and B). This is surprising as mMSCs up regulated all three chondrocyte specific genes when cultured on a 0.5 MPa gel in the presence of TGF β . Mwale, et al demonstrated that Aggrecan may be constitutively active in hMSCs before induction of chondrogenesis (Mwale *et al.*, 2006). Therefore, the knockdown

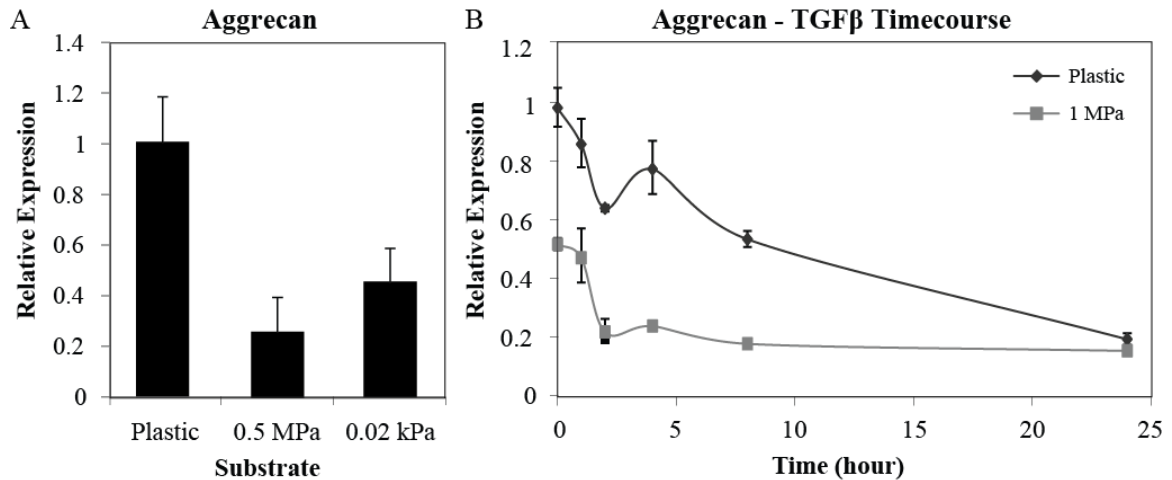


Figure 6.3: Aggrecan gene expression is repressed in hMSCs by cartilage-like substrates and TGFβ. In hMSCs cultured for 7 days in chondrogenic media, aggrecan gene expression is repressed more than 70% on 0.5 MPa substrates (A). At short time points, aggrecan gene expression is also repressed by TGFβ treatment, regardless of stiffness (B).

observed in hMSCs here could indicate an initial reprogramming event before commitment to the chondrocyte lineage.

Col2α1 expression was low in hMSCs regardless of substrate stiffness. Analysis of the melt curves after QPCR revealed that none of the hMSC RNA samples were producing any PCR products for Colα1, even though PCR products for the housekeeping gene 18S was generated as normal (Figure 6.4). This is surprising since Sox9 is induced in hMSCs on 0.5 MPa substrates and mMSCs induce both Sox9 and Col2α1 on 0.5 MPa substrates at such high levels. In all hMSC experiments cultured for longer than 24 hours, chondrogenic media was supplemented with 200 μM ascorbic acid. Ascorbic acid inhibits Col2α1 mRNA expression (Sabatini *et al.*, 2004), therefore the lack of Col2α1 expression in hMSCs may be a result of media formulation. Alternatively, a cartilage-like stiffness may be sufficient to promote selection of a chondrocyte lineage, but not sufficient to support induction of Col2α1 and Aggrecan mRNA expression. Analysis of

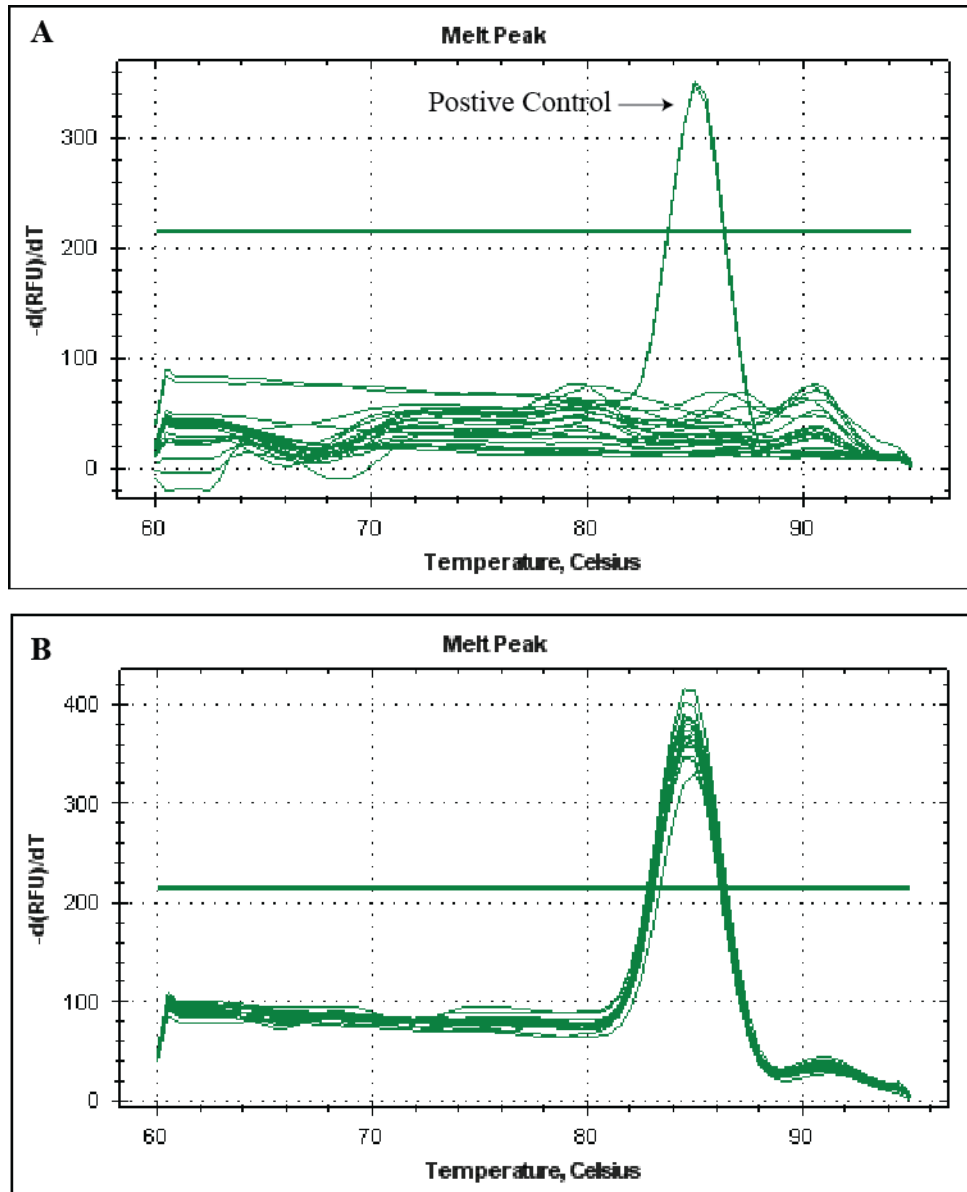


Figure 6.4: hMSCs fail to produce Col2 α 1 PCR product. Melt curves reveal that hMSCs fail to produce a PCR product from Col2 α 1 primers (A). A Col2 α 1 RNA sample is used as a positive control for comparison. PCR products for the housekeeping gene 18S were generated as normal (B).

other lineage markers and expression at several time points may be required to troubleshoot lack of hMSC Col2 α 1 expression on cartilage-like substrates.

ECM Stiffness and TGFβ Synergistic Induction of Sox9 Expression in hMSCs

As demonstrated in Chapter 5, TGFβ treatment synergistically enhances chondrocyte specific gene expression in ATDC5s cultured on cartilage-like substrates. To determine the effect of TGFβ treatment on stiffness sensitive chondrogenic gene expression, hMSCs were cultured on plastic and 0.5 MPa substrates for 7 days in chondrogenic media in the

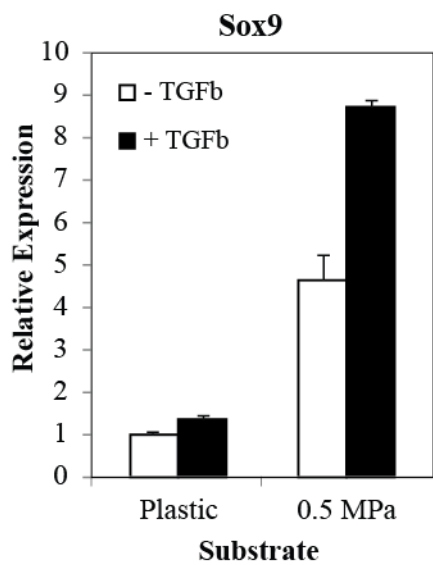


Figure 6.5: Substrate stiffness and TGFβ synergize to induce Sox9 expression. hMSCs cultured for 7 days on 0.5 MPa greatly induce Sox9 gene expression in response to TGFβ (5 ng/ml), relative to cells cultured on plastic in the absence of TGFβ.

presence or absence of TGFβ. Again, Sox9 gene expression is induced in hMSCs cultured on 0.5 MPa substrates 4.5-fold over plastic controls (Figure 6.5). Moreover, treatment with TGFβ enhances Sox9 expression in hMSCs, specifically on 0.5 MPa substrates. While Sox9 expression is driven to an 8.5-fold induction with TGFβ treatment on 0.5 MPa substrates, it has little effect on hMSCs cultured on

plastic (Figure 6.5). Therefore, while in ATDC5s, TGFβ treatment induces chondrocyte specific gene expression regardless of the stiffness of the ECM, hMSCs in monolayer require culture on a 0.5 MPa

substrate for TGFβ-induced Sox9 expression.

Rounded, Chondrocyte-like Morphology is Rapidly Induced by Culture on a Gel

Undifferentiated MSCs have a fibroblastic morphology; but as they undergo chondrogenesis, they adopt the rounded morphology normally found in mature chondrocytes (Daniels and Solursh, 1991). Culture on a cartilage-like stiffness (0.5 MPa)

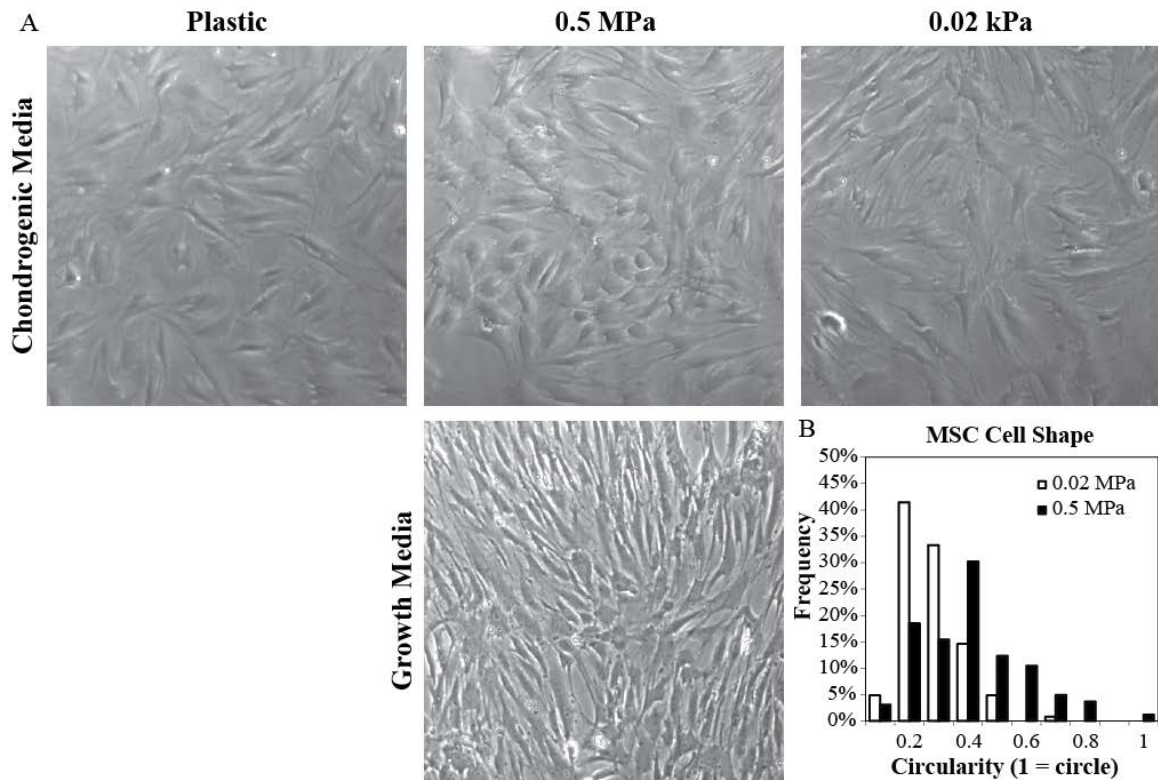


Figure 6.6: hMSCs adopt a rounded morphology on 0.5 MPa substrates. hMSCs cultured for 3 days on 0.5 MPa substrates in the presence of chondrogenic media adopt a more rounded morphology compared to cells cultured on softer or stiffer substrates (A). hMSCs fail to round on 0.5 MPa substrates in growth media. Quantification of hMSC cells shape at day 4 reveals a higher percentage of hMSCs are rounded compared to hMSCs on overly compliant substrates (B).

induces MSC rounding. In Figure 6.6A, after 3 days of culture, MSCs in chondrogenic media are noticeably more rounded on a 0.5 MPa substrate than on either softer or stiffer substrates. This pattern of rounding mirrors the preferential induction of Sox9 expression in hMSCs grown on 0.5 MPa substrates. Quantification of MSC morphology after 4 days of culture demonstrates that a higher percentage of cells adopt a rounded morphology on a 0.5 MPa substrate than on overly compliant substrates (Figure 6.6B). This stiffness-induced change in morphology is chondrogenic media dependent, as MSCs cultured in growth media on a 0.5 MPa substrate do not round by day 3 (Figure 6.6A, lower panel).

Stiffness-sensitive Chondrogenesis in hMSCs May Require Autocrine TGF β and ROCK

Signaling

As seen in Chapter 5, chondrocyte specific gene expression in ATDC5 is induced on 0.5 MPa substrates in response to autocrine TGF β 1 expression. To determine whether a similar mechanism regulates stiffness-sensitive Sox9 expression in hMSCs, PAI1 expression, a classical TGF β responsive gene, was analyzed after 7 days of culture in the presence of chondrogenic media. In Figure 6.7A, on plastic in the presence of TGF β , PAI1 expression in hMSCs is induced 4-fold. However, even in the absence of exogenous TGF β treatment, PAI1 mRNA expression in hMSCs cultured on 0.5 MPa substrates is induced 6-fold over plastic controls, indicating activation of the TGF β pathway in this

condition. Addition of TGF β on 0.5 MPa substrates provides no further induction, suggesting that PAI1 expression is at a maximal level on 0.5 MPa substrates even before addition of exogenous TGF β . These results indicate that hMSCs may be producing

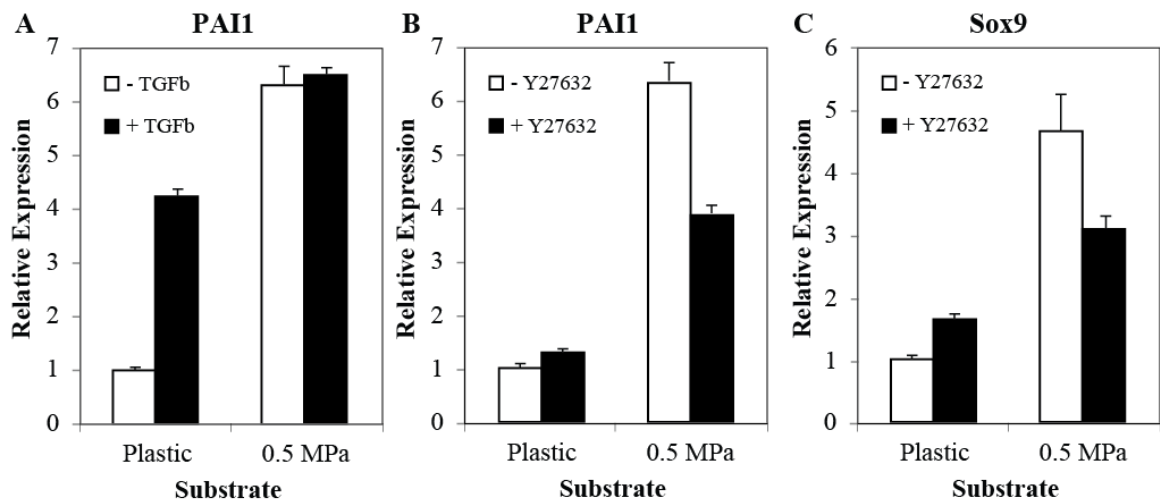


Figure 6.7: Stiffness-sensitive Sox9 expression may require ROCK-regulated activation of the TGF β pathway. PAI1, a classic TGF β -responsive gene, is up-regulated in hMSCs cultured on 0.5 MPa substrates for 7 days, even in the absence of TGF β (A). ROCK inhibition with Y27632 (10 μ M) represses PAI1 (B) and Sox9 (C) induction in hMSCs on 0.5 MPa substrates.

autocrine TGF β 1 in response to culture on a 0.5 MPa substrate similar to ATDC5s and primary murine chondrocytes.

In Chapter 5, stiffness-sensitive induction of autocrine TGF β 1 in ATDC5s on 0.5 MPa substrates is regulated by ROCK signaling. PAI1 expression in hMSCs cultured for 7 days on a 0.5 MPa substrate is knocked down by 40% in the presence of the ROCK inhibitor, indicating that a similar mechanism may be regulating the activation of the TGF β pathway (Figure 6.7B). Moreover, in hMSCs cultured on 0.5 MPa substrates, treatment with a chemical ROCK inhibitor (Y27632) for 7 days results in a loss of Sox9 induction (Figure 6.7C). Therefore, similar to ATDC5 and primary murine chondrocytes (Chapter 5), ROCK signaling is required for stiffness-sensitive induction of the TGF β pathway and induction of Sox9 in hMSCs.

Discussion

In summary, similar to the results found in Chapter 5, we have identified that MSCs up regulate chondrocyte specific genes in response to culture on a cartilage-like stiffness. However, induction of chondrogenic genes is isolated to Sox9 expression in hMSCs. This stiffness-induced Sox9 expression is accompanied by a rapid change in cell shape to a more rounded morphology on cartilage-like substrates. Sox9 gene expression is synergistically enhanced by addition of exogenous TGF β . An up-regulation in PAI1 expression on 0.5MPa gels indicates that autocrine TGF β may also be induced in hMSCs in response to a cartilage-like stiffness. Moreover, Sox9 and PAI1 induction in response to a cartilage-like substrate are ROCK sensitive.

While several chondrocyte specific genes were up regulated in murine MSCs and mature chondrocytes in Chapter 5, induction of chondrogenic gene expression was isolated to Sox9 for hMSCs. This difference could be a result of differences in the species of the cells. Possibly human chondrogenesis requires a stiffness that is distinct from the stiffness that induces murine chondrogenesis. The shape change observed in hMSCs is also distinct from the trend observed in Chapter 5. ATDC5s demonstrate no significant change in shape with a change in substrate stiffness. Primary murine chondrocytes retain a rounded morphology on substrates of 0.5 MPa or less. Indeed in experiments that lacked chondrogenic media, hMSCs exhibited no shape change but there was still an induction in Sox9 expression, although the induction was not as substantial as it was in chondrogenic media conditions. Moreover, in a short time course Sox9 is rapidly induced on 0.5 MPa substrates much earlier than noticeable rounding occurs. These two observations taken together suggest that chondrogenesis in response to

substrate stiffness may act independently of shape change, or a rounded morphology may be secondary to Sox9 induction in hMSCs.

Interestingly, exogenously added TGF β produces no significant induction in Sox9 expression in hMSCs culture on plastic. Only when hMSCs are cultured on a gel is there a marked induction in Sox9 expression with exogenously added TGF β . This response does not seem to indicate a lack of responsiveness to TGF β , as PAI1 gene expression is still induced on plastic, but rather an inability of TGF β to specifically induce Sox9 gene expression in this particular cell culture context. This is of course in sharp contrast to our results in Chapter 5, in which Sox9 and other chondrocyte specific genes are up-regulated in response to TGF β regardless of the substrate stiffness. It is well known that, in contrast to monolayer culture, 3D culture, or chemical inhibition of cytoskeletal tension, acts as a permissive signal upon which biochemical factors can be applied to induce chondrogenesis in hMSCs (Benya *et al.*, 1988; Benya and Shaffer, 1982; Brown and Benya, 1988; von der Mark *et al.*, 1977; Woods *et al.*, 2005). As seen in Chapter 5 in ATDC5 cells and primary murine chondrocytes, culture on a cartilage-like substrate reduces internal cellular tension and stress fiber formation. As with a 3D environment, culture on cartilage-like substrates may act as a permissive signal by reducing internal cellular tension in hMSCs to allow Sox9 induction in response to TGF β .

Recent research into stiffness-induced chondrogenesis in MSCs at first glance appears to disagree with the findings described in this chapter. Park *et al.* demonstrates that hMSCs induce Col2 α 1 mRNA expression when cultured on substrate far more compliant than cartilage ECM stiffness (~1 kPa)(Park *et al.*, 2011). In a study by Williamson *et al.*, the stiffness of bovine articular cartilage increases 3-fold with

development (Williamson *et al.*, 2001), therefore the optimal stiffness for chondroinduction may change with chondrocyte maturation. Indeed, Engler et al found that osteogenesis in hMSCs was activated on a stiffness (~25 kPa) far softer than bone matrix, hypothesizing that this stiffness may mimic unmineralized osteoid microenvironment encountered by hMSCs in early osteogenesis (Engler *et al.*, 2006). As the stiffnesses investigated in this dissertation are several orders of magnitude stiffer than those used in other studies, directly comparing hMSCs cultured on 1MPa and 1kPa may further reveal the mechanisms behind stiffness-induced chondrogenesis.

Future work should focus on identifying whether the TGF β pathway is similarly impacted by culture of hMSCs on a cartilage-like substrate. The results in this chapter suggest that a similar autocrine TGF β mechanism has a role in stiffness-induced chondrogenesis. Moreover, it would be interesting to explore the mechanisms that allow chondrogenesis on a cartilage-like substrate, but block induction on plastic even in the presence of TGF β . This phenomenon suggests that stiffness, in addition to regulating autocrine TGF β , relaxes additional barriers to chondrogenesis that have yet to be identified. A more in depth understanding of the mechanisms that regulate the initiation of chondrogenesis will add in the development of tissue engineering strategies for articular cartilage.

CHAPTER 7

Summary and Future Directions

In summary, we have adapted polyacrylamide (PA) gel substrates to facilitate innovative studies into the complex physical and biochemical properties of articular cartilage. These PA gel substrates were layered to act as mechanical models of the stratified material properties of articular cartilage. Development of a mathematical model from the loading behavior of stratified PA gels led to the novel observation that osteoarthritis (OA) drives the material properties of the cartilage extracellular matrix (ECM) towards homogeneity. Homogeneous PA gels in the stiffness range reported for articular cartilage were used as cell culture substrates to identify the cellular mechanisms that integrate physical and biochemical cues in the control of chondrocyte differentiation. Specifically, substrate stiffness primes the TGF β pathway to induce chondrocyte differentiation through both Smad and non-Smad mediated pathways. We have found that chondrocyte differentiation is specifically induced by culture on a cartilage-like substrate (0.5 MPa). Treatment with exogenous TGF β on a cartilage-like substrate induces a synergistic effect that drives chondrocyte gene expression far above that of either cue alone. Culture of both ATDC5 cells and primary murine chondrocytes on 0.5 MPa substrates reveals that autocrine TGF β is required for stiffness-induced chondrocyte differentiation. Substrate stiffness also hierarchically regulates Smad3 phosphorylation, nuclear localization, and transcription. When TGF β is added exogenously, synergistic induction of chondrocyte gene expression becomes Smad3 independent, acting instead

through the p38 MAPK pathway. We have identified similar mechanisms in human mesenchymal stem cells (hMSCs), although isolated to Sox9 gene expression. The differences in gene inducibility between hMSCs and mature chondrocytes indicates that the interaction between substrate stiffness and TGF β , highly tuned to a specific stiffness in mature chondrocytes, may require another as yet unidentified mechanism in the regulation of chondrogenesis.

Although this dissertation describes several novel mechanisms through which cells integrate signaling from ECM stiffness and TGF β , our understanding of the mechanisms by which cells integrate physical and biochemical cues remain incomplete. Future work should focus on the questions left unanswered by the work in this dissertation. For example, the mechanisms that specify the induction of chondrocyte differentiation only on a cartilage-like stiffness remain to be explored. In Chapter 5, chondroinduction on a 0.5 MPa substrate requires autocrine TGF β . While TGF β mRNA expression and ligand production increases with compliance reaching a maximum on the softest gel (Figure 5.4C), there is not a concurrent increase in Smad3 phosphorylation on overly compliant substrates (Figure 5.5A). While the lack of Smad3 phosphorylation on overly stiff substrates is most likely a result of low autocrine TGF β production, Smad3 phosphorylation is expected on overly compliant substrates where cells are expressing autocrine TGF β . The mechanism that prevents TGF β -inducible Smad3 phosphorylation on overly compliant substrates is unknown, but must lie between production of the ligand and effector activation, narrowing the possibilities (Figure 5.7). Post-translational modification of TGF β activation may be involved, as myocyte stretch-activated release of TGF β 1 from the latency associated peptide occurs on stiff, but not compliant, substrates

(Hinz, 2009; Wells and Discher, 2008). Moreover, as crosstalk between integrins and growth factor receptors is important in the regulation of cell behavior (Eliceiri, 2001), it is possible that stiffness, in regulating integrin clustering, also affects growth factor receptor clustering or availability.

Cell shape and substrate stiffness are strongly linked (Yeung *et al.*, 2005), therefore it is difficult to separate these two cues from one another. The work of Chris Chen has elegantly demonstrated that cell shape itself can regulate apoptosis and stem cell lineage selection independent of substrate stiffness (Chen *et al.*, 1997; Gao *et al.*, 2010; McBeath *et al.*, 2004; Shao *et al.*, 2012). There are several observations about cell shape in Chapters 5 and 6: ATDC5 cells do not exhibit a cell shape change with stiffness; primary chondrocytes lose their rounded phenotype with increasing substrate stiffness; and hMSCs obtain a rounded morphology specifically on 0.5 MPa substrates, but only in the presence of chondrogenic media. As ATDC5 cells, unlike primary chondrocytes, do not require rounded morphology for chondrocyte differentiation, they may provide insight into the relationship between substrate stiffness and cell shape. As the mechanisms involved in the interaction between substrate stiffness and TGF β can be observed in ATDC5 without any shape change, it would seem that a change in cell shape may be secondary to stiffness in regulation of chondrocyte differentiation. However, substrate stiffness does have such a strong effect on cell morphology in non-transformed cells (murine primary chondrocytes and hMSCs) and therefore it is difficult to interpret the importance of cell morphology as a physical cue in chondroinduction. Indeed, numerous studies have indicated the importance of a rounded morphology in inducing both chondrogenesis and maintenance of chondrocyte phenotype (Benya and Shaffer,

1982; Gao *et al.*, 2010; Glowacki *et al.*, 1983; Shao *et al.*, 2012; Takahashi *et al.*, 2007). In Chapter 6, hMSCs cultured on plastic adopt an elongated shape and in the presence of TGF β will not induce Sox9 expression. hMSCs cultured on a 0.5 MPa gel exhibit a rounded morphology and synergistically induce of Sox9 expression with TGF β treatment (Figure 6.5). It is possible that, in addition to an interaction between substrate stiffness and TGF β , a change in cell shape may be required for the proper induction of chondrogenesis.

It is well known that dimensionality is a factor in cellular mechanosensing studies. Several studies have found that similar stiffnesses induces cellular differentiation in 2D and 3D (Janmey and Miller, 2011). However, other studies have demonstrated that dimensionality can affect integrin ligation, cell contraction, and intercellular signals (Griffith and Swartz, 2006). Further studies should focus on whether the cellular mechanisms that integrate physical and biochemical cues identified here in 2D are maintained in a 3D environment. Though murine chondrocytes adopt a rounded morphology on cartilage-like substrate, they are cultured in monolayer and therefore may best represent chondrocytes from the thin superficial layer of articular cartilage. It would be interesting to determine, just as the moduli of articular cartilage vary with depth, whether chondrocytes harvested from different zones of cartilage have different optimal substrate stiffnesses and whether the mechanisms combining physical and biochemical cues vary as well.

As it appears that substrate stiffness affects chondrocyte differentiation, it would follow that this physical cue plays a role in the development of osteoarthritis. Indeed, the shear stress and physical manipulation by ultrasound have been shown affect the

osteoarthritic phenotype. Shear stress from fluid flow induces expression of matrix metalloprotease 9 and nitric oxide and decreases Col2a1 and aggrecan mRNA production in osteoarthritic chondrocytes (Lee *et al.*, 2002; Smith *et al.*, 1995). In a rat OA model, low-intensity pulsed ultrasound increased collagen II production and decreased histologically-assessed cartilage matrix damage (Naito *et al.*, 2010). Moreover, as osteoarthritis can arise from both a physical and biochemical impetus, studying the complex interactions between these two types of cues in the context of the disease may lead to innovative ideas about the true cause of osteoarthritis. Future work into the response of osteoarthritic chondrocytes to a range of substrate stiffnesses and TGF β treatment may elucidate new therapeutic targets.

While the work here describes an interaction between one physical and one biochemical cue, there are numerous others that may be important in differentiation of chondrocytes or other cells types. The ECM, while providing numerous physical cues, also binds soluble growth factors and controls diffusion rates, creating concentration gradients (Griffith and Swartz, 2006). Interstitial fluid flow, in addition to its role as a mechanical cue, functions to transport soluble factors through the ECM. Studies have found that interstitial flow can regulate the distribution of proteoglycans and proteases and can even synergize with VEGF in angiogenesis (Griffith and Swartz, 2006).

While exploring interaction between physical and biochemical cues is challenging, this strategy has proven relevant for tissue engineering applications. Many factors have to be considered to recapitulate the properties of the original healthy tissue. In this vein, synthetic gels have been developed that control growth factor binding sites, and restrict internalization while providing an tunable physical environment (Griffith and

Swartz, 2006). Aligned nanofibers synergize with bFGF in wound healing (Patel *et al.*, 2007). High shear stress combined with endothelial growth factor synergistically induces differentiation of Placenta-derived multipotent cells (Wu *et al.*, 2008). The cellular microenvironment is so complex, that the success of tissue engineering therapies may bank on a better understanding of how disparate cues work together to regulate tissue maintenance and function.

REFERENCES

- Aigner, T. and Dudhia, J. (2003). Genomics of osteoarthritis. *Curr Opin Rheumatol* *15*, 634-640.
- Aigner, T., Kurz, B., Fukui, N. and Sandell, L. (2002). Roles of chondrocytes in the pathogenesis of osteoarthritis. *Curr Opin Rheumatol* *14*, 578-584.
- Akizuki, S., Mow, V. C., Muller, F., Pita, J. C., Howell, D. S. and Manicourt, D. H. (1986). Tensile properties of human knee joint cartilage: I. Influence of ionic conditions, weight bearing, and fibrillation on the tensile modulus. *J Orthop Res* *4*, 379-392.
- Alvarez, J., Sohn, P., Zeng, X., Doetschman, T., Robbins, D. J. and Serra, R. (2002). TGFbeta2 mediates the effects of hedgehog on hypertrophic differentiation and PTHrP expression. *Development* *129*, 1913-1924.
- Amano, M., Chihara, K., Kimura, K., Fukata, Y., Nakamura, N., Matsuura, Y. and Kaibuchi, K. (1997). Formation of actin stress fibers and focal adhesions enhanced by Rho-kinase. *Science* *275*, 1308-1311.
- Annes, J. P., Munger, J. S. and Rifkin, D. B. (2003). Making sense of latent TGFbeta activation. *J Cell Sci* *116*, 217-224.
- Arany, P. R., Flanders, K. C., Kobayashi, T., Kuo, C. K., Stuelten, C., Desai, K. V., Tuan, R., Rennard, S. I. and Roberts, A. B. (2006). Smad3 deficiency alters key structural elements of the extracellular matrix and mechanotransduction of wound closure. *Proc Natl Acad Sci U S A* *103*, 9250-9255.
- Assoian, R. K. and Klein, E. A. (2008). Growth control by intracellular tension and extracellular stiffness. *Trends Cell Biol* *18*, 347-352.
- Baker, B. M. and Chen, C. S. (2012). Deconstructing the third dimension - how 3D culture microenvironments alter cellular cues. *J Cell Sci*
- Balooch, G., et al. (2005). TGF-beta regulates the mechanical properties and composition of bone matrix. *Proc Natl Acad Sci U S A* *102*, 18813-18818.
- Benya, P. D., Brown, P. D. and Padilla, S. R. (1988). Microfilament modification by dihydrocytochalasin B causes retinoic acid-modulated chondrocytes to reexpress the differentiated collagen phenotype without a change in shape. *J Cell Biol* *106*, 161-170.
- Benya, P. D. and Shaffer, J. D. (1982). Dedifferentiated chondrocytes reexpress the differentiated collagen phenotype when cultured in agarose gels. *Cell* *30*, 215-224.
- Bian, L., Zhai, D. Y., Tous, E., Rai, R., Mauck, R. L. and Burdick, J. A. (2011). Enhanced MSC chondrogenesis following delivery of TGF-beta3 from alginate microspheres within hyaluronic acid hydrogels in vitro and in vivo. *Biomaterials* *32*, 6425-6434.
- Blaney Davidson, E. N., Remst, D. F., Vitters, E. L., van Beuningen, H. M., Blom, A. B., Goumans, M. J., van den Berg, W. B. and van der Kraan, P. M. (2009). Increase in ALK1/ALK5 ratio as a cause for elevated MMP-13 expression in osteoarthritis in humans and mice. *J Immunol* *182*, 7937-7945.
- Blaney Davidson, E. N., van der Kraan, P. M. and van den Berg, W. B. (2007). TGF-beta and osteoarthritis. *Osteoarthritis Cartilage* *15*, 597-604.

- Broom, N. D. (1984). Further insights into the structural principles governing the function of articular cartilage. *J Anat* *139 (Pt 2)*, 275-294.
- Brown, P. D. and Benya, P. D. (1988). Alterations in chondrocyte cytoskeletal architecture during phenotypic modulation by retinoic acid and dihydrocytochalasin B-induced reexpression. *J Cell Biol* *106*, 171-179.
- Butcher, D. T., Alliston, T. and Weaver, V. M. (2009). A tense situation: forcing tumour progression. *Nat Rev Cancer* *9*, 108-122.
- Buxboim, A., Ivanovska, I. L. and Discher, D. E. (2010). Matrix elasticity, cytoskeletal forces and physics of the nucleus: how deeply do cells 'feel' outside and in? *J Cell Sci* *123*, 297-308.
- Chang, J. L., et al. (2010). Tissue-specific calibration of extracellular matrix material properties by transforming growth factor-beta and Runx2 in bone is required for hearing. *EMBO Rep* *11*, 765-771.
- Chen, A. C., Bae, W. C., Schinagl, R. M. and Sah, R. L. (2001). Depth- and strain-dependent mechanical and electromechanical properties of full-thickness bovine articular cartilage in confined compression. *J Biomech* *34*, 1-12.
- Chen, C. G., Thuillier, D., Chin, E. N. and Alliston, T. (2012). Chondrocyte-intrinsic Smad3 represses RunX2-inducible MMP-13 expression to maintain articular cartilage and prevent osteoarthritis. *Arthritis Rheum* *Accepted*,
- Chen, C. S., Mrksich, M., Huang, S., Whitesides, G. M. and Ingber, D. E. (1997). Geometric control of cell life and death. *Science* *276*, 1425-1428.
- Chen, S. S., Falcovitz, Y. H., Schneiderman, R., Maroudas, A. and Sah, R. L. (2001). Depth-dependent compressive properties of normal aged human femoral head articular cartilage: relationship to fixed charge density. *Osteoarthritis Cartilage* *9*, 561-569.
- Clancy, R. M., Rediske, J., Tang, X., Nijher, N., Frenkel, S., Philips, M. and Abramson, S. B. (1997). Outside-in signaling in the chondrocyte. Nitric oxide disrupts fibronectin-induced assembly of a subplasmalemmal actin/rho A/focal adhesion kinase signaling complex. *J Clin Invest* *100*, 1789-1796.
- Damljanovic, V., Lagerholm, B. C. and Jacobson, K. (2005). Bulk and micropatterned conjugation of extracellular matrix proteins to characterized polyacrylamide substrates for cell mechanotransduction assays. *Biotechniques* *39*, 847-851.
- Daniels, K. and Solursh, M. (1991). Modulation of chondrogenesis by the cytoskeleton and extracellular matrix. *J Cell Sci* *100 (Pt 2)*, 249-254.
- Darling, E. M., Wilusz, R. E., Bolognesi, M. P., Zauscher, S. and Guilak, F. (2010). Spatial mapping of the biomechanical properties of the pericellular matrix of articular cartilage measured in situ via atomic force microscopy. *Biophys J* *98*, 2848-2856.
- de Rooij, J., Kerstens, A., Danuser, G., Schwartz, M. A. and Waterman-Storer, C. M. (2005). Integrin-dependent actomyosin contraction regulates epithelial cell scattering. *J Cell Biol* *171*, 153-164.
- Derynck, R., Piek, E., Schneider, R. A., Choy, L. and Alliston, T. (2008). TGF-beta Family Signaling in Mesenchymal Differentiation. In: *The TGF-beta Family*, ed. R. Derynck and K. Miyazono, New York: Cold Spring Harbor Laboratory Press, 613-666.

- Derynck, R. and Zhang, Y. E. (2003). Smad-dependent and Smad-independent pathways in TGF-beta family signalling. *Nature* 425, 577-584.
- Discher, D. E., Janmey, P. and Wang, Y. L. (2005). Tissue cells feel and respond to the stiffness of their substrate. *Science* 310, 1139-1143.
- Dong, C., Li, Z., Alvarez, R., Jr., Feng, X. H. and Goldschmidt-Clermont, P. J. (2000). Microtubule binding to Smads may regulate TGF-beta activity. *Mol Cell* 5, 27-34.
- Dupont, S., et al. (2011). Role of YAP/TAZ in mechanotransduction. *Nature* 474, 179-183.
- Eliceiri, B. P. (2001). Integrin and growth factor receptor crosstalk. *Circ Res* 89, 1104-1110.
- Engler, A. J., Sen, S., Sweeney, H. L. and Discher, D. E. (2006). Matrix elasticity directs stem cell lineage specification. *Cell* 126, 677-689.
- Feng, X. H., Filvaroff, E. H. and Derynck, R. (1995). Transforming growth factor-beta (TGF-beta)-induced down-regulation of cyclin A expression requires a functional TGF-beta receptor complex. Characterization of chimeric and truncated type I and type II receptors. *J Biol Chem* 270, 24237-24245.
- Ferguson, C. M., Schwarz, E. M., Reynolds, P. R., Puzas, J. E., Rosier, R. N. and O'Keefe, R. J. (2000). Smad2 and 3 mediate transforming growth factor-beta1-induced inhibition of chondrocyte maturation. *Endocrinology* 141, 4728-4735.
- Flanagan, L. A., Ju, Y. E., Marg, B., Osterfield, M. and Janmey, P. A. (2002). Neurite branching on deformable substrates. *Neuroreport* 13, 2411-2415.
- Furumatsu, T., Tsuda, M., Taniguchi, N., Tajima, Y. and Asahara, H. (2005). Smad3 induces chondrogenesis through the activation of SOX9 via CREB-binding protein/p300 recruitment. *J Biol Chem* 280, 8343-8350.
- Gao, L., McBeath, R. and Chen, C. S. (2010). Stem cell shape regulates a chondrogenic versus myogenic fate through Rac1 and N-cadherin. *Stem Cells* 28, 564-572.
- Garamszegi, N., Garamszegi, S. P., Samavarchi-Tehrani, P., Walford, E., Schneiderbauer, M. M., Wrana, J. L. and Scully, S. P. (2010). Extracellular matrix-induced transforming growth factor-beta receptor signaling dynamics. *Oncogene* 29, 2368-2380.
- Geiger, B., Spatz, J. P. and Bershadsky, A. D. (2009). Environmental sensing through focal adhesions. *Nat Rev Mol Cell Biol* 10, 21-33.
- Georges, P. C. and Janmey, P. A. (2005). Cell type-specific response to growth on soft materials. *J Appl Physiol* 98, 1547-1553.
- Glowacki, J., Trepman, E. and Folkman, J. (1983). Cell shape and phenotypic expression in chondrocytes. *Proc Soc Exp Biol Med* 172, 93-98.
- Goldring, M. B. and Goldring, S. R. (2007). Osteoarthritis. *J Cell Physiol* 213, 626-634.
- Goldring, M. B., Tsuchimochi, K. and Ijiri, K. (2006). The control of chondrogenesis. *J Cell Biochem* 97, 33-44.
- Grad, S., Eglin, D., Alini, M. and Stoddart, M. J. (2011). Physical stimulation of chondrogenic cells in vitro: a review. *Clin Orthop Relat Res* 469, 2764-2772.
- Griffith, L. G. and Swartz, M. A. (2006). Capturing complex 3D tissue physiology in vitro. *Nat Rev Mol Cell Biol* 7, 211-224.

- Guilak, F., Cohen, D. M., Estes, B. T., Gimble, J. M., Liedtke, W. and Chen, C. S. (2009). Control of stem cell fate by physical interactions with the extracellular matrix. *Cell Stem Cell* 5, 17-26.
- Guilak, F., Ratcliffe, A. and Mow, V. C. (1995). Chondrocyte deformation and local tissue strain in articular cartilage: a confocal microscopy study. *J Orthop Res* 13, 410-421.
- Gunnell, L. M., Jonason, J. H., Loisel, A. E., Kohn, A., Schwarz, E. M., Hilton, M. J. and O'Keefe, R. J. (2010). TAK1 regulates cartilage and joint development via the MAPK and BMP signaling pathways. *J Bone Miner Res* 25, 1784-1797.
- Hansma, P., et al. (2009). The tissue diagnostic instrument. *Rev Sci Instrum* 80, 054303.
- Haudenschild, D. R., Chen, J., Pang, N., Lotz, M. K. and D'Lima, D. D. (2010). Rho kinase-dependent activation of SOX9 in chondrocytes. *Arthritis Rheum* 62, 191-200.
- Hauselmann, H. J., Fernandes, R. J., Mok, S. S., Schmid, T. M., Block, J. A., Aydelotte, M. B., Kuettner, K. E. and Thonar, E. J. (1994). Phenotypic stability of bovine articular chondrocytes after long-term culture in alginate beads. *J Cell Sci* 107 (Pt 1), 17-27.
- Henderson, J. H. and Carter, D. R. (2002). Mechanical induction in limb morphogenesis: the role of growth-generated strains and pressures. *Bone* 31, 645-653.
- Herakovich, C. T. (1997). Mechanics of Fibrous Composites. New York, John Wiley & Sons, Inc.
- Hinz, B. (2009). Tissue stiffness, latent TGF-beta1 activation, and mechanical signal transduction: implications for the pathogenesis and treatment of fibrosis. *Curr Rheumatol Rep* 11, 120-126.
- Hu, J. C. Y. and Athanasiou, K. A. (2003). Structure and Function of Articular Cartilage. In: *Handbook of Histology Methods for Bone and Cartilage*, ed. Y. H. An and K. L. Martin, Totowa: Humana Press Inc., 73-95.
- Huang, C. Y., Soltz, M. A., Kopacz, M., Mow, V. C. and Ateshian, G. A. (2003). Experimental verification of the roles of intrinsic matrix viscoelasticity and tension-compression nonlinearity in the biphasic response of cartilage. *J Biomech Eng* 125, 84-93.
- Huang, S. and Ingber, D. E. (2005). Cell tension, matrix mechanics, and cancer development. *Cancer Cell* 8, 175-176.
- Imer, R., Akiyama, T., N, F. d. R., Stolz, M., Aebi, U., N, F. F. and Staufer, U. (2009). The measurement of biomechanical properties of porcine articular cartilage using atomic force microscopy. *Arch Histol Cytol* 72, 251-259.
- Ingber, D. E. (2003). Mechanobiology and diseases of mechanotransduction. *Ann Med* 35, 564-577.
- Janmey, P. A. and Miller, R. T. (2011). Mechanisms of mechanical signaling in development and disease. *J Cell Sci* 124, 9-18.
- Kamaraju, A. K. and Roberts, A. B. (2005). Role of Rho/ROCK and p38 MAP kinase pathways in transforming growth factor-beta-mediated Smad-dependent growth inhibition of human breast carcinoma cells in vivo. *J Biol Chem* 280, 1024-1036.
- Kanchanawong, P., Shtengel, G., Pasapera, A. M., Ramko, E. B., Davidson, M. W., Hess, H. F. and Waterman, C. M. (2010). Nanoscale architecture of integrin-based cell adhesions. *Nature* 468, 580-584.

- Kadow, C. E., Georges, P. C., Janmey, P. A. and Beningo, K. A. (2007). Polyacrylamide hydrogels for cell mechanics: steps toward optimization and alternative uses. *Methods Cell Biol* 83, 29-46.
- Kawakami, Y., Rodriguez-Leon, J. and Izipisua Belmonte, J. C. (2006). The role of TGFbetas and Sox9 during limb chondrogenesis. *Curr Opin Cell Biol* 18, 723-729.
- Kempson, G. E., Muir, H., Swanson, S. A. and Freeman, M. A. (1970). Correlations between stiffness and the chemical constituents of cartilage on the human femoral head. *Biochim Biophys Acta* 215, 70-77.
- Kiviranta, P., Lammentausta, E., Toyras, J., Kiviranta, I. and Jurvelin, J. S. (2008). Indentation diagnostics of cartilage degeneration. *Osteoarthritis Cartilage* 16, 796-804.
- Kleemann, R. U., Krockner, D., Cedraro, A., Tuischer, J. and Duda, G. N. (2005). Altered cartilage mechanics and histology in knee osteoarthritis: relation to clinical assessment (ICRS Grade). *Osteoarthritis Cartilage* 13, 958-963.
- Klein, T. J., Chaudhry, M., Bae, W. C. and Sah, R. L. (2007). Depth-dependent biomechanical and biochemical properties of fetal, newborn, and tissue-engineered articular cartilage. *J Biomech* 40, 182-190.
- Klein, T. J., Schumacher, B. L., Schmidt, T. A., Li, K. W., Voegtline, M. S., Masuda, K., Thonar, E. J. and Sah, R. L. (2003). Tissue engineering of stratified articular cartilage from chondrocyte subpopulations. *Osteoarthritis Cartilage* 11, 595-602.
- Knecht, S., Vanwanseele, B. and Stussi, E. (2006). A review on the mechanical quality of articular cartilage - implications for the diagnosis of osteoarthritis. *Clin Biomech (Bristol, Avon)* 21, 999-1012.
- Kumar, D. and Lassar, A. B. (2009). The transcriptional activity of Sox9 in chondrocytes is regulated by RhoA signaling and actin polymerization. *Mol Cell Biol* 29, 4262-4273.
- Kwan, M. K., Lai, W. M. and Mow, V. C. (1984). Fundamentals of fluid transport through cartilage in compression. *Ann Biomed Eng* 12, 537-558.
- Lawrence, R. C., et al. (2008). Estimates of the prevalence of arthritis and other rheumatic conditions in the United States. Part II. *Arthritis Rheum* 58, 26-35.
- Lee, M. S., Trindade, M. C., Ikenoue, T., Schurman, D. J., Goodman, S. B. and Smith, R. L. (2002). Effects of shear stress on nitric oxide and matrix protein gene expression in human osteoarthritic chondrocytes in vitro. *J Orthop Res* 20, 556-561.
- Leight, J. L., Wozniak, M. A., Chen, S., Lynch, M. L. and Chen, C. S. (2012). Matrix rigidity regulates a switch between TGF-beta1-induced apoptosis and epithelial-mesenchymal transition. *Mol Biol Cell (Epub)*.
- Leipzig, N. D. and Shoichet, M. S. (2009). The effect of substrate stiffness on adult neural stem cell behavior. *Biomaterials* 30, 6867-6878.
- Li, C., Allen, J., Alliston, T. and Pruitt, L. A. (2011). The use of polyacrylamide gels for mechanical calibration of cartilage--a combined nanoindentation and unconfined compression study. *J Mech Behav Biomed Mater* 4, 1540-1547.
- Li, C., Pruitt, L. A. and King, K. B. (2006). Nanoindentation differentiates tissue-scale functional properties of native articular cartilage. *J Biomed Mater Res A* 78, 729-738.

- Li, T. F., et al. (2010a). Aberrant hypertrophy in Smad3-deficient murine chondrocytes is rescued by restoring transforming growth factor beta-activated kinase 1/activating transcription factor 2 signaling: a potential clinical implication for osteoarthritis. *Arthritis Rheum* 62, 2359-2369.
- Li, Y., Xu, L. and Olsen, B. R. (2007a). Lessons from genetic forms of osteoarthritis for the pathogenesis of the disease. *Osteoarthritis Cartilage* 15, 1101-1105.
- Li, Z., Dranoff, J. A., Chan, E. P., Uemura, M., Sevigny, J. and Wells, R. G. (2007b). Transforming growth factor-beta and substrate stiffness regulate portal fibroblast activation in culture. *Hepatology* 46, 1246-1256.
- Li, Z., Kupcsik, L., Yao, S. J., Alini, M. and Stoddart, M. J. (2010b). Mechanical load modulates chondrogenesis of human mesenchymal stem cells through the TGF-beta pathway. *J Cell Mol Med* 14, 1338-1346.
- Lin, X., Liang, M. and Feng, X. H. (2000). Smurf2 is a ubiquitin E3 ligase mediating proteasome-dependent degradation of Smad2 in transforming growth factor-beta signaling. *J Biol Chem* 275, 36818-36822.
- Lin, Y. C., Tambe, D. T., Park, C. Y., Wasserman, M. R., Treppe, X., Krishnan, R., Lenormand, G., Fredberg, J. J. and Butler, J. P. (2010). Mechanosensing of substrate thickness. *Phys Rev E Stat Nonlin Soft Matter Phys* 82, 041918.
- Livak, K. J. and Schmittgen, T. D. (2001). Analysis of relative gene expression data using real-time quantitative PCR and the 2(-Delta Delta C(T)) Method. *Methods* 25, 402-408.
- Lo, C. M., Wang, H. B., Dembo, M. and Wang, Y. L. (2000). Cell movement is guided by the rigidity of the substrate. *Biophys J* 79, 144-152.
- Maekawa, M., et al. (1999). Signaling from Rho to the actin cytoskeleton through protein kinases ROCK and LIM-kinase. *Science* 285, 895-898.
- Mak, A. F., Lai, W. M. and Mow, V. C. (1987). Biphasic indentation of articular cartilage--I. Theoretical analysis. *J Biomech* 20, 703-714.
- Massague, J. (1998). TGF-beta signal transduction. *Annu Rev Biochem* 67, 753-791.
- Matukas, V. J., Panner, B. J. and Orbison, J. L. (1967). Studies on ultrastructural identification and distribution of protein-polysaccharide in cartilage matrix. *J Cell Biol* 32, 365-377.
- McBeath, R., Pirone, D. M., Nelson, C. M., Bhadriraju, K. and Chen, C. S. (2004). Cell shape, cytoskeletal tension, and RhoA regulate stem cell lineage commitment. *Dev Cell* 6, 483-495.
- McCormack, T. and Mansour, J. M. (1998). Reduction in tensile strength of cartilage precedes surface damage under repeated compressive loading in vitro. *J Biomech* 31, 55-61.
- Miranti, C. K. and Brugge, J. S. (2002). Sensing the environment: a historical perspective on integrin signal transduction. *Nat Cell Biol* 4, E83-90.
- Moriguchi, T., et al. (1996). A novel kinase cascade mediated by mitogen-activated protein kinase kinase 6 and MKK3. *J Biol Chem* 271, 13675-13679.
- Mow, V. C., Gibbs, M. C., Lai, W. M., Zhu, W. B. and Athanasiou, K. A. (1989). Biphasic indentation of articular cartilage--II. A numerical algorithm and an experimental study. *J Biomech* 22, 853-861.
- Mullen, A. C., et al. Master transcription factors determine cell-type-specific responses to TGF-beta signaling. *Cell* 147, 565-576.

- Munger, J. S., et al. (1999). The integrin alpha v beta 6 binds and activates latent TGF-beta 1: a mechanism for regulating pulmonary inflammation and fibrosis. *Cell* 96, 319-328.
- Munger, J. S. and Sheppard, D. (2011). Cross talk among TGF-beta signaling pathways, integrins, and the extracellular matrix. *Cold Spring Harb Perspect Biol* 3, (Epub).
- Mwale, F., Stachura, D., Roughley, P. and Antoniou, J. (2006). Limitations of using aggrecan and type X collagen as markers of chondrogenesis in mesenchymal stem cell differentiation. *J Orthop Res* 24, 1791-1798.
- Naito, K., Watari, T., Muta, T., Furuhashi, A., Iwase, H., Igarashi, M., Kurosawa, H., Nagaoka, I. and Kaneko, K. (2010). Low-intensity pulsed ultrasound (LIPUS) increases the articular cartilage type II collagen in a rat osteoarthritis model. *J Orthop Res* 28, 361-369.
- Nehrer, S., Breinan, H. A., Ramappa, A., Young, G., Shortkroff, S., Louie, L. K., Sledge, C. B., Yannas, I. V. and Spector, M. (1997). Matrix collagen type and pore size influence behaviour of seeded canine chondrocytes. *Biomaterials* 18, 769-776.
- Nishikori, T., Ochi, M., Uchio, Y., Maniwa, S., Kataoka, H., Kawasaki, K., Katsube, K. and Kuriwaka, M. (2002). Effects of low-intensity pulsed ultrasound on proliferation and chondroitin sulfate synthesis of cultured chondrocytes embedded in Atelocollagen gel. *J Biomed Mater Res* 59, 201-206.
- Nofal, G. A. and Knudson, C. B. (2002). Latrunculin and cytochalasin decrease chondrocyte matrix retention. *J Histochem Cytochem* 50, 1313-1324.
- Oyen, M., Cook, R. F., Emerson, J. A. and Moody, N. R. (2004). Indentation responses of time-dependent films on stiff substrates. *J. Mater. Res.* 19, 2487-3121.
- Park, J. S., Chu, J. S., Tsou, A. D., Diop, R., Tang, Z., Wang, A. and Li, S. (2011). The effect of matrix stiffness on the differentiation of mesenchymal stem cells in response to TGF-beta. *Biomaterials* 32, 3921-3930.
- Parkkinen, J. J., Lammi, M. J., Helminen, H. J. and Tammi, M. (1992). Local stimulation of proteoglycan synthesis in articular cartilage explants by dynamic compression in vitro. *J Orthop Res* 10, 610-620.
- Parvizi, J., Wu, C. C., Lewallen, D. G., Greenleaf, J. F. and Bolander, M. E. (1999). Low-intensity ultrasound stimulates proteoglycan synthesis in rat chondrocytes by increasing aggrecan gene expression. *J Orthop Res* 17, 488-494.
- Paszek, M. J., et al. (2005). Tensional homeostasis and the malignant phenotype. *Cancer Cell* 8, 241-254.
- Patel, S., Kurpinski, K., Quigley, R., Gao, H., Hsiao, B. S., Poo, M. M. and Li, S. (2007). Bioactive nanofibers: synergistic effects of nanotopography and chemical signaling on cell guidance. *Nano Lett* 7, 2122-2128.
- Pujol, J. P., Chadjichristos, C., Legendre, F., Bauge, C., Beauchef, G., Andriamanalijaona, R., Galera, P. and Boumediene, K. (2008). Interleukin-1 and transforming growth factor-beta 1 as crucial factors in osteoarthritic cartilage metabolism. *Connect Tissue Res* 49, 293-297.
- Qiao, B., Padilla, S. R. and Benya, P. D. (2005). Transforming growth factor (TGF)-beta-activated kinase 1 mimics and mediates TGF-beta-induced stimulation of type II collagen synthesis in chondrocytes independent of Col2a1 transcription and Smad3 signaling. *J Biol Chem* 280, 17562-17571.

- Reinhart-King, C. A., Dembo, M. and Hammer, D. A. (2005). The dynamics and mechanics of endothelial cell spreading. *Biophys J* 89, 676-689.
- Roth, V. and Mow, V. C. (1980). The intrinsic tensile behavior of the matrix of bovine articular cartilage and its variation with age. *J Bone Joint Surg Am* 62, 1102-1117.
- Saarakkala, S., Julkunen, P., Kiviranta, P., Makitalo, J., Jurvelin, J. S. and Korhonen, R. K. (2010). Depth-wise progression of osteoarthritis in human articular cartilage: investigation of composition, structure and biomechanics. *Osteoarthritis Cartilage* 18, 73-81.
- Sabatini, M., Pastoureaux, P. and De Ceuninck, F., Eds. (2004). Cartilage and Osteoarthritis. Methods in Molecular Medicine. Totowa, Humana Press.
- Saeki, K., Hilton, J. F., Alliston, T., Habelitz, S., Marshall, S. J., Marshall, G. W. and DenBesten, P. (2007). Elevated TGF-beta2 signaling in dentin results in sex related enamel defects. *Arch Oral Biol* 52, 814-821.
- Sakai, K., Mohtai, M. and Iwamoto, Y. (1998). Fluid shear stress increases transforming growth factor-beta 1 expression in human osteoblast-like cells: modulation by cation channel blockades. *Calcif Tissue Int* 63, 515-520.
- Sasaki, A., Masuda, Y., Ohta, Y., Ikeda, K. and Watanabe, K. (2001). Filamin associates with Smads and regulates transforming growth factor-beta signaling. *J Biol Chem* 276, 17871-17877.
- Schinagl, R. M., Gurskis, D., Chen, A. C. and Sah, R. L. (1997). Depth-dependent confined compression modulus of full-thickness bovine articular cartilage. *J Orthop Res* 15, 499-506.
- Schinagl, R. M., Ting, M. K., Price, J. H. and Sah, R. L. (1996). Video microscopy to quantitate the inhomogeneous equilibrium strain within articular cartilage during confined compression. *Ann Biomed Eng* 24, 500-512.
- Schulze-Tanzil, G., de Souza, P., Villegas Castrejon, H., John, T., Merker, H. J., Scheid, A. and Shakibaei, M. (2002). Redifferentiation of dedifferentiated human chondrocytes in high-density cultures. *Cell Tissue Res* 308, 371-379.
- Serra, R., Johnson, M., Filvaroff, E. H., LaBorde, J., Sheehan, D. M., Derynck, R. and Moses, H. L. (1997). Expression of a truncated, kinase-defective TGF-beta type II receptor in mouse skeletal tissue promotes terminal chondrocyte differentiation and osteoarthritis. *J Cell Biol* 139, 541-552.
- Serra, R., Karaplis, A. and Sohn, P. (1999). Parathyroid hormone-related peptide (PTHrP)-dependent and -independent effects of transforming growth factor beta (TGF-beta) on endochondral bone formation. *J Cell Biol* 145, 783-794.
- Seto, H., et al. (2004). Distinct roles of Smad pathways and p38 pathways in cartilage-specific gene expression in synovial fibroblasts. *J Clin Invest* 113, 718-726.
- Setton, L. A., Elliott, D. M. and Mow, V. C. (1999). Altered mechanics of cartilage with osteoarthritis: human osteoarthritis and an experimental model of joint degeneration. *Osteoarthritis Cartilage* 7, 2-14.
- Shao, H. J., Ho, C. C., Lee, Y. T., Chen, C. S., Wang, J. H. and Young, T. H. (2012). Chondrogenesis of human bone marrow mesenchymal cells by transforming growth factors beta1 through cell shape changes on controlled biomaterials. *J Biomed Mater Res A*

- Shieh, A. C. and Athanasiou, K. A. (2003). Principles of cell mechanics for cartilage tissue engineering. *Ann Biomed Eng* 31, 1-11.
- Smith, R. L., et al. (1995). Effects of fluid-induced shear on articular chondrocyte morphology and metabolism in vitro. *J Orthop Res* 13, 824-831.
- Sneddon, I. N. (1965). The relationship between load and penetration in the axisymmetric boussinesq problem for a punch of arbitrary profile. *Int J Engng Sci* 3, 47-57.
- Stanton, L. A., Underhill, T. M. and Beier, F. (2003). MAP kinases in chondrocyte differentiation. *Dev Biol* 263, 165-175.
- Stolz, M., et al. (2009). Early detection of aging cartilage and osteoarthritis in mice and patient samples using atomic force microscopy. *Nat Nanotechnol* 4, 186-192.
- Streuli, C. H., Schmidhauser, C., Kobrin, M., Bissell, M. J. and Derynck, R. (1993). Extracellular matrix regulates expression of the TGF-beta 1 gene. *J Cell Biol* 120, 253-260.
- Takahashi, T., Ogasawara, T., Asawa, Y., Mori, Y., Uchinuma, E., Takato, T. and Hoshi, K. (2007). Three-dimensional microenvironments retain chondrocyte phenotypes during proliferation culture. *Tissue Eng* 13, 1583-1592.
- Tang, S. Y., Mathews, P., Randall, C., Yurtsev, E., Fields, K., Wong, A., Kuo, A., Alliston, T. and Hansma, P. (2010). In situ Materials Characterization using the Tissue Diagnostic Instrument. *Polym Test* 29, 159-163.
- Thirion, S. and Berenbaum, F. (2004). Culture and phenotyping of chondrocytes in primary culture. *Methods Mol Med* 100, 1-14.
- Tomasek, J. J., Gabbiani, G., Hinz, B., Chaponnier, C. and Brown, R. A. (2002). Myofibroblasts and mechano-regulation of connective tissue remodelling. *Nat Rev Mol Cell Biol* 3, 349-363.
- Tuli, R., Tuli, S., Nandi, S., Huang, X., Manner, P. A., Hozack, W. J., Danielson, K. G., Hall, D. J. and Tuan, R. S. (2003). Transforming growth factor-beta-mediated chondrogenesis of human mesenchymal progenitor cells involves N-cadherin and mitogen-activated protein kinase and Wnt signaling cross-talk. *J Biol Chem* 278, 41227-41236.
- van de Laar, I. M., et al. (2011). Mutations in SMAD3 cause a syndromic form of aortic aneurysms and dissections with early-onset osteoarthritis. *Nat Genet* 43, 121-126.
- van der Kraan, P. M., Blaney Davidson, E. N., Blom, A. and van den Berg, W. B. (2009). TGF-beta signaling in chondrocyte terminal differentiation and osteoarthritis: modulation and integration of signaling pathways through receptor-Smads. *Osteoarthritis Cartilage* 17, 1539-1545.
- Varelas, X., Sakuma, R., Samavarchi-Tehrani, P., Peerani, R., Rao, B. M., Dembowy, J., Yaffe, M. B., Zandstra, P. W. and Wrana, J. L. (2008). TAZ controls Smad nucleocytoplasmic shuttling and regulates human embryonic stem-cell self-renewal. *Nat Cell Biol* 10, 837-848.
- Veilleux, N. H., Yannas, I. V. and Spector, M. (2004). Effect of passage number and collagen type on the proliferative, biosynthetic, and contractile activity of adult canine articular chondrocytes in type I and II collagen-glycosaminoglycan matrices in vitro. *Tissue Eng* 10, 119-127.
- von der Mark, K., Gauss, V., von der Mark, H. and Muller, P. (1977). Relationship between cell shape and type of collagen synthesised as chondrocytes lose their cartilage phenotype in culture. *Nature* 267, 531-532.

- Wang, C. C., Deng, J. M., Ateshian, G. A. and Hung, C. T. (2002). An automated approach for direct measurement of two-dimensional strain distributions within articular cartilage under unconfined compression. *J Biomech Eng* 124, 557-567.
- Wang, C. C., Hung, C. T. and Mow, V. C. (2001). An analysis of the effects of depth-dependent aggregate modulus on articular cartilage stress-relaxation behavior in compression. *J Biomech* 34, 75-84.
- Wang, G., Woods, A., Sabari, S., Pagnotta, L., Stanton, L. A. and Beier, F. (2004). RhoA/ROCK signaling suppresses hypertrophic chondrocyte differentiation. *J Biol Chem* 279, 13205-13214.
- Wang, H. B., Dembo, M. and Wang, Y. L. (2000). Substrate flexibility regulates growth and apoptosis of normal but not transformed cells. *Am J Physiol Cell Physiol* 279, C1345-1350.
- Wang, J. H. and Thampatty, B. P. (2006). An introductory review of cell mechanobiology. *Biomech Model Mechanobiol* 5, 1-16.
- Wang, M., Shen, J., Jin, H., Im, H. J., Sandy, J. and Chen, D. (2011a). Recent progress in understanding molecular mechanisms of cartilage degeneration during osteoarthritis. *Ann N Y Acad Sci* 1240, 61-69.
- Wang, Y. K., Yu, X., Cohen, D. M., Wozniak, M. A., Yang, M. T., Gao, L., Eyckmans, J. and Chen, C. S. (2011b). Bone Morphogenetic Protein-2-Induced Signaling and Osteogenesis Is Regulated by Cell Shape, RhoA/ROCK, and Cytoskeletal Tension. *Stem Cells Dev* (Epub).
- Wang, Y. L. and Pelham, R. J., Jr. (1998). Preparation of a flexible, porous polyacrylamide substrate for mechanical studies of cultured cells. *Methods Enzymol* 298, 489-496.
- Watanabe, H., de Caestecker, M. P. and Yamada, Y. (2001). Transcriptional cross-talk between Smad, ERK1/2, and p38 mitogen-activated protein kinase pathways regulates transforming growth factor-beta-induced aggrecan gene expression in chondrogenic ATDC5 cells. *J Biol Chem* 276, 14466-14473.
- Wells, R. G. (2008). The role of matrix stiffness in regulating cell behavior. *Hepatology* 47, 1394-1400.
- Wells, R. G. and Discher, D. E. (2008). Matrix elasticity, cytoskeletal tension, and TGF-beta: the insoluble and soluble meet. *Sci Signal* 1, 13.
- Wiersma, J. A., Bos, M. and Pennings, A. J. (1994). High strength poly(meth)acrylamide copolymer hydrogels. *Polymer Bulletin* 33, 615-622.
- Williamson, A. K., Chen, A. C. and Sah, R. L. (2001). Compressive properties and function-composition relationships of developing bovine articular cartilage. *J Orthop Res* 19, 1113-1121.
- Wilson, W., Huyghe, J. M. and van Donkelaar, C. C. (2007). Depth-dependent compressive equilibrium properties of articular cartilage explained by its composition. *Biomech Model Mechanobiol* 6, 43-53.
- Wipff, P. J., Rifkin, D. B., Meister, J. J. and Hinz, B. (2007). Myofibroblast contraction activates latent TGF-beta1 from the extracellular matrix. *J Cell Biol* 179, 1311-1323.
- Woo, S. L., Simon, B. R., Kuei, S. C. and Akeson, W. H. (1980). Quasi-linear viscoelastic properties of normal articular cartilage. *J Biomech Eng* 102, 85-90.

- Woods, A. and Beier, F. (2006). RhoA/ROCK signaling regulates chondrogenesis in a context-dependent manner. *J Biol Chem* 281, 13134-13140.
- Woods, A., Wang, G. and Beier, F. (2005). RhoA/ROCK signaling regulates Sox9 expression and actin organization during chondrogenesis. *J Biol Chem* 280, 11626-11634.
- Woods, A., Wang, G. and Beier, F. (2007). Regulation of chondrocyte differentiation by the actin cytoskeleton and adhesive interactions. *J Cell Physiol* 213, 1-8.
- Wrana, J. L. (2000). Regulation of Smad activity. *Cell* 100, 189-192.
- Wu, C. C., Chao, Y. C., Chen, C. N., Chien, S., Chen, Y. C., Chien, C. C., Chiu, J. J. and Linju Yen, B. (2008). Synergism of biochemical and mechanical stimuli in the differentiation of human placenta-derived multipotent cells into endothelial cells. *J Biomech* 41, 813-821.
- Wu, J. Z. and Herzog, W. (2002). Elastic anisotropy of articular cartilage is associated with the microstructures of collagen fibers and chondrocytes. *J Biomech* 35, 931-942.
- Yang, X., Chen, L., Xu, X., Li, C., Huang, C. and Deng, C. X. (2001). TGF-beta/Smad3 signals repress chondrocyte hypertrophic differentiation and are required for maintaining articular cartilage. *J Cell Biol* 153, 35-46.
- Yeung, T., et al. (2005). Effects of substrate stiffness on cell morphology, cytoskeletal structure, and adhesion. *Cell Motil Cytoskeleton* 60, 24-34.
- Zawel, L., Dai, J. L., Buckhaults, P., Zhou, S., Kinzler, K. W., Vogelstein, B. and Kern, S. E. (1998). Human Smad3 and Smad4 are sequence-specific transcription activators. *Mol Cell* 1, 611-617.
- Zhang, X., Ziran, N., Goater, J. J., Schwarz, E. M., Puzas, J. E., Rosier, R. N., Zuscik, M., Drissi, H. and O'Keefe, R. J. (2004). Primary murine limb bud mesenchymal cells in long-term culture complete chondrocyte differentiation: TGF-beta delays hypertrophy and PGE2 inhibits terminal differentiation. *Bone* 34, 809-817.
- Zhang, Y., Chang, C., Gehling, D. J., Hemmati-Brivanlou, A. and Derynck, R. (2001). Regulation of Smad degradation and activity by Smurf2, an E3 ubiquitin ligase. *Proc Natl Acad Sci U S A* 98, 974-979.

APPENDIX A

JOURNAL OF THE MECHANICAL BEHAVIOR OF BIOMEDICAL MATERIALS 4 (2011) 1540–1547



available at www.sciencedirect.com



journal homepage: www.elsevier.com/locate/jmbbm



Technical note

The use of polyacrylamide gels for mechanical calibration of cartilage — A combined nanoindentation and unconfined compression study

Cheng Li^{a,*}, Jessica Allen^a, Tamara Alliston^{b,a}, Lisa A. Pruitt^{c,a}

^aUCSF and UC Berkeley Joint Graduate Group in Bioengineering, University of California, Berkeley, CA, 94720, United States

^bDepartment of Orthopaedic Surgery, University of California, San Francisco, SF, CA, 94143, United States

^cDepartment of Mechanical Engineering, University of California, Berkeley, Berkeley, CA, 94720, United States

ARTICLE INFO

Article history:

Received 6 November 2009

Received in revised form

4 February 2011

Accepted 8 February 2011

Published online 24 February 2011

Keywords:

Nanoindentation

Unconfined compression

Biomaterials

Soft tissues

Mechanics

Cartilage

Polyacrylamide gels

Mechanical calibration

ABSTRACT

This study investigates polyacrylamide (PA) gel as a calibration material to measure the nanomechanical compressive modulus of cartilage using nanoindentation. Both nanoindentation and unconfined compression testing were performed on PA gel and porcine rib cartilage. The equilibrium moduli measured by the two methods were discernable. Nanoindentation has the advantage of distinguishing between spatially dependent constituent properties that affect tissue mechanical function in heterogeneous and hierarchically structured tissues such as cartilage. Both sets of measurements exhibited similar positive correlation with increasing gel crosslinker concentration. The compressive modulus measurements from compression in the PA gels ranged from 300 kPa–1.4 MPa, whereas those from nanoindentation ranged from 100 kPa–1.1 MPa. Using this data, a method for relating nanoindentation measurements to conventional mechanical property measurements is presented for porcine rib cartilage. It is shown that based on this relationship, the local tissue modulus as measured from nanoindentation (1.1–1.4 MPa) was able to predict the overall global modulus of the same sample of rib cartilage (2.2 MPa), as confirmed by experimental measurements from unconfined compression. This study supports the use of nanoindentation for the local characterization of cartilage tissues and may be applied to other soft tissues and constructs.

Published by Elsevier Ltd

1. Introduction

The complex structures and heterogeneity of cartilage presents challenges to characterizing its material properties. Commonly employed mechanical tests, such as confined

and unconfined compression, at best treat the tissue as a poroelastic, multi-phasic, isotropic material (Armstrong and Mow, 1982; Athanasiou et al., 1994; Kempson et al., 1971; Sokoloff, 1966; Hayes and Mockros, 1971). These methods give information about the global behavior of the tissue as

* Corresponding address: UCSF and UC Berkeley Joint Graduate Program in Bioengineering, 2121 Etcheverry Hall, University of California, Berkeley, CA 94720, United States. Tel.: +1 510 457 5683, +1 650 587 1513.

E-mail address: limeow@gmail.com (C. Li).

1751-6161/\$ - see front matter. Published by Elsevier Ltd

doi:10.1016/j.jmbbm.2011.02.004

described by, for example, the equilibrium aggregate modulus and the time constant (Mow et al., 1980). Further, these experiments are limited in revealing and characterizing a micrometer length scale (a few μm to hundreds of μm) structure–property relationships key to cartilage function. There is a strong need for more in-depth knowledge of the *in-situ* local tissue properties in a spatially-dependent manner. This would help resolve the mechanical contributions from the spatially varied structural and constituent units to the overall behavior and function of cartilage.

Local mechanical characterization of articular cartilage exploring multi-scale structure–property relationships has been limited due to a number of factors. Such factors include the paucity of mechanical tools that facilitate these measurements, the development of appropriate testing and analysis techniques, as well as the identification of materials that can serve as baseline measures for such systems. In the last decade nanoindentation has evolved as a promising tool for structure–property characterization of tissues and soft biomaterials (Kaufman et al., 2007; Ebenstein et al., 2004; Franke et al., 2007; Gupta et al., 2005; Ferguson et al., 2003; Gupta et al., 2007; Li et al., 2006; Akhtar et al., 2009; Chaudhry et al., 2009). Studies have addressed a number of important factors in nanomechanical testing methodology including large deformations, surface detection, adhesion, hydration, surface roughness and time-dependent behavior (Ebenstein et al., 2004; Gupta et al., 2007; Li et al., 2006; Ebenstein and Pruitt, 2006; Ebenstein and Wahl, 2006; Hansma et al., 2009; Kesari et al., 2010; Donnelly et al., 2006). Nanoindentation analysis typically relies on applying Hertz contact theory to a material volume under the probe with the assumptions of material homogeneity, isotropy, and linearly elastic or elastic–plastic material response. Application of the appropriate indenter tip size and geometry, as well as the indentation protocol can be used to target localized material volumes of interest, and isolate steady state material matrix properties. For example, a 100 μm ideal conospherical tip can effectively target a region with a contact diameter of 30–50 μm at 1–3 μm of penetration depth. This may be appropriate for probing, for example, particular cellular regions within cartilage zones, or of the extracellular matrix of cartilage. It is important to note that in indenting, soft tissues like cartilage have inherent surface roughness due to natural grooves, protrusions, and pockets from protein components and cellular regions (tens of micrometers in wavelength and several micrometers in amplitude) (Mow et al., 1992). These micro- and nano-scale roughness features deform and release pockets of fluid to provide lubrication (Walker et al., 1968; Hou et al., 1990) or to support other essential tissue functions. In indentation of soft tissues, these surface roughness features yield easily during initial loading (and conform to the rigid indenter with contact diameters of 40–50 μm) as fluid is pushed out and before the tissue volume can sustain significant load. Therefore the “roughness” of hydrated soft materials under indentation does not contribute significantly to the differences in contact area and load–displacement data, but rather can be considered as another aspect of tissue heterogeneity that contributes to variation in the measurement. Similar to creep and stress relaxation experiments described by Mow et al. (1980), the nanoindentation technique can be

controlled to rid the fluid flux-driven time-dependent behavior and capture solid matrix properties in a solid–fluid biphasic material. However, cartilage, like most soft biomaterials, has more complex behavior than can be fully described by current material models, particularly at the micrometer and smaller length scales where conventional continuum mechanics assumptions do not necessarily apply. Moreover, the complex stress field in the cartilage under the indenter tip is not fully understood. Given these limitations associated with applying the nanoindentation technique to soft biomaterials, the measurements are not true material properties, but rather are relative measures for making comparisons and discoveries. The measured modulus may be interpreted as an *in-situ* tissue modulus distinct from the global elastic modulus of the entire tissue structure as measured by conventional large-scale mechanical testing.

A challenge in developing a protocol for nanomechanical characterization of cartilage is the availability of a control material. An appropriate reference material is one whose physical and mechanical properties resemble that of cartilage but are controllable and predictable, and hence can be more consistently characterized. Previous investigators have utilized agarose gels to serve as a reference material for soft biomaterials and biological tissues (Ebenstein and Pruitt, 2006; Scandiucci de Freitas et al., 2006; Li, 2008). However, not only are the microstructures of agarose gels variable depending on the natural source of the agarose powder and method of gel preparation, they are also unstable and susceptible to degradation within a few days owing to disentanglement of its physical chain network (Scandiucci de Freitas et al., 2006; Stolz et al., 2004; Normand et al., 2000). An alternative material, polyacrylamide (PA) gel used commonly in biological research (Hansma et al., 2009) is a synthetic chemical compound that solidifies to form one large chemically crosslinked molecule that is more stable compared to agarose gel and from our experience is able to retain its mechanical integrity for well over a week. PA gels can also be tailored to span the elastic moduli range of 0.2 MPa to over 1 MPa, which is within the modulus range of cartilage tissue (Mow et al., 1980; Kleeemann et al., 2005; Kiviranta et al., 2008). This study proposes to use PA gels as a reference material for the mechanical characterization of cartilage and other soft biomaterials. We hypothesize that there is a link between the material and its structural and compositional units and that there is a relationship relating the global elastic modulus and the nanoindentation derived tissue modulus. The goal of this pilot study is to propose a method using mechanically graded polyacrylamide gels against which nanoindentation of cartilage and other complex soft biomaterials can be calibrated.

2. Materials and methods

2.1. Polyacrylamide gels

Materials for making polyacrylamide (PA) gels were obtained from Bio-Rad (Hercules, CA). For this study, the monomer acrylamide concentration of each gel was held constant (at 20% or 30% w/v) while the Piperazine diacrylamide (PDA) crosslinker concentration was varied from 0.5% to 3% w/v.

Table 1 – Gel composition and test scheme of polyacrylamide gel specimens.

Gel type	%w/v Acrylamide	%w/v PDA	Nanoindentation	Compression
20:0.5	20	0.5	×	×
20:1.5	20	1.5	×	×
20:2	20	2	×	×
20:2.5	20	2.5	×	n/a
30:1	30	1	×	×
30:2	30	2	×	×
30:3	30	3	×	×

The unit w/v is measured in grams of solute per mL of solution, and is commonly used in chemistry to represent the concentration of a solution. A summary of the PA gels and the test schemes is provided in Table 1. The desired acrylamide and piperazine diacrylamide volumes were added to a solution containing a 0.01 M Hepes Buffer (pH 8.5) and TEMED (1/2000 dilution) in deionized water. The Hepes solution was vortexed for 30 s and degassed in a vacuum chamber for 1 h. To initiate the polymerization reaction, 10% (w/v) ammonium persulfate solution was added to the degassed mixture at a 1/200 dilution (final conc. 0.05% (w/v)). The solution was carefully mixed with a pipette and then poured into a vertical mold that was 7 cm by 8 cm in width and height respectively and approximately 1 mm in thickness. Gels were stored in the 0.01 M Hepes solution overnight at 4 °C before testing. For each gel formulation, 3–5 specimens were cut from the gel slab with a 6 mm cylindrical punch and then subjected to unconfined compression. In addition, each gel formulation was subjected to 7 or more indents using nanoindentation (described below).

2.2. Porcine cartilage

Fresh rib cartilage was obtained from a local abattoir and immediately dissected. Cylindrical specimens of porcine cartilage ($n = 4$) were obtained with biopsy punches. These specimens were 6.8 mm in diameter and 4–6 mm in thickness and were taken from porcine rib cartilage slices in the sagittal plane and subsequently stored in phosphate buffered saline (PBS) at 4°C until use. The rib cartilage disks excluded the bone. The disks were tested as soon as they were dissected; however, storage times varied from one to three days due to schedule constraints around completing unconfined compression and nanoindentation tests on the same specimens. Four specimens were tested in unconfined compression, and on one of these specimens, 17 indents were performed using nanoindentation. Only one specimen was tested using nanoindentation because it was decided a priori that the nanoindentation data should be collected within 24 h of bulk testing. This takes into consideration accelerated tissue degradation *ex vivo*.

2.3. Unconfined compression tests

The compression loading protocols were fine-tuned for either the gel or cartilage in order to minimize testing time and to span the relevant linear stress–strain regions. The Bose Electroforce 3200 mechanical test system (Bose Corporation, Eden Prairie, MN) was used for unconfined compression. A 10 N load cell and two custom compression platens 2 cm

in diameter were used to test the delicate gel samples. Each PA gel was immersed in Hepes buffer (0.01 M, pH 8.5) and loaded between the two metal platens at room temperature. Contact was established at 0.1–0.2 N of preload. Each gel sample was ramp loaded at 0.02 mm/s at each of the 1% strain steps (~0.01 mm in displacement) up to a total strain of 8%, and allowed to relax at each step for up to 360 s. The gel samples were more delicate and prone to fracture compared to the harvested cartilage samples. Therefore, the loading protocol—pre-load, strain rate, total strain, and time of relaxation, were optimized specifically to measure the equilibrium stresses for the gel and cartilage samples in their respective linear loading regimes. To accommodate testing of the cartilage samples, a higher 450 N load cell and larger platens 5 cm in diameter were used. Initial sample contact with platens was established at 0.7–0.8 N of preload. Each cartilage specimen was ramp loaded at 0.008 mm/s through three 5% strain steps (~0.25 mm in displacement) up to a total strain of 15%, and allowed to relax at each step for up to 600 s. The loading schemes and relaxation responses are illustrated in Fig. 1, and the load relaxation response at each step was verified to reach a load decay rate of at least 0.03 N/s. Stresses and strains at the end of the relaxation periods were captured and graphed on a stress–strain plot. The equilibrium modulus was defined as the best-fit linear slope of the stress versus strain data. The R squared values of the curve fit ranged from 0.97 to 0.99.

2.4. Nanoindentation tests

Nanoindentation was performed using a Hysitron TriboIndenter (Hysitron Inc., Minneapolis, MN) with a 100 μ m cono-spherical diamond fluid tip. The indenter tip is connected to the transducer, which was displacement-controlled, and data is presented as load versus displacement plots for loading, hold, and unloading. For all samples, indentation started with the nanoindenter tip approaching the sample from off-contact. The sample surface was clearly evident as seen by the rapid increase in load with displacement (Li, 2008). Typical nanoindentation load and displacement data for gel and cartilage are shown in Fig. 2.

The total displacements into the sample ranged from 2000 to 3000 nm with relaxation times of at least 30 s at maximum displacement. The loading rates ranging from 500 nm/s and 2000 nm/s was found to not affect the relaxation behavior. Hence data from all loading curves were used to calculate the quasi-equilibrium modulus. The Hertz equilibrium modulus is defined as:

$$E_H = \frac{3P_{eq}}{4\sqrt{R}h_{eq}^{\frac{3}{2}}} \quad (1)$$

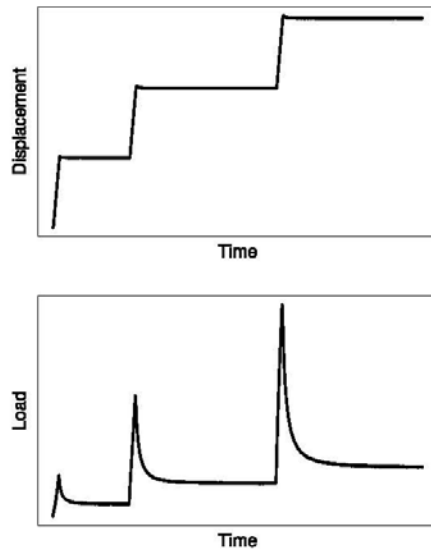


Fig. 1 - Representation of a loading scheme consisting of three sequential loading steps (top) and their corresponding load relaxation response over time (bottom) during unconfined compression. The loading schemes for PA gel and cartilage samples were each tailored to their properties and geometry. Gel sample: linear loading range = 8% strain, loading step = 1% strain increments, ramp rate = 0.02 mm/s, hold time = 360 s. Cartilage sample: linear loading range = 15% strain, loading step = 5% strain, ramp rate = 0.008 mm/s, hold time = 600 s.

where P_{eq} is the quasi-equilibrium load, h_{eq} is the corresponding displacement, and R is the radius of curvature of the spherical indenter (Hertz, 1881). The elastic modulus is related to E_H as

$$E = E_H(1 - \nu^2) \quad (2)$$

where ν is the Poisson's ratio of the specimen and is assumed a value of 0.499, that of an incompressible material. The stress relaxation segment of load versus time data was fitted with a power law function and the theoretical equilibrium load was determined from the curve fit. The goodness-of-fit was calculated as the R squared value and ranged from 0.62 to 0.98. The load decay rate for gel at the end of the hold step was on the order of 0.1 $\mu\text{N/s}$, whereas that for cartilage ranged from orders of 0.1 to 1 $\mu\text{N/s}$.

3. Results and discussion

3.1. Polyacrylamide gel data

The equilibrium compressive modulus for the seven gel types spanning a range of crosslinker content were measured using unconfined compression and nanoindentation. These results are plotted in Fig. 3 and also summarized in Table II. The results demonstrate controllable mechanical properties

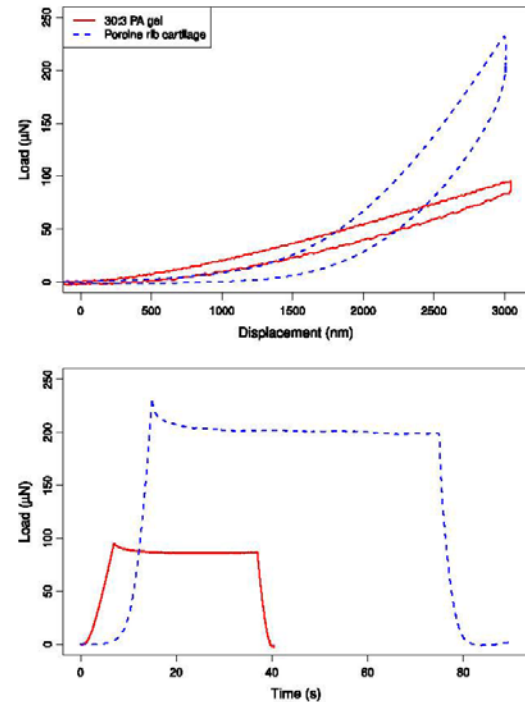


Fig. 2 - Representative load vs. displacement data (top) and load vs. time data (bottom) for PA gel and cartilage during nanoindentation.

within the linear range of stress-strain behavior for the PA gels with the range of crosslinker concentrations. The range of elastic modulus from unconfined compression for the gels was 0.3-1.4 MPa while that from nanoindentation was 0.1-1.1 MPa (Table 2). These values are comparable to both engineered cartilage constructs (Martinez-Diaz et al., 2010; Katakai et al., 2009) and native cartilage tissues (Kempson et al., 1971; Mow et al., 1980; Kleemann et al., 2005; Kiviranta et al., 2008).

The equilibrium modulus values of the PA gels were found to be stable over the two-week time frame without any degradation in the modulus (Li, 2008). The results of these modulus measurements support the premise that PA gels can be prepared with homogeneous microstructures that are reproducible (Normand et al., 2000; Peyton and Putnam, 2005). Moreover, the chemically crosslinked microstructure (Peyton and Putnam, 2005) offers a much greater consistency and stability than was found in agarose gels. These results suggest that PA gel would be an excellent control material for characterization of cartilage tissue modulus as in evaluating diseased cartilage or tissue engineering constructs.

As shown in Fig. 3, the trend of increasing equilibrium modulus with greater crosslinker concentration is consistent in unconfined compression and nanoindentation data. The modulus values measured by unconfined compression are higher than those from nanoindentation tests. However at the higher crosslinker concentration, the modulus values from the two methods appear to deviate from the linear

Table 2 – Summary of mean (SD) of equilibrium modulus of PA gel and porcine cartilage measured from unconfined compression and nanoindentation.

Gel sample	Unconfined compression modulus (MPa) Mean (SD), n = 3	Nanoindentation modulus (MPa) Mean (SD), k ≥ 7
20:0.5	0.3 (0.07)	0.1 (0.08)
20:1.5	0.5 (0.16)	0.3 (0.03)
20:2	0.8 (0.16)	0.3 (0.03)
20:2.5	N/A	0.5 (0.02)
30:1	0.5 (0.07)	0.2 (0.03)
30:2	1.2 (0.1)	0.5(0.03)
30:3	1.4 (0.06)	1.1 (0.08)
Porcine rib cartilage sample	Mean (SD), n = 4	Mean (SD), k = 17
A	2.2 (0.3)	2.7 (1.0)

n = number of samples of gel or cartilage, k = number of indents.

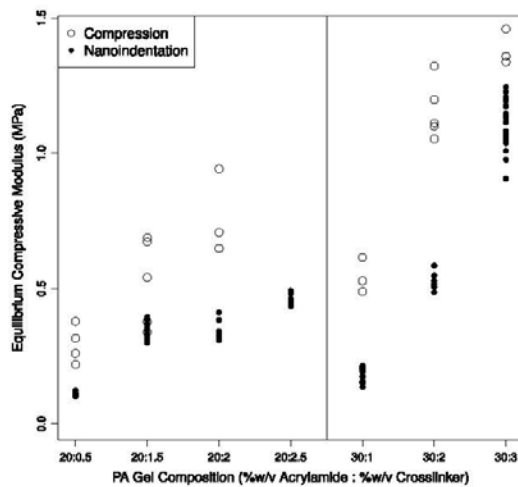


Fig. 3 – Comparison of equilibrium modulus values for the polyacrylamide gel types from unconfined compression and from nanoindentation. The vertical line helps to visually separate the 20% PA gel data on the left and the 30% PA gel data on the right.

correlation, possibly due to the saturation of crosslinks within the polymer network. Also, over the range of crosslinking, there is a smaller variation in nanoindentation measurements of the equilibrium modulus than for the bulk compression tests. However this is not consistent in all PA gel formulations. This could point to the relatively greater homogeneous material properties at the local level of an area of tens of squared micrometers due to a locally uniform microstructure, compared to the global properties of an area of tens of squared millimeters. However, the difference in the variation is also likely due to the variations intrinsic to the selected test method and its execution. Since the relaxation states of samples in this study are comparable based on load decay measurement at the assumed steady state, the authors do not believe that the relaxation states of the tissue are responsible for the higher mean values for unconfined compression compared to nanoindentation. The data from unconfined compression equilibrium reached a

lower decay rate (0.03 N/s) following relaxation from peak loads of several Newtons in PA gels (tens of Newtons in cartilage samples) than the decay rate (0.1 μ N/s) reached by data from nanoindentation following stress relaxation from peak loads of tens of μ N in PA gels (hundreds of μ N in cartilage samples).

Based on the mean values of quasi-equilibrium modulus measured by nanoindentation and unconfined compression, a calibration curve, as shown in Fig. 4, was plotted which converts the local modulus to the global modulus of the material. Fitting this data to a log function produced a quantitative relationship with a Pearson's correlation coefficient R of 0.94 for the PA gel measurements. This suggests that the local and global properties of the gels are distinguishable, with the local measurements collectively contributing to the overall tissue modulus. This also validates that the assumptions of material isotropy, homogeneity, and elasticity are satisfied in the case of PA gels for both nanoindentation and unconfined compression. This calibration curve is unique in that it can relate measures of local heterogeneities to an averaged global measure of the material as a whole.

It should be noted that for the 20:1.5 PA gel, the unconfined compression data deviated further from the curve fit than other data points. Nanoindentation did not discriminate the local compressive modulus of this gel formulation from that of the next higher crosslinker concentration. This suggests that fundamental differences in the local vs. global properties can perhaps be further clarified by using both of these complimentary measurement techniques. However, as noted above, overall trends in both unconfined and nanoindentation modulus measurements of the 20% w/v PA gel formulations indicate a plateau in the equilibrium modulus at higher crosslinker concentrations. Further studies with higher concentrations of the acrylamide gel formulations with various crosslinker concentrations will elucidate material property changes at crosslinker saturation levels.

3.2. Porcine cartilage data

The quasi-equilibrium modulus values of porcine rib cartilage were measured using the unconfined compression and nanoindentation test protocols described above. Four specimens of porcine rib cartilage were measured by

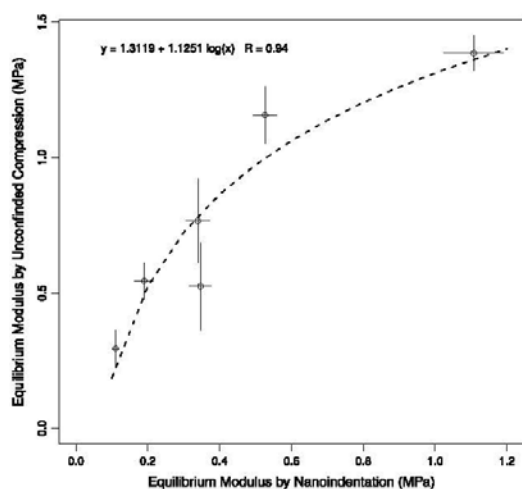


Fig. 4 – Mean (SD) equilibrium modulus values measured by nanoindentation vs. Mean (SD) equilibrium modulus values from unconfined compression fit to a log function. The equation for the fit is determined to be: $y = 1.3119 + 1.1251 \log(x)$, where y is the equilibrium modulus measured by unconfined compression, and x is that measured by nanoindentation.

unconfined compression, and one of these specimens, with a measured modulus of 2.2 MPa using unconfined compression, was further subjected to nanoindentation testing. The results of the unconfined compression and nanoindentation tests are provided in Fig. 5. The average equilibrium modulus for the unconfined compression tests was 2.2 MPa (ranging from 1.8–2.6 MPa) while for the nanoindentation tests it was 2.7 MPa (ranging from 1.1–4.4 MPa).

Unlike articular cartilage, porcine rib cartilage is known to be a generally more homogeneous tissue with random collagen orientation throughout the hyaline cartilage (Mattice et al., 2006; Forman and Kent, 2010); thus it was expected that its material behavior would be more similar to that of PA gels compared to articular cartilage. In fact, the mean equilibrium modulus values of porcine rib cartilage, 1.4 MPa and 1.1 MPa corresponding to unconfined compression and nanoindentation respectively, are on the same order of magnitude as the stiffest 30:3 (% w/v acrylamide:% w/v crosslinker) gel formulation (Table 2). However, in contrast to PA gels, the variation within the nanoindentation data for cartilage was greater than variation within the unconfined compression data—a standard deviation of 1.0 vs. 0.3. This is consistent with the larger range of data on relaxation states observed under nanoindentation compared to compression. This would slightly overestimate the true equilibrium value of cartilage taken with the nanoindentation technique. The relatively large variation in the cartilage nanoindentation data however is also related to the greater heterogeneity that exists within the cartilage tissue – chondrocytes and extracellular matrix structures over an area of tens of squared micrometers – that are not present in the PA gels. This data also supports the notion that the nanoindentation modulus

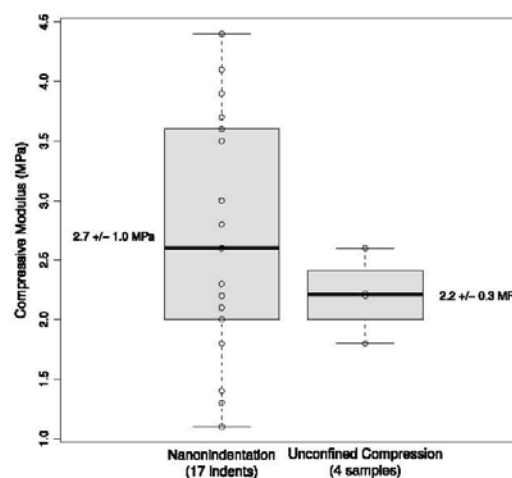


Fig. 5 – Unconfined compression and nanoindentation measurements for quasi-equilibrium modulus of porcine rib cartilage. Note the mean (SD) reported for four samples of cartilage measured with unconfined compression, and one sample (17 indents) measured with nanoindentation.

measurement can be a good indicator for evaluating local property variations within the tissue. Such spatial property information can be very useful for mapping cartilage quality for particular cellular and structural units over a given tissue area that appears homogeneous at the global tissue level.

Despite this difference, and considering the overall similarity in physical properties and in mean equilibrium modulus between the PA gels and the cartilage tissue, the measurements obtained from nanoindentation for cartilage were converted to their equivalent global value using the relationship shown in Fig. 4 (developed for the PA gels). The equivalent average modulus using this conversion is 1.8 MPa and this is within 1 standard deviation of the actual values measured by unconfined compression (Fig. 5). A summary of the porcine cartilage measurements is included in Table II for ease of comparison to the PA gels. These findings reveal the extent to which the PA gel calibration curve can be applied over the specified modulus property range and extrapolated to predict local and global material property relationships for rib cartilage.

4. Conclusions

This work demonstrates that polyacrylamide gels can serve as effective calibration materials for nanoindentation of cartilage and likely other soft hydrated biomaterials. The results of unconfined compression and nanoindentation tests indicate the modulus of the PA gels can be tailored with crosslinking to match approximate modulus values of the cartilage tissue. A method for relating nanoindentation measurements to conventional global mechanical property measurements has been suggested for both PA gels and porcine rib cartilage; the potential application of this relationship to more heterogeneous tissues with

predominant preferred microstructural orientation such as articular cartilage requires further study. Nanoindentation can be used to measure the local properties of interest. In homogeneous and isotropic materials, it can be interpreted at the macroscale level to give a sense of its functionality as a whole structure. This pilot study supports the use of nanoindentation for the localized characterization of cartilage tissues and engineered cartilage constructs.

Bulk mechanical testing of healthy articular cartilage reveals that the equilibrium compressive elastic modulus is on the order of 1 MPa (Armstrong and Mow, 1982; Athanasiou et al., 1994; Kempson et al., 1971; Sokoloff, 1966); however, this global modulus of the tissue may not provide insight into local property changes that occur in disease progression, nor constituent contributions to the structural behavior of this complex tissue. A quantifiable measurement of spatially varying elastic modulus values at the constituent length scales can offer valuable information about the local biochemical and biomechanical transformations at work in the progression of osteoarthritis or in tissue remodeling (Tang et al., in press). The knowledge gained from nanoindentation experiments of tissues and biomaterials can then be extended to efforts in disease prevention and tissue repair.

Acknowledgements

The authors would like to thank Drs. Philipp Thurner, Kevin Cheng, Kurt Koester, and Shikha Gupta for their expertise and support with testing. Funding was provided by NSF ADEPT (Applied Design and Engineering Project Teams) Fellowship.

REFERENCES

- Akhtar, R., Schwarzer, N., Sherratt, M.J., Watson, R.E., Graham, H.K., Trafford, A.W., Mummery, P.M., Derby, B., 2009. Nanoindentation of histological specimens: mapping the elastic properties of soft tissues. *J. Mater. Res.* 24 (3), 638–646.
- Armstrong, C.G., Mow, V.C., 1982. Variations in the intrinsic mechanical properties of human articular cartilage with age, degeneration, and water content. *J. Bone Joint Surg. Am.* 64 (1), 88–94.
- Athanasiou, K.A., Agarwal, A., Dzida, F.J., 1994. Comparative-study of the intrinsic mechanical-properties of the human acetabular and femoral-head cartilage. *J. Orthop. Res.* 12 (3), 340–349.
- Chaudhry, B., Ashton, H., Muhamed, A., Yost, M., Bull, S., Frankel, D., 2009. Nanoscale viscoelastic properties of an aligned collagen scaffold. *J. Mater. Sci. Mater. Med.* 20 (1), 257–263.
- Donnelly, E., Baker, S.P., Boskey, A.L., van der Meulen, M.C., 2006. Effects of surface roughness and maximum load on the mechanical properties of cancellous bone measured by nanoindentation. *J. Biomed. Mater. Res. Ser. A* 77 (2), 426–435.
- Ebenstein, D.M., Kuo, A., Rodrigo, J.J., Reddi, A.H., Ries, M., Pruitt, L., 2004. A nanoindentation technique for functional evaluation of cartilage repair tissue. *J. Mater. Res.* 273–281.
- Ebenstein, D.M., Pruitt, L.A., 2006. Nanoindentation of soft hydrated materials for application to vascular tissues. *J. Biomed. Mater. Res. Ser. A* 69 (2), 222–232.
- Ebenstein, D.M., Wahl, K.J., 2006. A comparison of JKR-based methods to analyze quasi-static and dynamic indentation force curves. *J. Colloid Interface Sci.* 298 (2), 652–662.
- Ferguson, V.L., Bushby, A.J., Boyde, A., 2003. Nanomechanical properties and mineral concentration in articular calcified cartilage and subchondral bone. *J. Anat.* 203 (2), 191.
- Forman, J.L., Kent, R.W., 2010. Modeling costal cartilage using local material properties with consideration for gross heterogeneities. *J. Biomech.*
- Franke, O., Durst, K., Maier, V., Goken, M., Birkholz, T., Schneider, H., Hennig, F., Gelse, K., 2007. Mechanical properties of hyaline and repair cartilage studied by nanoindentation. *Acta Biomater.* 3 (6), 873–881.
- Gupta, S., Carrillo, F., Li, C., Pruitt, L., Puttlitz, C., 2007. Adhesive forces significantly affect elastic modulus determination of soft polymeric materials in nanoindentation. *Mater. Lett.* 61 (2), 448–451.
- Gupta, H.S., Schratte, S., Tesch, W., Roschger, P., Berzlanovich, A., Schoeberl, T., Klaushofer, K., Fratzl, P., 2005. Two different correlations between nanoindentation modulus and mineral content in the bone-cartilage interface. *J. Struct. Biol.* 149 (2), 138–148.
- Hansma, P., Yu, H., Schultz, D., Rodriguez, A., Yurtsev, E.A., Orr, J., Tang, S., Miller, J., Wallace, J., Zok, F., Li, C., Souza, R., Proctor, A., Brimer, D., Nogues-Solan, X., Mellbovsky, L., Pena, M.J., Diez-Ferrer, O., Mathews, P., Randall, C., Kuo, A., Chen, C., Peters, M., Kohn, D., Buckley, J., Li, X., Pruitt, L., Diez-Perez, A., Alliston, T., Weaver, V., Lotz, J., 2009. The tissue diagnostic instrument. *Rev. Sci. Instrum.* 80 (5), 054303.
- Hayes, W.C., Mockros, L.F., 1971. Viscoelastic properties of human articular cartilage. *J. Appl. Physiol.* 31 (4), 562–568.
- Hertz, H., 1881. On the contact of elastic solids. *J. Reine Angew. Math.* 92, 156–171.
- Hou, J.S., Holmes, M.H., Lai, W.M., Mow, V.C., 1990. Squeeze film lubrication for articular cartilage with synovial fluid. In: *Biomechanics of Diarthrodial Joints*. Springer-Verlag, New York.
- Katakai, D., Imura, M., Ando, W., Tateishi, K., Yoshikawa, H., Nakamura, N., Fujie, H., 2009. Compressive properties of cartilage-like tissues repaired in vivo with scaffold-free, tissue engineered constructs. *Clin. Biomech. (Bristol, Avon)* 24 (1), 110–116.
- Kaufman, J.D., Song, J., Klapperich, C.M., 2007. Nanomechanical analysis of bone tissue engineering scaffolds. *J. Biomed. Mater. Res. Ser. A* 81 (3), 611–623.
- Kempson, G.E., Freeman, M.A., Swanson, S.A., 1971. The determination of a creep modulus for articular cartilage from indentation tests of the human femoral head. *J. Biomech.* 4 (4), 239–250.
- Kesari, H., Doll, J.C., Pruitt, B.L., Cai, W., Lew, A.J., 2010. Role of surface roughness in hysteresis during adhesive elastic contact. *Philos. Mag. Lett.* 90 (12), 891–902.
- Kiviranta, P., Lammentausta, E., Toyras, J., Kiviranta, I., Jurvelin, J.S., 2008. Indentation diagnostics of cartilage degeneration. *Osteoarthritis Cartilage* 16 (7), 796–804.
- Kleemann, R.U., Krockner, D., Cedraró, A., Tuischer, J., Duda, G.N., 2005. Altered cartilage mechanics and histology in knee osteoarthritis: relation to clinical assessment (ICRS grade). *Osteoarthritis Cartilage* 13 (11), 958–963.
- Li, C., 2008. Local properties of articular cartilage—a combined nanoindentation and biochemical characterization approach. University of California, Berkeley.
- Li, C., Pruitt, L.A., King, K.B., 2006. Nanoindentation differentiates tissue-scale functional properties of native articular cartilage. *J. Biomed. Mater. Res. Ser. A* 78 (4), 729–738.
- Martinez-Diaz, S., Garcia-Giralt, N., Lebourg, M., Gomez-Tejedor, J.A., Vila, G., Caceres, E., Benito, P., Pradas, M.M., Nogues, X., Ribelles, J.L., Monllau, J.C., 2010. In vivo evaluation of 3-dimensional polycaprolactone scaffolds for cartilage repair in rabbits. *Am. J. Sports Med.* 38 (3), 509–519.

- Mattice, J.M., Lau, A.G., Oyen, M.L., 2006. Spherical indentation load-relaxation of soft biological tissues. *J. Mater. Res.* 21 (8).
- Mow, V.C., Kuei, S.C., Lai, W.M., Armstrong, C.G., 1980. Biphasic creep and stress-relaxation of articular cartilage in compression—theory and experiments. *Trans. ASME, J. Biomech. Eng.* 102 (1), 73-84.
- Mow, V.C., Ratcliffe, A., Poole, A.R., 1992. Cartilage and diarthrodial joints as paradigms for hierarchical materials and structures. *Biomaterials* 13 (2), 67-97.
- Normand, V., Lootens, D.L., Amici, E., Plucknett, K.P., Aymard, P., 2000. New insight into agarose gel mechanical properties. *Biomacromolecules* 1 (4), 730-738. Winter.
- Peyton, S.R., Putnam, A.J., 2005. Extracellular matrix rigidity governs smooth muscle cell motility in a biphasic fashion. *J. Cell. Physiol.* 204 (1), 198-209.
- Scandiucci de Freitas, P., Wirz, D., Stolz, M., Gopfert, B., Friederich, N.F., Daniels, A.U., 2006. Pulsatile dynamic stiffness of cartilage-like materials and use of agarose gels to validate mechanical methods and models. *J. Biomed. Mater. Res. B: Appl. Biomater.* 78 (2), 347-357.
- Sokoloff, L., 1966. Elasticity of aging cartilage. *Fed. Proc.* 25 (3), 1089-1095.
- Stolz, M., Raiteri, R., Daniels, A.U., VanLandingham, M.R., Baschong, W., Aebi, U., 2004. Dynamic elastic modulus of porcine articular cartilage determined at two different levels of tissue organization by indentation-type atomic force microscopy. *Biophys. J.* 86 (5), 3269-3283.
- Tang, S., Souza, R., Hansma, P., Ries, M., Alliston, T., Li, X., Local tissue properties of human osteoarthritic cartilage correlate with magnetic resonance T1rho relaxation times. *J. Orthop. Res.* (in press).
- Walker, P.S., Dowson, D., Longfield, M.D., Wright, V., 1968. "Boosted lubrication" in synovial joints by fluid entrapment and enrichment. *Ann. Rheum. Dis.* 27 (6), 512-520.

APPENDIX B

REVIEW OF SCIENTIFIC INSTRUMENTS 80, 054303 (2009)

The tissue diagnostic instrument

Paul Hansma,¹ Hongmei Yu,² David Schultz,³ Azucena Rodriguez,³ Eugene A. Yurtsev,¹ Jessica Orr,³ Simon Tang,³ Jon Miller,⁴ Joseph Wallace,⁵ Frank Zok,⁶ Cheng Li,⁷ Richard Souza,⁸ Alexander Proctor,⁹ Davis Brimer,⁹ Xavier Nogues-Solan,¹⁰ Leonardo Mellbovsky,¹⁰ M. Jesus Peña,¹⁰ Oriol Diez-Ferrer,¹⁰ Phillip Mathews,¹ Connor Randall,¹ Alfred Kuo,³ Carol Chen,³ Mathilde Peters,⁴ David Kohn,⁵ Jenni Buckley,³ Xiaojuan Li,⁸ Lisa Pruitt,⁷ Adolfo Diez-Perez,¹⁰ Tamara Alliston,³ Valerie Weaver,² and Jeffrey Lotz³

¹Department of Physics, University of California, Santa Barbara, California 93106, USA

²Department of Surgery, Department of Anatomy, Department of Bioengineering and Therapeutics, and Center for Bioengineering and Tissue Regeneration, University of California, San Francisco, California 94143, USA

³Department of Orthopaedic Surgery, University of California, San Francisco, California 94143, USA

⁴Department of Dentistry, University of Michigan, Ann Arbor, Michigan 48109, USA

⁵Department of Biologic and Materials Sciences and Department of Biomedical Engineering, University of Michigan, Ann Arbor, Michigan 48109, USA

⁶Department of Materials, University of California, Santa Barbara, California 93106, USA

⁷UC Berkeley and UCSF Joint Graduate Group in Bioengineering, Berkeley, California 94720, USA

⁸Department of Radiology and Biomedical Imaging, University of California, San Francisco, California 94143, USA

⁹Active Life Technologies, 629 State St., Suite 213, Santa Barbara, California 93101, USA

¹⁰Hospital del Mar, Department of Internal Medicine, Autonomous University of Barcelona, P. Maritim 25-29, 08003 Barcelona, Spain

(Received 11 December 2008; accepted 13 April 2009; published online 27 May 2009)

Tissue mechanical properties reflect extracellular matrix composition and organization, and as such, their changes can be a signature of disease. Examples of such diseases include intervertebral disk degeneration, cancer, atherosclerosis, osteoarthritis, osteoporosis, and tooth decay. Here we introduce the tissue diagnostic instrument (TDI), a device designed to probe the mechanical properties of normal and diseased soft and hard tissues not only in the laboratory but also in patients. The TDI can distinguish between the nucleus and the annulus of spinal disks, between young and degenerated cartilage, and between normal and cancerous mammary glands. It can quantify the elastic modulus and hardness of the wet dentin left in a cavity after excavation. It can perform an indentation test of bone tissue, quantifying the indentation depth increase and other mechanical parameters. With local anesthesia and disposable, sterile, probe assemblies, there has been neither pain nor complications in tests on patients. We anticipate that this unique device will facilitate research on many tissue systems in living organisms, including plants, leading to new insights into disease mechanisms and methods for their early detection. © 2009 American Institute of Physics. [DOI: 10.1063/1.3127602]

I. INTRODUCTION

The tissue diagnostic instrument (TDI) was redesigned from the bone diagnostic instrument^{1,2} so as to measure tissue mechanical properties subcutaneously and *in vivo* with additional probe assemblies and an adjustable compliance (Fig. 1). It consists of a thin probe assembly that can penetrate skin and soft tissue to reach deep tissues. The disposable, sterilizable probe assembly consists of an outer reference probe made from a 23 gauge hypodermic needle and an inner test probe made from stainless steel wire ranging from 175 to 300 μm in diameter and from 2 to 90 mm in length. Since friction between the test probe and the reference probe increases with length, it is desirable to use only the length needed to access the desired tissue location. The test probe is held in a nickel tube that couples to a magnet, which in turn is linked to a force generator. During operation the force generator oscillates the probe within the tissue of interest and

concurrently measures the force and displacement. The maximum values for force and displacement are 12 N and 600 μm . The probe is typically operated at a frequency of 4 Hz because this is rapid enough to allow hand holding yet sufficiently slow to allow easy decoupling of the elastic and viscous response of the tissue (see supplementary material³ for more details including force and displacement ranges.)

II. MEASUREMENTS

We first illustrate TDI use in human spinal disks that are composed of a thick outer ligament (*annulus fibrosus*) and a central swelling hydrogel (*nucleus pulposus*). Spinal disk degeneration can be the underlying cause of back pain leading to significant morbidity and societal expense. Intervertebral disks are one of the most highly loaded tissues in the body, and consequently material property insufficiency can lead to damage accumulation, inflammation, and pain. Disk degen-

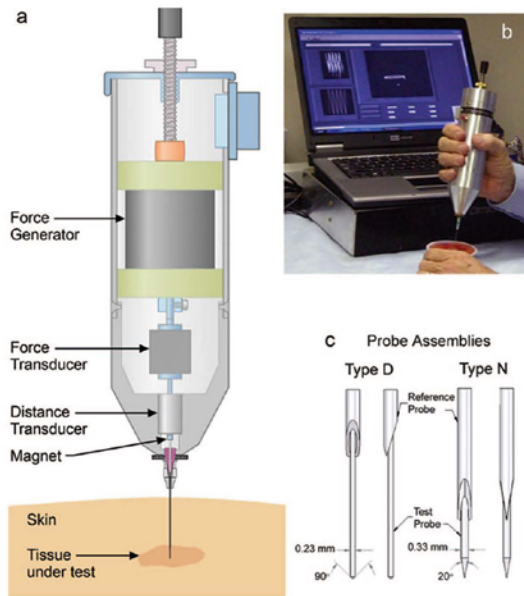


FIG. 1. (Color) The TDI. (a) The TDI can measure mechanical properties of tissues under test even if they are covered with skin and other soft tissues because it has a probe assembly that can be inserted subcutaneously into the tissue under test. (b) It can be handheld and is connected to a computer for data generation, acquisition, and processing. In this photo it is being used to measure differences in the mechanical properties of fruit and gel in a snack food. (c) A probe assembly for the TDI consists of a test probe, which moves displacements of the order of $200\ \mu\text{m}$ relative to the reference probe. The reference probe serves to shield the test probe from the influence of the skin and soft tissue that must be penetrated to reach the tissue under test. Type D probes are good for very soft tissue, such as the murine breast tissue in Fig. 3. Type N probes are good for stiffer tissue, such as the spinal disk tissue in Fig. 2. The screw at the top of the TDI (a) can adjust the compliance of the TDI, as discussed in the supplementary material.

eration is currently diagnosed using imaging techniques, such as magnetic resonance.⁴ Unfortunately, these methods can only indirectly suggest disk mechanical properties, which currently cannot be measured *in vivo*.

Using image-guided, percutaneous placement [Figs. 2(a) and 2(b)], disk material properties can now be measured safely *in vivo* using a type N probe assembly [Fig. 1(c)]. The novel sharpening of the reference probe for type N probe assembly decreases the problem of tissue being caught between the test probe and the reference probe during insertion and thus decreases the friction between the test probe and the reference probe. The friction between the test and reference probes is typically $\sim 0.02\ \text{N}$. The specific value is recorded by the software before testing a sample and is removed from the samples' force versus distance plot before analysis. The force versus displacement data are plotted in real time and recorded digitally [Figs. 2(c) and 2(d)]. The slope of the force versus displacement curve provides a measure of disk elasticity: in the case of a simple spring, the slope would be the spring constant. The energy dissipation in the force versus displacement curve is the area inside the curve and is a measure of the viscous behavior. Viscosity is absent from a simple spring yet is large for a purely viscous material such

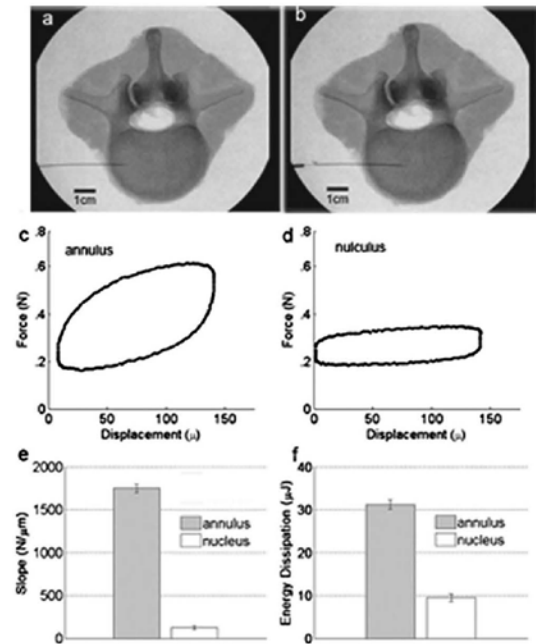


FIG. 2. Demonstration of the ability of the TDI to distinguish between the annulus and nucleus of a human intervertebral disk. (a) X-ray image of transverse view of a cadaver lumbar motion segment L12 with test probe located in annulus. (b) Similar view with probe centered in the nucleus. (c) Force vs displacement curve measured by the TDI during a cyclic load cycle (4 Hz) in the annulus. (d) Force vs displacement curve measured in the nucleus. Note that the annulus is much stiffer (higher slope) and dissipates more energy (higher area enclosed by the curve). (e) Histogram comparing the average least-squares slope for ten cycles in the annulus vs in the nucleus. (f) Histogram comparing the average energy dissipation for ten measurements in the annulus vs in the nucleus ($31.8 \pm 1.1\ \mu\text{J}$ vs $9.7 \pm 0.6\ \mu\text{J}$; $p < 0.01$). The error bars indicate standard deviation for the ten measurements within the annulus and within the nucleus in the disk.

as petroleum jelly, which has an elasticity near zero.

There are significant differences (p values of < 0.01) in slope (N/m) and energy dissipation (μJ) between the *annulus fibrosus* and the *nucleus pulposus* (Fig. 2). The *annulus fibrosus* has both higher slope and energy dissipation. These results are representative of our measurements on 11 disks: the slope and energy dissipation are always greater in the annulus than the nucleus. This observation of higher slope or stiffness in the annulus is consistent with previous experiments measuring the compressive properties of both annulus and nucleus.^{5,6} However, a precise comparison with established mechanical data is not readily available because mechanical testing in this manner at high spatial resolution has not been possible previously. Because these properties are known to change with age and degeneration, an eventual goal would be to determine whether *in vivo* measures of annulus and nucleus material properties provide novel data that improve back pain diagnosis and treatment. We note that the 23 gauge needle is consistent with the recent recommendation⁷ that a spinal needle smaller than or equal to 22 gauge should be used to prevent postsurgery leakage.

An epithelial tissue such as the mammary gland is an

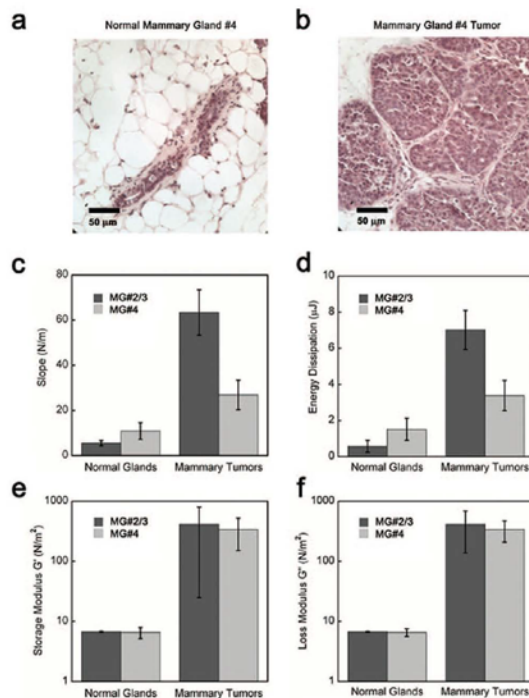


FIG. 3. (Color) Demonstration of the ability of the TDI to distinguish between normal mammary glands and tumors. Hematoxylin and eosin (H&E) staining of (a) the representative normal FVB murine mammary gland and (b) the matched malignant MMTV-PyMT⁺/₋ murine mammary gland that were tested in this experiment. (c) The mammary tumors have significantly ($P < 0.001$) higher slopes, a measure of elasticity, for both the thoracic # 2/3 and the inguinal # 4 tissues. (d) The mammary tumors have significantly higher energy dissipation for the thoracic # 2/3 tissue ($P < 0.001$), but the difference for the inguinal # 4 tumor was not significant. Histogram comparing (e) the elastic modulus and (f) the loss modulus, as measured by rheology, for the normal mammary glands and mammary tumors after the TDI measurements (two subregions for each mammary gland, ten measurements for each region). Note that the results for elasticity and loss modulus for the two techniques reproduce the same general trends. The error bars in the measurements indicate standard deviation for all the measurements.

example of the softest tissue that can be probed with the current TDI. Figure 3 shows a paired-comparison of the mammary glands #2/3 and #4 from normal Friend Virus B, mice and tumors arising in the matched mammary glands of their MMTV-PyMT⁺/₋ (Mouse Mammary Tumor Virus-Polyoma Middle T Antigen) littermates. These data are representative of the data in an ongoing study of various tumors. The results of that study are beyond the scope of this paper, but we can report that all 30 tumors are stiffer (have higher slope) than all 15 normal mammary glands in tissue site-matched and age-matched mice. Normal murine mammary glands have elastic modulus below 1 kPa as measured with a conventional rheometer and with the TDI device. This value is comparable with our calibration curves on polyacrylamide (PA) gels (see supplementary material) that demonstrate TDI sensitivity below 1 kPa. Normal and transformed human breast tissue is considerably stiffer than mouse tissue⁸ and is therefore well within the range of the TDI. Tissue stiffness

increases in many breast cancers. To quantify stiffness and improve breast tumor detection, imaging modalities such as sonoelastography and Magnetic Resonance elastography have been used.^{9,10} The TDI offers a tractable and economical approach to measure breast stiffness *in situ* with millimeter resolution. Our preliminary trials on human breast tissue from cadavers showed detectable variations in mechanical properties between different locations in the same specimen with a spatial resolution of 2 mm (data not shown). Based on these observations an eventual goal would be to use the TDI for localization of human breast cancer *in situ*. A foreseeable clinical application includes using the device to define margins of affected tissue and sites for biopsy. The TDI measurement could easily be combined with biopsy; the test probe could be withdrawn into the reference probe to collect a biopsy sample after mechanical testing. We are currently investigating the molecular mechanism of how the mechanical properties contribute to breast cancer; the TDI can be applied to clarify the molecular link between matrix materials properties of tissues and tumor risk (i.e., breast cancer in women with mammographically dense breasts^{11,12}).

Prior to clinically apparent symptoms of osteoarthritis, the material quality and mechanical function of cartilage matrix are compromised.¹³ The ability to noninvasively probe the material quality of this stratified tissue will complement and extend current diagnostic capabilities.¹³ Furthermore, detection of cartilage degeneration early in osteoarthritis may increase the success of therapeutic intervention. To that end, the ability of the TDI to distinguish the elastic modulus of synthetic materials with moduli comparable to cartilage was validated against well-established methods including atomic force microscopy, nanoindentation, and bulk stress relaxation (Fig. 4). In addition to accurately measuring the elastic modulus of PA gels with a range of moduli from 0.2 to 1 MPa, the TDI could measure the elastic modulus of a stiff gel that was inferior to a compliant gel, demonstrating its ability to noninvasively evaluate a stratified material [Fig. 4(d)]. When applied to cartilage, the TDI readily discriminated between a young healthy cadaveric specimen and an old degenerated surgical specimen that were probed *in situ* [Fig. 4(f)].

Human dentin is an example of the hard tissue that can be probed with our current device (Fig. 5). One unsolved problem for practicing dentists is deciding when a sufficient depth has been reached when drilling to remove carious dentin from a cavity. One proposed solution has been the development of a new experimental polymer bur (from SS White Burs, Inc., Lakewood, NJ), which is designed to remove soft decaying dentin but blunt on harder healthy dentin and thus self-limit the tissue amount removed. Here we show the properties of the remaining dentin after a first excavation by such a bur and then after a second excavation with a second polymer bur of the same type (Fig. 5). Next was a third excavation with a #4 round carbide bur and finally a cavity preparation into presumably sound dentin using a #330 carbide bur. Note that even after the cavity preparation, the dentin did not have the full elastic modulus of the healthy dentin. Our primary focus was on relative values as excavation proceeded. The elastic modulus, as calculated from force

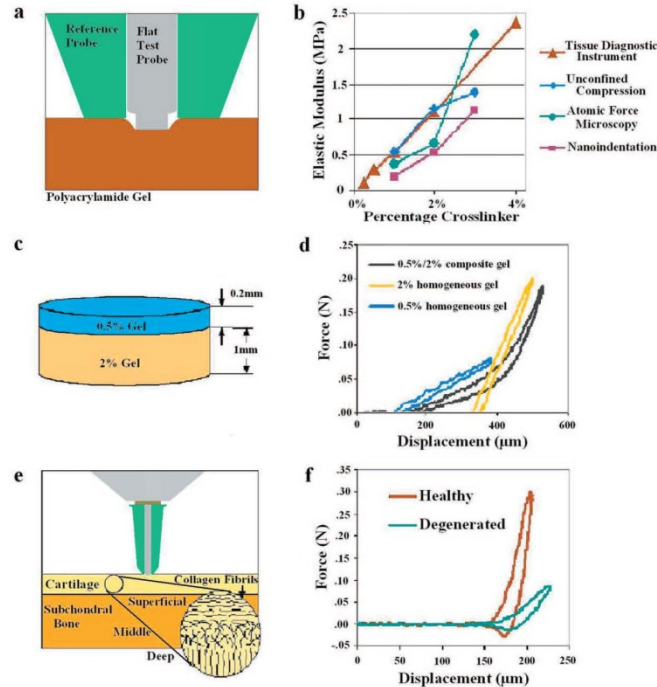


FIG. 4. (Color) Demonstration of the ability of the TDI to distinguish differences in moduli of stratified materials such as cartilage. (a) The elastic modulus can be determined with the type V probe assembly that indents soft materials rather than penetrating them, as above. (b) PA gels with elastic moduli in the range previously reported for cartilage (0.2–1 MPa) were used to validate the TDI relative to other established methods, including atomic force microscopy, nanoindentation, and bulk stress relaxation. PA gel moduli increased dose-dependently with cross-linker concentration ($p=0.012$). (c) To construct a stratified elastic modulus gel, a 0.2 mm thick layer of “compliant” PA gel was poured over a prepolymerized 1 mm thick “stiff” PA gel. (d) The force vs displacement curve produced by the TDI revealed two distinct slopes on the loading curve for the stratified gels. Each slope of the composite gel matches the corresponding slopes for homogeneous 0.5% and 2% PA gel, demonstrating the capability to analyze stratified materials, such as cartilage. (e) A schematic of the indentation tests performed on cartilage, which were performed in hydrated conditions with phosphate buffered saline. (f) Using similar test conditions, the TDI easily distinguished between young cadaveric cartilage and aged degenerated cartilage measured *in situ*.

versus displacement curves generated by the TDI and analyzed using a modified Oliver and Pharr¹⁴ method, for the dentin left in the cavity by the polymer bur was below that for healthy dentin far from the cavity [Fig. 5(c)]. Please see the appendix for the details of the modified method. The hardness, as calculated from force versus displacement curves generated by the TDI and analyzed using a modified Oliver and Pharr¹⁴ method, for the dentin left in the cavity by the polymer bur was below that for healthy dentin far from the cavity [Fig. 5(c)]. One-way analysis of variance gives values of $P < 0.0001$ for the elastic modulus and $P = 0.0008$ for the hardness, indicating that the variation among means is significantly greater than expected by chance. Thus the TDI has the potential to quantify the properties of dentin left in a cavity and could be used to study the outcome of various treatment strategies for how much degenerated dentin is removed before filling the cavity.

The absolute value for the elastic modulus of our “healthy dentin” is well within the range of existing measurements but below the value of 20–25 GPa recommended in a recent critical reevaluation of the literature.¹⁵ The reason is probably the storage of the teeth in water for weeks before measurement.¹⁶ To our knowledge, the TDI is the first instru-

ment that can measure elastic modulus and hardness inside irregularly shaped, fully hydrated dentin cavities. It could be used for research projects without further modification. For individual clinical use, a smaller, less expensive version with an angled probe would be desirable. The experiments on dentin reported here build on a rich history of measuring mechanical properties with indentation methods.^{14,17,18} Of special interest is recent work modeling size effects with finite element analysis¹⁹ because extensions of work such as this may lead to a more quantitative understanding of TDI measurements on soft tissue as well as hard tissue.

The hard tissue, bone, is of particular interest medically because of the growing incidence of debilitating bone fracture as our population ages.²⁰ Changes in bone material properties are believed to play a role in fracture risk.^{21–23} With the top screw backed off, as discussed in the supplementary materials,³ the TDI functions as a Bone Diagnostic Instrument,^{1,2} which may, after clinical tests, prove useful in quantifying the component of bone fragility due to degraded material properties. Figure 6 shows tests of the TDI, working as a bone diagnostic instrument, on a living patient to determine if the procedure is painful or results in complications. Neither this patient nor the others tested to date experienced

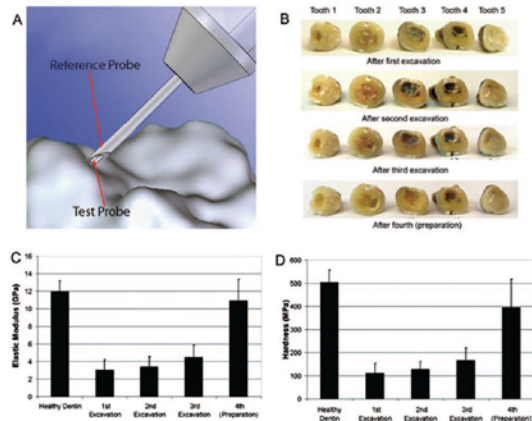


FIG. 5. (Color) Demonstration of the ability of the TDI to measure the elastic modulus and hardness of human dentin to quantify the properties of the dentin left in a tooth cavity after each of multiple excavations and finally preparation. (a) The probe assembly for these measurements was designed to indent the hard tissue. The reference probe was a hypodermic needle that rested on the surface under test. The test probe was sharpened into a 90° cone with a 30 μm radius at the end (drawing by Haykaz Mkrtchyan). (b) The teeth after the various excavations and finally preparation. At each successive stage of excavation and preparation more dentin was removed from the cavity. [(c) and (d)] The elastic modulus and hardness of the dentin remaining in the cavity was significantly ($p=.01$) less than that of healthy dentin. The error bars indicate standard deviation of the ten measurements that were taken on each of the five teeth (a total of 50 measurements). Note that the elastic modulus of the healthy dentin is over 10 GPa, over seven orders of magnitude greater than the normal mammary glands (Fig. 3), demonstrating the range of the TDI.

any pain beyond the initial “stick” when the local anesthesia was injected. There have been no complications.

III. DISCUSSION OF NEW POSSIBILITIES

It might, in the future, be possible for the TDI to measure the interaction forces between antibody coated test probes and tissues. This would allow measurements of single molecule interactions as is currently achieved with an atomic force microscope.²⁴ Rupture forces in the range of 20–140 pN have been measured for many receptor-ligand interactions with single-cell force spectroscopy.²⁵ With these interaction forces, we can make order of magnitude estimates of forces we might find when trying to rotate or translate a test probe that had bound to a tissue with many molecular bonds in parallel. Assuming a molecular density of 1 molecule/10 nm^2 , an interaction force per molecule of 50 pN, a coated region of area of $4 \times 10^{-6} \text{ m}^2$ (the exposed area of the type D probe), and a fractional binding of 1%, we would get a force of $50 \text{ pN/molecule} \times 4 \times 10^{-6} \text{ m}^2 \times 1 \text{ molecule}/10 \text{ nm}^2 \times .01 = 200 \text{ mN}$. The present lower limits of sensitivity of the TDI for forces come from the friction between the test probe and the reference probe, of the order of 10 mN, and from the force noise in our force transducer, of the order of 5 mN in a 1 kHz bandwidth. Thus forces of the magnitude that could be expected from molecular interactions with coated tips should be measurable. A big problem could be nonspecific interaction masking specific interactions. A proof of concept experimental approach to

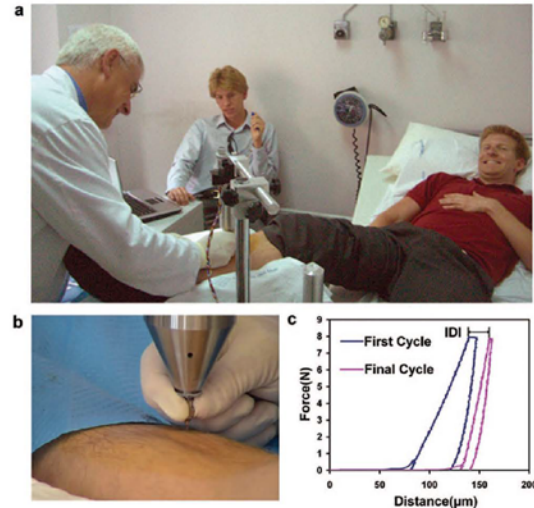


FIG. 6. (Color) Demonstration of the ability of the TDI to do measurements on a living patient. (a) The probe assembly of the TDI is lowered by a physician (A.D.P.) to penetrate the skin and soft tissue covering the tibia of the patient (D.B.) after the test site has been sterilized and locally anesthetized. (b) Close up of the physician’s hand on the probe assembly as he lowers it to the bone surface. (c) Representative force vs distance curves measured on the bone of the patient. This patient and the other patients tested to date experienced neither pain nor complications with the procedure. The most important parameter is the indentation distance increase (IDI) defined in the image as the increase in indentation distance from the first cycle to the last. In model systems the IDI is greater for more easily fractured bone. Other parameters such as the creep at nearly constant force (the plateau on the top of the curves), the elastic modulus, the energy dissipation, and the hardness can also be determined from analysis of the force vs distance curves.

overcoming this masking effect would be to use a test probe coated on just one side that was exposed to the tissue under test through a window in the wall of a closed-end reference probe. The difference in the forces between the test probe and the tissue under test for the coated versus uncoated side could be measured. This could naturally be extended with multiple coatings on multiple strips on the test probe, each exposed one by one through a slit in the wall of the closed-end reference probe. We emphasize, however, that proof of concept experiments will be necessary to evaluate this potential application of the TDI.

It is important to note that though the present instrument is able to make basic measurements in a wide range of tissues (almost all tissues in the human body from very soft breast tissue to hard, mineralized tissues), it is in a very early stage of development. More versatile instruments with more measurement modalities, such as mentioned above, and more user convenience features, such as wireless operation, are possible. Specialized instruments for specific measurements in specific tissues could be developed at a small fraction of the cost of the fully versatile instrument. The device could also be modified to assess materials properties of various bioengineered artificial three dimensional tissues.^{26,27}

ACKNOWLEDGMENTS

We thank the NIH for support of this work under Grant Nos. RO1 GM 065354 and RO1 AR 049770 and NIH Grant

No. AR049770, the DOD under Grant No. W81XWH-05-1-330, and the Fondo de Investigaciones Sanitarias (FIS) under Grant No. PI07/90912. We thank Angus Scrimgeour for asking us to do indentation measurements on bone, Robert Recker for encouraging us to plan for clinical trials even when the BDI was at an early stage of development, Paul Zaslansky for pointing us toward dental applications, and Georg Fantner, Jonathan Adams, Patricia Turner, Doug Rhen, Jason Lelujian, and Ralf Jungman for helping develop prototype BDIs, which then stimulated development of the more general TDI.

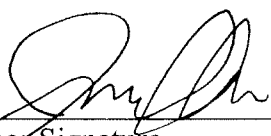
- ¹P. K. Hansma, P. J. Turner, and G. E. Fantner, *Rev. Sci. Instrum.* **77**, 075105 (2006).
- ²P. Hansma, P. Turner, B. Drake, E. Yurtsev, A. Proctor, P. Mathews, J. Lelujian, C. Randall, J. Adams, R. Jungmann, F. Garza-de-Leon, G. Fantner, H. Mkrtychyan, M. Pontin, A. Weaver, M. B. Brown, N. Sahar, R. Rossello, and D. Kohn, *Rev. Sci. Instrum.* **79**, 064303 (2008).
- ³See EPAPS Document No. E-RSINAK-80-032905 for details regarding the measurements and test methods of the TDI on various biomaterials. For more information on EPAPS, see <http://www.aip.org/pubservs/epaps.html>.
- ⁴C. W. A. Pfirrmann, A. Metzendorf, M. Zanetti, J. Hodler, and N. Boos, *Spine* **26**, 1873 (2001).
- ⁵S. M. Klisch and J. C. Lotz, *J. Biomech.* **32**, 1027 (1999).
- ⁶J. M. Cloyd, N. R. Malhotra, L. Weng, W. Chen, R. L. Mauck, and D. M. Elliott, *Eur. Spine J.* **16**, 1892 (2007).
- ⁷J. L. Wang, Y. C. Tsai, and Y. H. Wang, *Spine* **32**, 1809 (2007).
- ⁸G. D. A. Sarvazyan, E. Maevsky, and G. Oranskaja, Proceedings of the International Workshop on Interaction of Ultrasound with Biological Media, 1994, Valenciennes, France, p. 6981.
- ⁹A. Samani, J. Zubovits, and D. Plewes, *Phys. Med. Biol.* **52**, 1565 (2007).
- ¹⁰A. Samani and D. Plewes, *Phys. Med. Biol.* **52**, 1247 (2007).
- ¹¹M. J. Paszek, N. Zahir, K. R. Johnson, J. N. Lakin, G. I. Rozenberg, A. Gefen, C. A. Reinhart-King, S. S. Margulies, M. Dembo, D. Boettiger, D. A. Hammer, and V. M. Weaver, *Cancer Cells* **8**, 241 (2005).
- ¹²N. F. Boyd, H. Guo, L. J. Martin, L. M. Sun, J. Stone, E. Fishell, R. A. Jong, G. Hislop, A. Chiarelli, S. Minkin, and M. J. Yaffe, *N. Engl. J. Med.* **356**, 227 (2007).
- ¹³R. U. Kleemann, D. Krocker, A. Cedraro, J. Tuischer, and G. N. Duda, *Osteoarthritis Cartilage* **13**, 958 (2005).
- ¹⁴W. C. Oliver and G. M. Pharr, *J. Mater. Res.* **19**, 3 (2004).
- ¹⁵J. H. Kinney, S. J. Marshall, and G. W. Marshall, *Crit. Rev. Oral Biol. Med.* **14**, 13 (2003).
- ¹⁶S. Habelitz, G. W. Marshall, M. Balooch, and S. J. Marshall, *J. Biomech.* **35**, 995 (2002).
- ¹⁷W. D. Nix and H. J. Gao, *J. Mech. Phys. Solids* **46**, 411 (1998).
- ¹⁸W. C. Oliver and G. M. Pharr, *J. Mater. Res.* **7**, 1564 (1992).
- ¹⁹Y. Huang, F. Zhang, K. C. Hwang, W. D. Nix, G. M. Pharr, and G. Feng, *J. Mech. Phys. Solids* **54**, 1668 (2006).
- ²⁰Z. A. Cole, E. M. Dennison, and C. Cooper, Osteoporosis Epidemiology Update, *Curr. Rheumatol. Rep.* **10**, 92 (2008).
- ²¹E. Durchschlag, E. P. Paschalis, R. Zochrer, P. Roschger, P. Fratzl, R. Recker, R. Phipps, and K. Klaushofer, *J. Bone Miner. Res.* **21**, 1581 (2006).
- ²²H. S. Gupta, P. Fratzl, M. Kerschitzki, G. Benecke, W. Wagermaier, and H. O. K. Kirchner, *J. R. Soc., Interface* **4**, 277 (2007).
- ²³R. K. Nalla, J. J. Kruzic, J. H. Kinney, and R. O. Ritchie, *Bone* **35**, 1240 (2004).
- ²⁴M. Rief, F. Oesterhelt, B. Heymann, and H. E. Gaub, *Science* **275**, 1295 (1997).
- ²⁵J. Helenius, C. P. Heisenberg, H. E. Gaub, and D. J. Muller, *J. Cell Sci.* **121**, 1785 (2008).
- ²⁶L. G. Griffith and M. A. Swartz, *Nat. Rev. Mol. Cell Biol.* **7**, 211 (2006).
- ²⁷J. G. Jacot, S. Dianis, J. Schnall, and J. Y. Wong, *J. Biomed. Mater. Res. Part A* **79A**, 485 (2006).

Publishing Agreement

It is the policy of the University to encourage the distribution of all theses, dissertations, and manuscripts. Copies of all UCSF theses, dissertations, and manuscripts will be routed to the library via the Graduate Division. The library will make all theses, dissertations, and manuscripts accessible to the public and will preserve these to the best of their abilities, in perpetuity.

Please sign the following statement:

I hereby grant permission to the Graduate Division of the University of California, San Francisco to release copies of my thesis, dissertation, or manuscript to the Campus Library to provide access and preservation, in whole or in part, in perpetuity.



Author Signature

9/6/12
Date